Mobility Control by CO_2-foam Injection for Integrated EOR

Master Thesis in Reservoir Physics

Ingrid Eikemo Opdal

Department of Physics and Technology

University of Bergen

June 2014

Summary

This thesis investigated integrated enhanced oil recovery (IEOR) methods in fractured carbonate rocks. The objective was to study the oil recovery by miscible CO_2 injection in fractured rocks using different rock types and compare oil recovery performance by CO_2-foam injections. CO_2 injections were also performed on reservoir shale cores to evaluate permeability.

Routine analysis was performed on 48 outcrop (chalk and limestone) and 4 reservoir carbonate cores. Experiments by CO_2 injection have been performed on five setups at three different locations; Department of Physics and Technology, Bergen; Haukeland University Hospital, Bergen and Texas A&M University, College Station, Texas. Experiments were conducted at varying pressure and temperature and fractured networks. The fractured permeability was several orders of magnitude larger than the matrix permeability.

Pure supercritical CO_2 was injected prior to supercritical CO_2-foam injection in strongly water-wet outcrop cores, whole and fractured at pressure of 90 bar and temperature of 35°C. Oil recovery by pure supercritical CO_2 injection was most efficient in whole cores, above 85% OOIP, whereas in fractured cores the oil recovery and oil production rate was significantly reduced and oil was only produced by diffusion. Pre-generated foam injection showed increased oil recovery compared to pure CO_2 injection in limestone, but only minor increased oil recovery in chalk. Subsequent injection of CO_2-foam reduced the gas mobility in fractures and diverted flow into the oil-saturated matrix. *In situ* foam generation during tertiary foam injection in fractured limestone network showed increased differential pressure due to generation of strong foam and improved oil recovery, additional 6-10 % OOIP produced.

Waterfloods and tertiary CO_2 injections in heterogeneous reservoir carbonate cores were performed above minimum miscibility pressure of CO_2 and crude oil. Waterflood oil recovery ranged between 17 – 46% OOIP, whereas subsequent CO_2 injections showed significant enhanced oil recovery, above 85% OOIP for all cores.

A “best practice” for permeability and re-saturation of unpreserved shale core plugs was established.

Acknowledgement

First I would like to thank my supervisors Professor Arne Graue and Associate Professor Martin Fernø at the Department of Physics and Technology at University of Bergen for their guidance and support regarding this thesis, and for giving me the opportunity to do research abroad.

I would also like to thank Associated Professor Geir Ersland for help and good conversations. Thanks to PhD Candidate Bergit Brattekås and PhD Candidate Marianne Steinsbø for collaboration and guidance.

Thanks to Dr. Schechter for the opportunity to do experimental work at the laboratory at Texas A&M University in College Station. And thanks to PhD Candidate Øyvind Eide, MSc Fransisco Tuvar, MSc Stig A. Langlo and MSc Tom Ydstebø for the experimental collaboration and the festivities at A&M.

Thanks to Inez Buzdugan for useful advises and help at the laboratory, and thanks to Haukeland University Hospital and Geir Espen Abell for collaboration with the PET/CT scanner.

Especially thanks to my friends and lab partners Rebecca Tunli and Kristine Bø for fun and busy hours at the lab, good conversations and all the encouragement. Thanks to my other friends at UoB for all the good memories through my studies, I will never forget.

Finally I would like to thank my parents and siblings (John, Liv, Grethe, Kristin and Håkon) for all support. Thanks to my funny nephew and cute niece. Last but not least tanks to all my friends for motivation and support. I love you!

June 2, 2014

Ingrid Eikemo Opdal

Table of contents

Introduction

The average of world's oil recovery factor is estimated to be 35% (Babadagli, 2007), indicating large amount of oil remained in the reservoirs after current oil recovery methods have been applied. To meet the world's energy demand it is of interest to increase the oil production. Primary recovery by pressure depletion and secondary recovery by water injection may result in low volumetric sweep efficiency and oil remained trapped in the reservoir. Thus there is major interest in Enhanced Oil Recovery (EOR) techniques. Examples of EOR methods are 1) thermal, 2) chemical and 3) miscible methods and is chosen with respect to the reservoir (Zolotukhin and Ursin, 2000). Carbonate reservoirs, holding 60% of the remaining oil reserves in the world (Ardèvol and Gutamanis, 2008) are all of some degree heterogeneous (Bertin et al., 1999) and more effective EOR techniques are needed to produce the remaining oil from these reservoirs.

By injecting gas and displace oil by a miscible process one can achieve sweep efficiency resulting in enhance oil recovery (Holm and Josendal, 1974). Injection of the greenhouse gas carbon dioxide (CO_2) combined with CO_2 storage has been studied the last decade due to increased focus on CO_2 as a climate changing gas. Recently, carbon capture, utilization and storage (CCUS) have received attention as a tool to inject CO_2 in the oil reservoir for oil recovery and, simultaneously, store the CO_2 underground (Halland et al., 2014b). Development of the technology and IEOR techniques are therefore vital for the oil production and to reduce the pollution. Thus research within these topics is of importance to obtain broader knowledge and get involved in these present topics.

The Norwegian Continental Shelf (NCS) has increased the initial estimated oil and gas production to a produced value of 44% OOIP (Tormodsgard, 2014) since the production started from the carbonate chalk field, Ekofisk 43 years ago and currently there are 78 fields in production on the NCS (Halland et al., 2014a). The production is declining (NorwegianPetroleumDirectorate, 2014) and thus EOR techniques are of great interest in this area to accelerate the oil production. EOR screening and examination with regard to CO_2 injection in several fields has been performed (Aarra and Skauge, 1994, Jensen et al., 2000, Awan et al., 2008) and the studies showed good potential. A major challenge is the injection of CO_2 as a low viscosity fluid in heterogeneous reservoirs which may lead to low sweep efficiency. Foam (combined surfactant and gas) injection may improve the gas sweep efficiency, due to control of the low viscous gas flow (Halland et al., 2014a), and improving the microscopic displacement efficiency by lowering interfacial tension between water and oil.

Because the importance and significant interest of gas injection around the world, the Department of Physics and Technology, UoB has in years studied CO_2 injection for storage and EOR and during the latest years it has been focused on improving the gas injection by increasing the viscosity by e.g.

injecting surfactant to create foam. This thesis has focused on this improvement of oil recovery and studied CO_2 injection and the influence of foam injection in fractured core plugs to gain a better understanding and contribute to the research within this subject.

The thesis is divided into four main parts, and further divided into 9 chapters including appendix. Part1 (chapter 1 and 2) characterize carbonate reservoir and their importance and contribution to petroleum reserves in the world, and describe recovery mechanisms during miscible CO_2 and CO_2-foam in fractured reservoirs. Part 2 review the experimental setups and procedure used in this thesis (chapter 3) and presents the experimental results and discussion on CO_2 EOR (chapter 4). CO_2 injection for permeability measurements in unconventional shale rocks is also discussed (chapter5). Part 3 (chapter 6 and 7) summarize and conclude based on the experimental results and discussion and give suggestions to further work. References used in this thesis are listed in the end (chapter 8) and appendix is a list of nomenclature, source of errors and example of uncertainty calculations.

PART I - Theory

1 Carbonate Reservoirs

The reservoirs out in the field are all of some degree heterogeneous (Bertin et al., 1999). Due to large heterogeneity more than 50 percent of the oil is left in the reservoir after water flooding (Lucia et al., 2003) and it is useful to examine fluid flow behavior and how it is possible to improve the oil recovery in these types of structures. When characterizing fluid distribution and flow behavior in heterogeneous reservoirs it all starts at pore level. The pore geometry and pore size have large impact on the petrophysical parameters and one of the parameters that controls the pore geometry is the relationship between porosity and permeability, φ/k (Marzouk et al., 1998). The variability in porosity and permeability demonstrate the heterogeneity of carbonate reservoirs, but these two properties have little correlation and what describes a carbonate reservoir is the rock fabric due to the vertical and lateral continuity (Wang et al., 1998, Jennings and Ward, 2000, Jennings and Lucia, 2003). Carbonate reservoirs are different from silica clastic reservoirs due to the high heterogeneity and wide range of petrophysical values. Modern research programs have developed methods and tried to understand this heterogeneity to make reliable predictions of the reservoirs and performance of oil production (Lucia et al., 2003). Understanding and examining the characterization and fluid flow in carbonate reservoirs are important because a significant amount, a total of 60% of the remaining oil reserves in the world are hold in carbonate reservoirs (Ardèvol and Gutamanis, 2008).

Fractures within the reservoirs influence and change the fluid flow behavior compared to fluid flow in matrix. Characterization of fractures, fracture networks and fractured porous media in oil and gas reservoirs are difficult but essential for exact planning, and the development cannot be economic without accurate identifications of fractures and their spatial distribution. Thus permeability measurements at different points in the reservoir are one key parameter that can provide information about this spatial distribution of fractures (Sahimi, 2011b). To better understand the different impacts of reservoir and fluid properties one hundred fractured reservoir was examined by Allan and Sun (2003). They divided naturally fractured reservoirs into four types of reservoirs dependent on 1) porosity and permeability of the matrix and the fractures, 2) the matrix and the fractures storage capacity, and 3) flow of hydrocarbons. The results showed wide range in porosity and permeability both for matrix and fractures, and these variation of the fluid storage capacity and the fluid-flow pathways was found both in matrix and fractures (Allan and Sun, 2003).

The production from fractured reservoirs may be difficult to predict due to the fractured network, compared to other conventional reservoirs, which are defined as easier and more economically to

produce from (CAPP, 2014). Conventional recovery methods such as pressure depletion and water injection in fractured reservoirs may result in short-lived field, rapid production declines, and low ultimate recovery due to the complex characteristic of the pore geometry, leaving behind a significant amount of petroleum reserves in the underground. Thus fractured reservoirs are large contributors to oil recovery by enhanced oil recovery techniques (Allan and Sun, 2003).

The void system in a limestone is characterized by a wide variation in the shapes and distribution of pore sizes and these variations are influenced by complicated processes of secondary solution, recrystallization and fracturing, which make it difficult to obtain representative sampling of the reservoirs (Craze, 1950). The limestone pore throat sizes ranges between 0.1 – 10 microns whereas the chalk core is a type of carbonate limestone with pore throat sizes ranging only between 0.1 – 1 micron. (Sahimi, 2011b).

In fractured domains capillarity or diffusion may be the main driving force under certain conditions (Yokoyama and Lake, 1981) when steep compositional and saturation gradients develop (Moortgat and Firoozabadi, 2012). The performance and oil recovery from heterogeneous and fractured reservoirs are significantly reduced due to the presence of high permeable zones, allowing the CO_2 to bypass the matrix oil regardless of pressure, temperature and miscibility. When CO_2 flows through the fractures only a small amount of the matrix oil will be contacted by molecular diffusion of CO_2. When CO_2 dissolves in the oil the oil swells and moves into the fractures resulting in more oil produced.

One need to do something to avoid CO_2 channeling through high permeable zones and one thing is to reduce the mobility of CO_2 by increasing its viscosity or decreasing the fracture permeability (Brautaset, 2009). This thesis focuses on how to affect the viscosity of the CO_2 to lower its mobility and thus achieve a more favorable mobility ratio and enhance the oil recovery.

1.1 Reservoir scale

Carbonate reservoirs represent over half of the world petroleum reserves (Høgnesen et al., 2005). Chalk and limestone are two rock types that represent carbonate reservoirs and the large amount of oil and gas are stored in the matrix in these reservoirs. Spontaneous imbibition into matrix is one of the major recovery mechanisms in many chalk reservoirs due to water- and mixed wet conditions (Torsaeter, 1984), but the recovery from these fields can be low because of the fractured nature of these reservoirs. Thus it is of high interest to study mechanisms that enhance the oil recovery, and for several years there have been studied injection schemes such as CO_2- and CO_2-foam injection.

There are several oil fields were CO_2-injection is performed to enhance oil recovery. The United States is a large contributor to the amount of carbonate reservoirs in the world. CO_2 injection was started at the SACROC unit in Texas in 1972, where CO_2 was supplied from gas field in South Texas. This flooding process was performed as a tertiary recovery method after pressure depletion and water injection (Crameik and Plassey, 1972). The efficiency of the CO_2 injection is dependent on the reservoir conditions, if the CO_2 is miscible with the oil or not, and by injecting CO_2 an immiscible or miscible displacement process occur dependent on the reservoir conditions, which affect the recovery of the residual oil. The performance of miscible CO_2 flooding is affected by the oil displacement efficiency at pore level and the sweep efficiency at field scale (Healy et al., 1994). Reservoirs in the world consist of oil with different compositions, light, intermediate and heavy hydrocarbons and the recovery of the hydrocarbons are dependent on the reservoir pressure and temperature. The benefit of CO_2 injection in the United States is the natural resources and accessibility of CO_2 from large gas reservoirs. But also on the Norwegian Continental Shelf there is potential for gas injection from fields nearby. The North Sea is one of the most important oil and gas producing provinces in the world, with Norway and UK as major producers.

The chalk field, on the Norwegian Continental Shelf (NCS), Ekofisk, was the first discovered field (1969) on the NCS and is one of the largest there. Production started in 1971 by pressure depletion followed by water injection for pressure maintenance and it has shown tremendous success, prognoses up to 50% oil recovery (Sheng, 2013). When the production from reservoir declines there will be of interest to recover the oil trapped in large volumes of the reservoir. Thus other recovery methods to enhance the oil recovery need to be evaluated and detailed screening of different EOR methods is performed, among these were WAG using CO_2. EOR surveys in the North Sea have been reported to evaluate the potential of EOR methods to increase the oil production (Teigland and Kleppe, 2006). Major challenges regarding oil recovery on the NCS is the offshore location, which leads to technical, logistical and economic difficulties regarding the storage and transport of large amount of gas used for production.

In 2006 there was reported about five different EOR technologies initiated in the North Sea (Teigland and Kleppe, 2006), where one of them was hydrocarbon miscible gas injection. But CO_2 injection as EOR technique has been examined and showed higher potential than hydrocarbon gas because of the properties of the CO_2 (Sjævland and Kleppe, 1992).

In reservoir where the structure is complicated (heterogeneous) and the rock material is fractured, such as the carbonate reservoirs in the world, area of high permeability pathways might result in flow of majority of the injected gas in these areas and bypassing oil stored in matrix blocks. To avoid bypassing oil by gas segregation, viscous fingering, gas override and gravity tongue one can improve the effectiveness of gas flooding by injection of surfactant simultaneously or alternating with the gas to gain mobility control (Farajzadeh et al., 2010).

1.2 Fluid interaction in porous medium

Originally, the reservoirs have only water present and as the hydro carbons migrate upwards due to specific gravity it penetrates into the water saturated rock. The amount of water present at a given height depends on the amount of oil that has displaced the water. The distribution of fluid saturations within a rock is explained by cohesive and adhesive forces between the different fluids and the fluids and the rock minerals, respectively. These phenomena are important to understand when evaluating the reservoir and the production to better understand the mechanisms of fluid flow within the porous medium (Zolotukhin and Ursin, 2000).

The cohesive forces explain the attraction between molecules in fluids. For miscible fluids the attraction between molecules within the fluids is greater than the attraction of the molecules within one of the fluids. Immiscible fluids have greater molecular attraction inside its own fluid than the attraction to the molecules within the other fluid present. The adhesive force of the molecules within a fluid explains the attraction to the molecules of the rock minerals and indicates the wetting fluid. The wettability of the rock is the tendency of a fluid to spread on a surface when another immiscible fluid is present (Zolotukhin and Ursin, 2000). For water imbibition in fractured media, capillarity can drive cross-flow between the high-and low permeability layers and between fractures and the matrix and this can result in delayed water breakthrough, hence enhanced oil recovery. This is a result of the high oil recovery at the Ekofisk Field, on the Norwegian continental Shelf, where total recovery of the reserves was initially estimated to 17 - 18% but are extended to approximately 50% (Criscione, 2012). In the case of a gas-oil drainage processes, the gas-oil capillary pressure gradients is generally damaging the gravitational segregation of gas at the top of the domain and flow of oil towards production wells at the bottom (Moortgat and Firoozabadi, 2012). Capillary pressure is defined as the molecular pressure difference across the interface of immiscible fluids present in narrow channels, such as rock pore channels.

If water and oil are present in a vertically water-wet capillary, water displaces the oil to some height, determined by the equilibrium between the pressure difference and the fluid gravity. The equation of capillary pressure, P_c, depends on the pore radius and for two immiscible fluids in a pipe the equation is given as

$$P_c = p_{nw} - p_w = \sigma_{nw-w}\left(\frac{1}{R_1} + \frac{1}{R_2}\right) = \frac{2\sigma_{nw-w}\cos\theta_c}{r_c} \qquad [1.1]$$

where p_c, p_{nw} and p_w are the capillary pressure, pressure of the non-wetting fluid and pressure of the wetting fluid, respectively. $\sigma_{n\text{-}nw}$ is the interfacial tension, IFT, between non-wetting and wetting fluid,

R_1 and R_2 is the radius of the curvature of the meniscus between the two miscible fluids, θ_c is the wetting angle and r_c is the capillary pipe's radius.

During an immiscible or miscible displacement by gas in a porous medium there are four drive mechanisms that play a vital role; gravity, viscous and capillary forces and diffusion. One important relationship between two of these forces, is the ratio between viscous and capillary forces, termed capillary number, N_c. This number characterizes the fluid flow and is related to the residual wetting and non-wetting phase saturations. It is a dimensionless number and it contains dynamic parameters, given by equation 1.2

$$N_c = \frac{\upsilon \mu}{\sigma \cos\theta} \qquad [1.2]$$

Where N_c is the capillary number, υ is the velocity [ml/s], μ is the viscosity [cP], σ is the IFT of the two fluids and θ is the wetting angle. Figure 1.1 shows a capillary desaturation curve, where a normal range of capillary number after a water flooding is 10^{-7} to 10^{-5} (Zolotukhin and Ursin, 2000). For enhanced oil recovery it is preferable to increase the capillary number by increasing the velocity and/or lowering the interfacial tension, by adding surfactants.

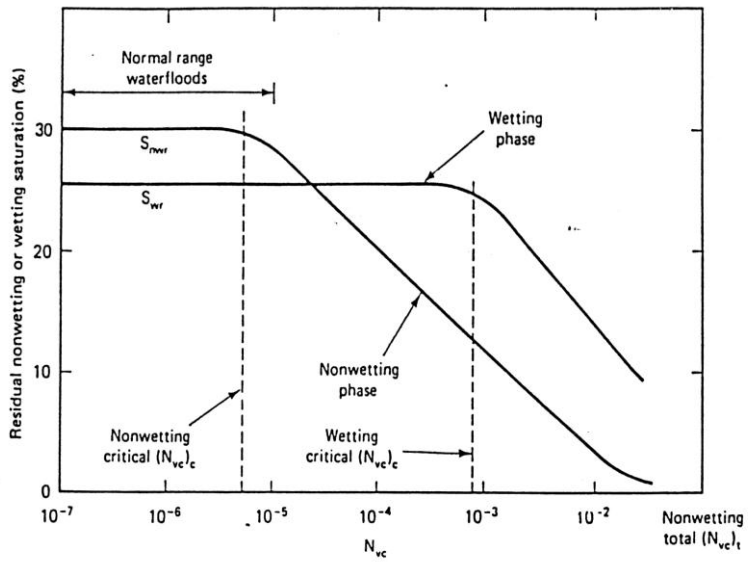

Figure 1.1 – Capillary desaturation curve: Plot of capillary number vs. percent residual (non-flowing) saturation of the non-wetting and wetting phases. (Lake, 1989).

Another vital characterization of fluid flow in porous media is the mobility of the fluid, which is explained by the ratio between permeability and viscosity (Aronofsky and Ramey, 1956). Mobility ratio is defined by the ratio of the mobility of the displacing fluid to the mobility of the displaced fluid and for a water-oil displacement the ratio is given by equation 1.3 (Seright, 2010)

$$M = \frac{\lambda_w}{\lambda_o} = \frac{\frac{k_{rw}}{\mu_w}}{\frac{k_{ro}}{\mu_o}} \qquad [1.3]$$

Where M is the mobility ratio, λ_i is the mobility, k_r is the relative permeability and μ_i is the viscosity. The nomenclature *w* and *o* are indicating water and oil phase, respectively.

According to equation 1.3, efficient floods with stable displacement front is indicated by low mobility ratio, $M < 1$, because then the mobility of the displacing fluid is lower than the displaced fluid and there is low possibility of viscous fingering. Because gas has lower viscosity than oil, gas injection in heterogeneous reservoirs with high permeability streaks leads to poor gas sweep efficiency, denoted by high mobility ratio, $M \geq 1$ (Zolotukhin and Ursin, 2000).

2 CO_2 for Enhanced Oil Recovery

Oil recovery is divided into primary, secondary and tertiary recovery method based on the dominating displacement mechanisms in the reservoir. Primary recovery methods are pressure depletion, secondary is mainly water flooding to maintenance the pressure and tertiary recovery methods, also known as Enhanced Oil Recovery (EOR) methods, are chemical, miscible and thermal flooding. These techniques also improve the oil displacement and may in addition maintenance the pressure and thus increase the lifetime of the field (Lake et al., 1992).

2.1 CO_2

The carbon dioxide gas consists of one carbon atom and two oxygen atoms which lay in a straight line. The oxygen atoms are slightly negative charged and the carbon atom is slightly positive charged. Even though the CO_2 molecule is not dipole it has polar molecules that react with other polar solvents such as water, H_2O, and make the water acidic. The CO_2 may also contain impurities and injection of CO_2 may result in corrosion of equipment used in experiments at the laboratory and pipelines in the industry (Beck et al., 2011). Despite the corrosion, this gas is used for enhanced oil recovery and one of the reasons for that is the advantages of carbon dioxide to be extracted from the effluent gas production and reinjected, which makes it cheaper to use (Wellington and Vinegar, 1985).

At standard temperature and pressure conditions (STP) T = 15 °C and P = 1 atm (1.013 bar), respectively (Lake, 2007), carbon dioxide is a gas, but with increasing pressure and temperature it will change phase into liquid or supercritical condition. CO_2 reaches a supercritical state at pressure of P = 73.8 bar and temperature of T = 30.95 °C ((NIST), 2011). In the supercritical state the carbon dioxide has properties both like a liquid and a gas, and a phase diagram is shown in Figure 2.1.

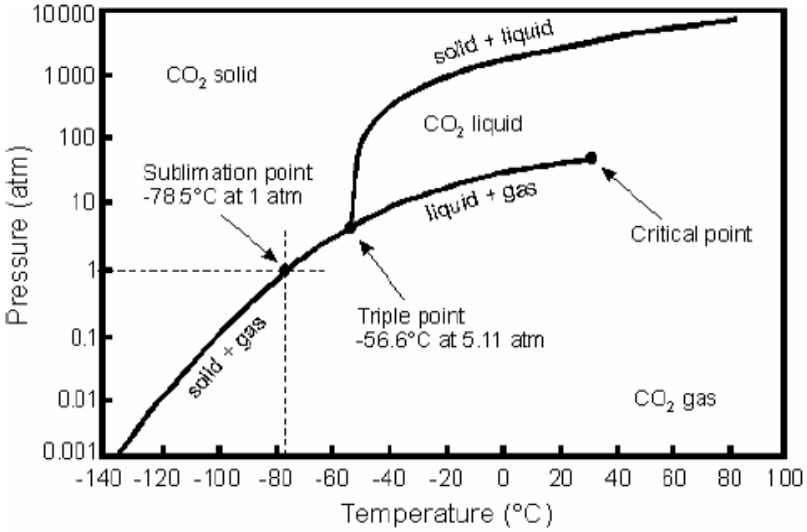

Figure 2.1: Pressure-temperature phase diagram of CO_2 (Picha, 2007).

CO_2 has both disadvantages and advantages when it is used for oil recovery as mentioned. This is due to the properties of the material in the range of pressure and temperature of oil reservoirs. At typical reservoir condition of 1000 psia (68.948 bar) to 3000 psia (206.843 bar) and 60 °C the CO_2 has a viscosity hundred times less than the viscosity of the oil to be displaced (Wellington and Vinegar, 1985). The high mobility of carbon dioxide may result in viscous fingering/channeling of CO_2 through high permeability zones, such as fractures, rather than efficiently displace oil and since the mobility ratio controls the volumetric sweep efficiency this is one of the biggest concerns for gas flooding in EOR project (Kulkarni and Rao, 2004). Viscosity as function of pressure at different temperatures is shown in Figure 2.2. This diagram shows the large variation in viscosity at low constant temperatures and increasing pressure, and less variation in the case of higher constant temperatures. This is because the CO_2 changes state from gas to liquid with temperatures below critical temperature and whereas this change decrease as CO_2 changes state from gas to supercritical. In supercritical state the viscosity increase less when pressure increases compared to that of liquid state.

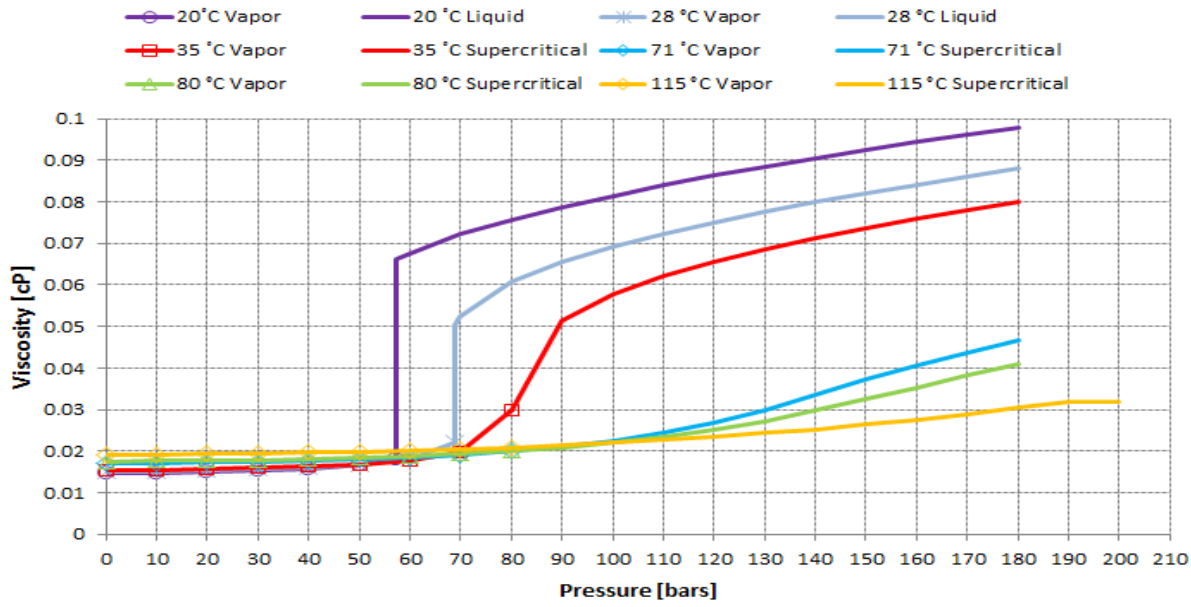

Figure 2.2 – Viscosity of CO_2 as function of pressure. The different colors indicate different temperatures. Where the marks end is the respectively temperature and pressure when phase changes. The graph changes from point to line when the CO_2 goes from one state to another. Viscosity values according to NIST.

Density as function of pressure at different temperatures is shown in Figure 2.3 which shows the same trend as the viscosity diagram in Figure 2.2. Below the critical temperature there is a significant difference in density at vapor and liquid phase, but decreases as the temperature increases, which yields for viscosity as well. When CO_2 changes from vapor or liquid to supercritical this difference decrease due to properties more similar like a liquid and gas. Compared to other gases used in oil recovery e.g. N_2 and HC, the density of CO_2 is higher, hence more favorable than e.g. CH_4 and N_2, due to lower density difference between displacing fluid and displaced fluid, resulting in less gravity segragation (Kulkarni and Rao, 2004).

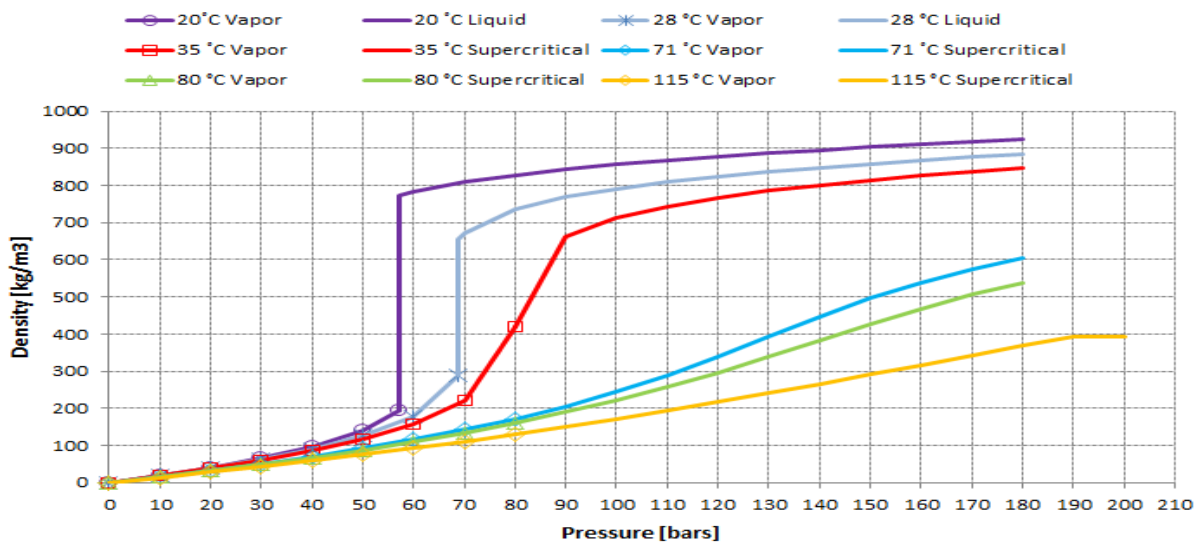

Figure 2.3 – Density of CO_2 as function of pressure. The different colors indicate different temperatures. The graph changes from point to line when the CO_2 goes from one state to another (Haugen, 2012).

The viscosity- and density differences between CO_2 and both brine and oil in the reservoir may lead to early gas breakthrough, gas override and viscous fingering, leaving behind oil-rich zones e.g. deeper down in the reservoir (Stalkup, 1983). In heterogeneous and fractured reservoir lack of mobility control during a gas-displacement may lead to poor volumetric sweep due to significant permeability differences, and this volumetric sweep efficiency may be improved by mobility control (Kovscek and Radke, 1994).

CO_2 applied for gas injection has shown interesting results in the field, and among efficient CO_2 injection is the Wellman Unit in Terry County, Texas, which is considered to be one of the best performing CO_2 injection on the record (Nagai and Redmond, 1982, Bangia et al., 1993, Schechter et al., 1998). To achieve an efficient CO_2 injection it is desirable to have a miscible or near-miscible displacement. CO_2 with density in the range of 500 to 900 kg/m^3 is total miscible with oil presented as ethane, C_2H_6 to hydrocarbons with 14 or more carbon atoms (Ely and Hanley, 1987). Several reservoirs consist of heavier hydrocarbons than C_{14}, and test has shown that CO_2 is miscible with hydrocarbons up to 30, thus CO_2 is a prominent feature for gas injection.

2.2 Mechanisms by miscible CO_2 displacement

2.2.1 Miscible process

Petroleum industry defines miscibility within a reservoir as that physical condition between two or more fluids that permits them to mix in all proportions without any existence of interface between them (Holm, 1986). Miscible CO_2 injection is more favorable than traditional recovery methods, because it may result in producing mobile oil from matrix which is bypassed from previous water injection. Studies of immiscible and miscible CO_2 flooding have shown that the latter one has a higher recovery where the results from the work done by Kulkarni and Rao in 2004 and 2005 showed 23% against 93.7% recovery for immiscible CO_2 and miscible CO_2 flooding, respectively (Kulkarni and Rao, 2004, Kulkarni and Rao, 2005).

Triangular phase diagram also known as ternary phase diagram is used to describe a miscible displacement process. These diagrams cannot explain the thermodynamic of the multicomponent reservoir fluids, but shows schematic mixing of gas and liquid at a certain constant pressure and temperature (Hutchinson and Braun, 1961). Figure 2.4 shows an example of a ternary phase diagram of a first-contact miscible, a vaporizing gas drive and a condensing gas drive process, the two latter are called multi-contact miscibility processes (Holm, 1986). The three different corners of the triangle in Figure 2.4 represent light, intermediate and heavy components of the reservoir fluid. The blue curved line to the left inside of the triangle is the boundary of the two-phase region, which inside this area the fluid is both in gas and liquid phase. This curved line is divided by the plait point (dark circle) into a dew point line (upper part) and a bubble point line (lower line). Outside the dew point line the fluid composition is saturated with gas molecules and outside the bubble point line the fluid composition is saturated with liquid molecules. The blue dashed line outside the two-phase region, termed critical tie-line, is the tangent to the two-phase region and goes through the plait point. Mixing between gas and oil is determined by the composition of the injection gas and reservoir oil. (Hutchinson and Braun, 1961). In the case when the dilution path does not intersect the two-phase region, the displacement process will consist of a single hydrocarbon phase which changes in composition. Injecting gas that is miscible with the reservoir fluid at constant reservoir pressure and temperature, leads to a miscible displacement. If the injection gas, at reservoir temperature and pressure, is consistently within one hydrocarbon phase the process is called first-contact miscible (Organick and Brown, 1952), shown in Figure 2.4 as the line between I_2-I_3.

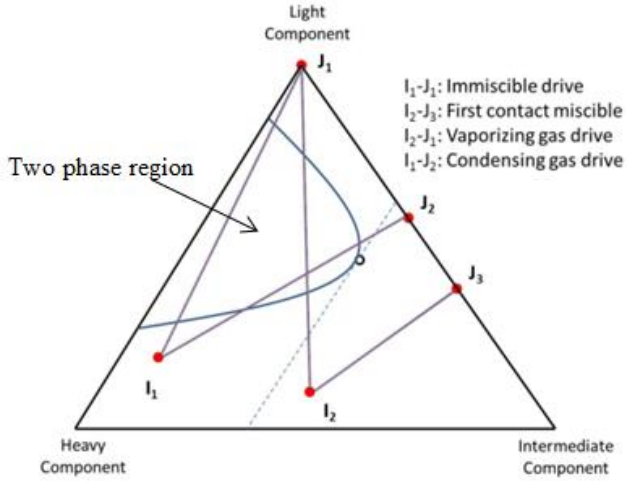

Figure 2.4: Ternary phase diagram. The three corners indicate different components. Red dots are composition of fluids and the lines between the red marks are different dilution paths dependent on whether the process is immiscible (I_1-J_1), first-contact miscible (I_2-J_3), vaporizing gas drive (I_2-J_1) or condensing gas drive (I_1-J_2). Modified from (Mathiassen, 2003).

Vaporizing gas drive is when injection of a lean gas, consisting of light components, and the hydrocarbons within the reservoir fluid start vaporizing into the gas phase (Hutchinson and Braun, 1961), and the lean gas becomes heavier. If the reservoir fluid consists of high concentration of lighter components, such as C_2-C_6 the recovery process becomes favorable. When CO_2 is injected into the reservoir it may result in a multi-contact miscible displacement of the crude oil, because the CO_2 can extract heavy components all up to C_{30} (Gernert and Brigham, 1964, Holm and Josendal, 1974) (Sjævland and Kleppe, 1992). The mixing zone between the injection gas and reservoir fluid termed transition zone (Kasraie and Ali, 1984), consist of a front completely miscible with the reservoir fluid and the back of it is completely miscible with the CO_2 (Hutchinson and Braun, 1961).

2.2.2 MMP

To achieve a miscible displacement of oil by CO_2, the average reservoir pressure needs to be greater than the Minimum Miscibility Pressure (MMP) of CO_2 and the reservoir oil. The MMP is minimum pressure required to achieve miscibility for two fluids and can be measured in a slimtube experiment (Yarborough and Smith, 1970, Yellig and Metcalfe, 1980), using beads or unconsolidated sands packed in narrow and long tubes. The slimtube is saturated with oil and gas is injected at high pressures. At one end there is a fixed pressure and the pressure gradients are neglected since the permeability of the medium is large. One looks at the results of percent recovery vs. pressure. Figure 2.5 shows the MMP at the lowest pressure in the case of maximum recovery. This graph is from a

slimtube experiment with a fixed oil composition and the MMP for CO_2 varies with different oil compositions at different temperatures (Yellig and Metcalfe, 1980).

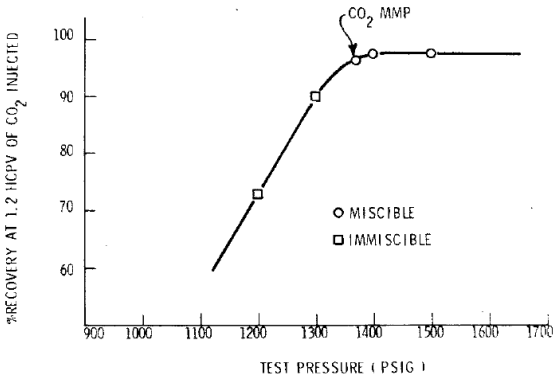

Figure 2.5: Test result from a slimtube experiment with fixed oil composition and fixed temperature: CO_2 displacement tests conducted at various pressure levels, where the CO_2 MMP was reported as the lowest test-pressure level for miscible displacement (Yellig and Metcalfe, 1980).

2.2.3 Oil swelling by CO_2

The mixing process of CO_2 and crude oil has been studied through experiments of single-contact phase-behavior of CO_2 and crude oil, where swelling/extraction of hydrocarbons from the crude oil by CO_2 has been examined. This was studied and compared to MMP results from slimtube experiments by Hand and Pinczewski, 1990 and showed that mixing CO_2 with oil at increasing pressure and constant temperature resulted in denser fluids and oil swelling as a result of that CO_2 dissolved in the oil (Hand and Pinczewski, 1990). The oil swelling depends on the amount of methane in the oil, because when CO_2 contacts the reservoir oil it will not displace all of the methane and, hence more methane in the oil results in less swelling (Sjævland and Kleppe, 1992).

2.2.4 Dispersion in porous media

In oil recovery there are several important phenomena when fluid flows through the porous media. During a CO_2 injection one of the phenomena explaining a miscible displacement process is dispersion. During a miscible displacement process dispersion mechanisms contribute to mixing of fluids within the porous media (Sahimi, 2011a), and there exists two different dispersion mechanisms; molecular diffusion and convective mixing (Bear, 1972, Lake, 1989), and it is either in the same direction as fluid flow, longitudinal dispersion and in opposite as fluid flow, transversal dispersion (Perkins and Johnston, 1963). The dispersion in a field-scale porous media is purely mechanical, dependent on the variations of the permeability of the medium, while the dispersion in stratified porous media is dependent on porosity, fluid velocity and the local transverse and longitudinal dispersion (Sahimi, 2011a). Figure 2.4 shows a simple model of a porous medium where the fluid disperses within the porous media.

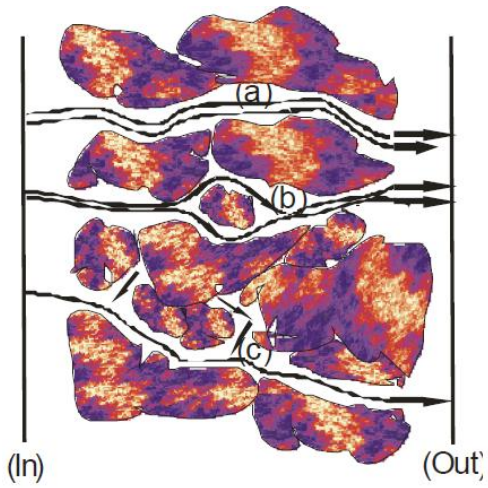

Figure 2.4 - Dispersion within a porous medium, where red and blue shapes are indicating grains: Tracer particles (dark arrows) injected at the inlet (In) and transported by advection and diffusion through the pore space and measured at the outlet (Out). Particles mix due to a) random hopping between streamlines within channels, b) mixing at pore intersections and c)diffusion-like mixing at low velocity regions (Bijeljic and Blunt, 2006).

At pore-scale, heterogeneities in the porous media causes fluctuations of fluid velocity, where grains lay in the path way and decelerate some of the fluid velocity. These heterogeneities is a reason for the convective mixing (da Silva and Belery, 1989, Rage, 1996). Among the variables that can affect the dispersion in addition to heterogeneities of the media are 1) viscosity difference, 2) density difference and 3) turbulence (Perkins and Johnston, 1963). The overall oil recovery from a fractured reservoir is a

result of the complex interplay of several mechanisms during a CO_2 injection (Darvish et al., 2006), and among these, extraction by molecular diffusion play a vital role.

2.2.5 Molecular diffusion

In fractured reservoir the hydrocarbons are stored in the matrix and the fractures act as flow channels (Darvish et al., 2006). During a miscible displacement process of two fluids, such as oil and CO_2, the interface between these two fluids will over a time be a diffuse mixing zone due to random distribution of the molecules within the fluids (Perkins and Johnston, 1963). Experiments and simulation has shown the importance of the diffusion mechanism for oil recovery from tight matrix (Darvish et al., 2006, Lie, 2013). Figure 2.5 shows a schematic of diffusion.

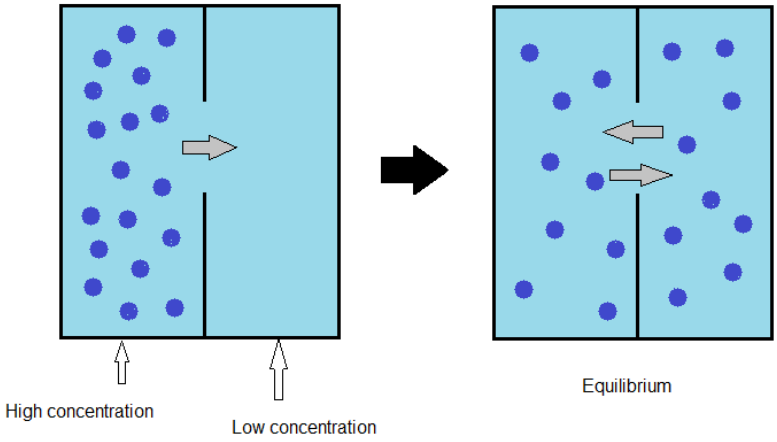

Figure 2.5 - Schematic figure of diffusion. High concentration of a fluid, shown as blue dots, mixed with another fluid, the light blue color, is diffusing over time and reaches equilibrium within the fluid.

If there is constant volume during the mixing of the fluids, the change in diffusional flux over time is described by Fick's second law of diffusion (Perkins and Johnston, 1963), given in Equation 2.1

$$\frac{\partial G}{\partial t} = -D_m A' \frac{\partial^2 C}{\partial x^2} \qquad [2.1]$$

where G is the quantity of material diffusing across a plane, t [sec] is time, D_m $\left[\frac{\text{cm}^2}{\text{sec}}\right]$ is the molecular diffusion coefficient, A' [cm^2] is the cross sectional area for diffusion, C [volume fraction] is the concentration and x [cm] is the position.

The diffusional coefficient describes the molecular diffusivity of the solute in the solvent and is typically given as a function of concentration. According to Fick's second law, with a constant concentration at the boundary, the rate of diffusion is proportional to the square root of time. The rate of diffusion decreases significantly as a solvent diffuses further into a solute, which makes

concentration related to square root of time (Cussler, 2009). The miscibility between the CO_2 and the oil is vital for the displacement process at micro level (Kulkarni and Rao, 2005), thus diffusion which occur at pore scale plays a major role in the laboratory experiment.

2.2.6 Water shielding

CO_2 may displace oil efficiently in a miscible displacement process, but studies of high water saturations present in the porous media showed reduced displacement efficiency. Water barrier shielding the oil from the CO_2 restricted the access of the contact between the CO_2 and the oil. Experiment where oil was trapped in a "dead-end" pore and water was blocking the pore throat was performed on micro models and the results showed later oil recovery, compared to no water barrier present. But as a result of CO_2 diffusion, after some considerable time, the oil swelled and displaced the water from the pore throat and the oil moved out from the dead-end pore (Campbell and Orr, 1985). This mechanism is severe in water wet media and under low gas/oil interfacial tension- and low gas/oil capillary pressure conditions (Gabitto, 1998). Figure 2.6 shows a schematic of this process.

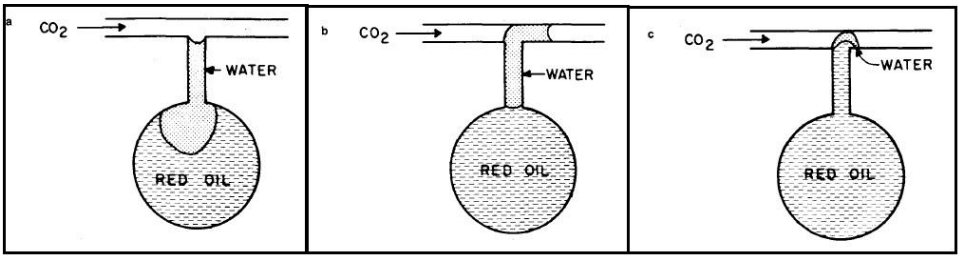

Figure 2.6: Schematic of trapped oil in "dead-end" pore blocked by water and recovered by diffusion of CO_2 leading to oil swelling. a) Start of CO_2 injection; b) position of water barrier after 18 hours c) position of water barrier after 26.5 hours, modified from (Campbell and Orr, 1985).

2.3 Foam

Gas injection as oil recovery method may lead instability problem such as gas fingering or gas override (Sahimi, 2011b), due to unfavorable mobility ratio. To prevent these events, one can inject the gas simultaneously with surfactant to create foam, which will decrease the mobility of the gas and hence delay the gas breakthrough (Blaker et al., 2002). Decreased mobility reduces the instability problem at field scale such as 1) gas fingering, 2) gas override and 3) gas channeling. Vital studies of mechanisms that are involved when injection CO_2 and surfactant, either simultaneously or alternating has been conducted (Hirasaki and Lawson, 1985, Rossen, 1988, Kovscek and Radke, 1994) and these are described below.

Foam consists of gas bubbles dispersed in liquid and a continuous liquid film called lamellae separates the gas bubbles. To achieve the dispersion of small bubbles within liquid, one needs to add energy to the system; a surfactant can be used as a foaming agent and as mentioned reduce the surface tension. Thus a protective film is formed at the bubble surfaces to prevent coalescence with other bubbles (Schramm and Wassmuth, 1994). Figure 2.9 shows a generalized foam system in 2D.

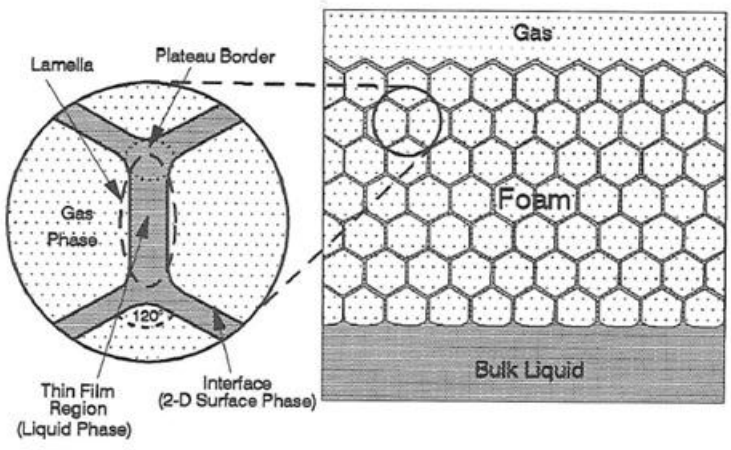

Figure 2.7: A generalized foam system. The gas phase is white-dotted and the liquid is shaded (Schramm and Wassmuth, 1994).

Adding surfactant chemical to brine at concentration on the order of 0.1 to 1 wt % will make effective foam (Kovscek and Bertin, 2002). The quality of foam is the ratio of gas volume to total volume at given pressure and temperature (Grundmann and Lord, 1983), but the quality may also be characterized as the ratio between gas and liquid flow rates (Farajzadeh et al., 2012), and can be expressed by the equation:

$$f_g \frac{q_g}{q_g + q_{liq}} \quad [2.2]$$

where f_g is the gas fraction, q_g is the gas flow rate and q_{liq} is the liquid flow rate.

The mobility of the foam is dependent on different factors such as bubble size, foam texture (small bubbles are less mobile than larger bubbles) and the tendency of gas bubbles to trap or remain stationary (Kovscek and Bertin, 2002). Studies of foam has shown that the bubble size of the foam depends on the rock material; permeability and porosity, surfactant type and concentration, and the velocity of liquid and gas (Kovscek and Bertin, 2002). The key variable in prediction of foam flow in porous media is the foam texture because this variable distinguishes between ordinary gas flow and foam flow. The foam texture is also the dominant parameter in the gas mobility (Hirasaki, 1989).

It is separated between two different classes of foam; "continuous-gas" foam and "discontinuous-gas" foam. The former does not have large reduction of gas mobility, but the latter one has large reduction due to resistance of displaced lamellae, which need to be included in the gas mobility (Hirasaki, 1989). Figure 2.8 shows schematic of these two scenarios.

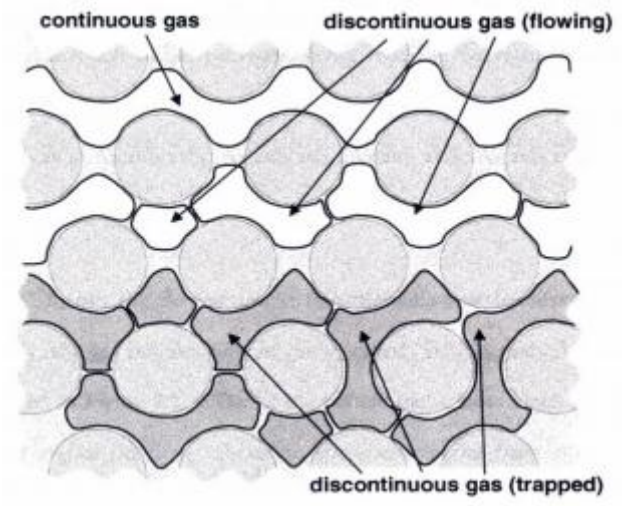

Figure 2.8: Schematic of "continuous-gas" foam and "discontinuous-gas" foam. Flowing gas is white and trapped gas is grey. Circles indicates grains (Farajzadeh et al., 2012).

Foam flow in smooth capillaries was examined by Hirasaki and Lawson, 1985, who found the number of lamellae per unit length to be the most important factor of foam flow, due to resistance of flow. From their experiments they concluded with three significant factors that resist the flow of foam; the viscosity of liquid between bubbles; the viscous resistance of liquid between the foam bubbles and the capillary wall and; the surface tension gradient in surfactant concentration (Hirasaki and Lawson, 1985, Falls et al., 1989).

Surfactant

Surfactant solution can be injected into the reservoir to reduce the interfacial tension (IFT) between oil and brine. When adding surfactants to brine-oil-system it is possible to recover the capillary trapped oil, which may constitute more than half of the residual oil in the reservoir (Zolotukhin and Ursin, 2000). There are different types of surfactants dependent on the polarity of the molecules. The anionic surfactant (negative charged) is the most used one for oil recovery, due to their solubility in aqueous phase. They reduce IFT efficiently, are relatively resistant to retention, stable and cheap (Zolotukhin and Ursin, 2000). When surfactants are added to brine-oil system the polar end reacts with the water and the non-polar end reacts with oil.

Adsorption and Retention

Surfactant can also react at the surface of the rock and the rock can adsorb the surfactant. This is important to take into account when surfactant is injected into the reservoir. If the rock surface adsorbs surfactants it hence reduces surfactant concentration in the liquid flowing from injector to producer. The adsorption is dependent on rock wettability and in some cases it can even change the wettability of the rock (Gogoi, 2011). The adsorption is dependent on the anionic and cationic molecules and a positively charged carbonate surface (Ca^{2+}) can adsorb an anionic surfactant (Esmaeilzadeh et al., 2011). Temperature is a factor that can influence the surfactant as well by degradation (Heller, 1984), and the surfactant need to be carefully chosen to match the reservoir conditions and avoid adsorption and retention. Surfactant is expensive thus it is important to calculate the right amount of surfactants for a successful foam injection.

2.3.1 Foam mobility in porous media: apparent viscosity

Foam flowing through a porous medium passes through capillaries in the sense of pores and pore throats and the mobility of foam in porous media is related to the apparent viscosity. Apparent viscosity is defined as the relationship between flow rate and pressure drop for the flow of foam through a capillary (Hirasaki and Lawson, 1985). Results from the experiments where apparent viscosity measured by foam flowing in tubes performed by Patton et. al. (1983), also confirmed theoretically by Hirasaki and Lawson (1985) showed that the apparent viscosity was dependent on the diameter of the tubes, on the rate of flow and the length of the tube (Patton et al., 1983)

2.3.2 Foam generation in porous media: Lamellae

Foam formation, or generation, at pore-level is explained by the three main mechanisms: "snap-off", "leave-behind" and lamellae division.

"Snap-off" mechanism

Snap-off is a mechanical process, which occurs during multiphase flow in porous media and this process also explains the origin of residual oil. When gas moves through pore throats and enters liquid filled pores capillary pressure is increasing and results in snap-off of the continuous gas film (Kovscek and Radke, 1994). Figure 2.12 shows a schematic snap-off event.

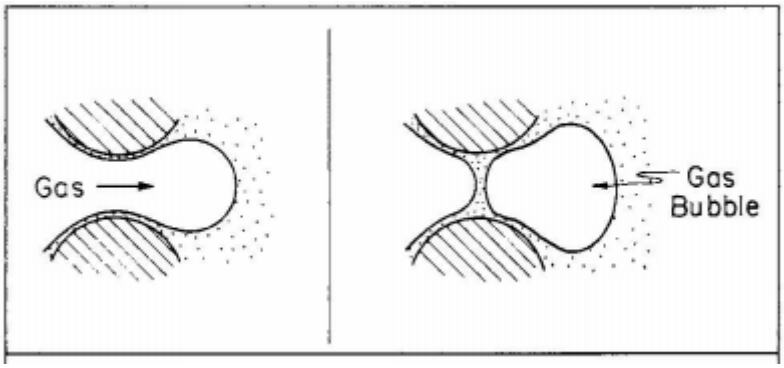

Figure 2.9: Schematic of snap-off mechanism. Modified from (Ransohoff and Radke, 1988).

"Leave-behind" mechanism

The "leave-behind" mechanism is when two gas fronts from different directions enter the same liquid filled pore and squeeze liquid between the two fronts and create lamella. Dependent on the surfactant the lamella is either stable or it ruptures (Ransohoff and Radke, 1988). Figure 2.10 shows schematic of "leave-behind" mechanism.

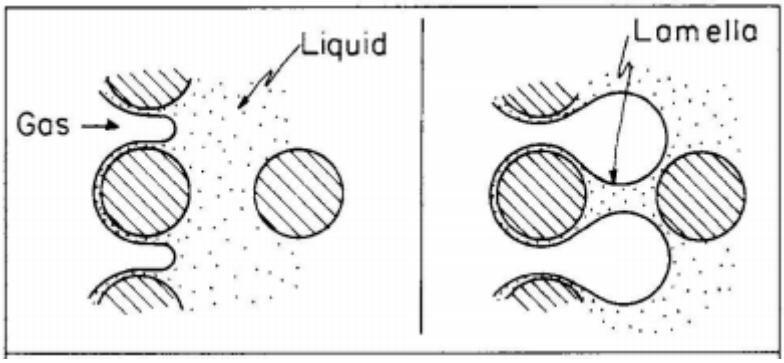

Figure 2.10: Schematic of foam formation by the mechanism "leave-behind" (Ransohoff and Radke, 1988).

Lamellae division

Lamella division is the third mechanism that creates foam. When lamella is moving into a pore body consisting of two or several pore throats, the lamella may spread into different direction and create new lamella in the pore throats where there is no existing stationary lamella. This mechanism only occurs if there is already existing foam and the foam is flowing, thus it is also called secondary foam generation (Ransohoff and Radke, 1988). Figure 2.11 shows schematic of lamellae division.

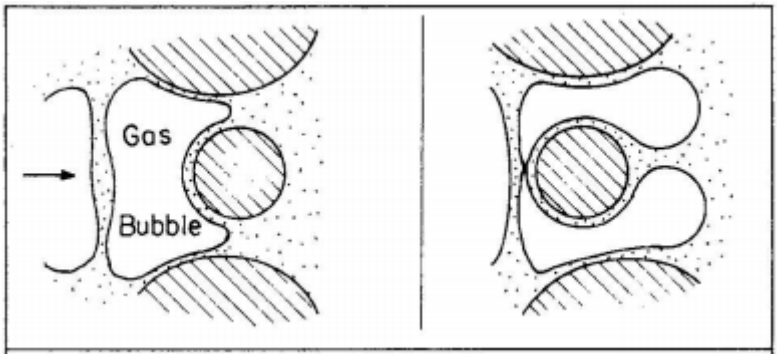

Figure 2.11: Schematic of lamellae division mechanism. Modified from (Ransohoff and Radke, 1988)

Porous medium characteristics, such as pore size and shape, permeability and capillary pressure in combination with gas and liquid phase velocities ultimately determine bubble size and therefore gas mobility in porous media (Hirasaki and Lawson, 1985)

2.3.3 Foam Propagation and Stability

Produced lamella may only translating a short distance before it ruptures (Kovscek and Radke, 1994), and thus it needs to be stabilized. The stability of the foam in the porous media is a function of both foam film properties and petro-physical properties of the rock. And the strength of the foam is related to the magnitude of the pressure gradient over the medium (Farajzadeh et al., 2012). One can characterize the strength of generated foam by the mobility reduction factor (MRF) and it is often defined by the equation

$$MRF = \frac{\Delta P(foam)}{\Delta P(no-foam)} \qquad [2.3]$$

where MRF is the mobility reduction factor, $\Delta P(foam)$ and $\Delta P(no\text{-}foam)$ are the measured pressure across the porous medium with and without foam, respectively.

The foaming agent, hence the surfactant, added to the brine reduces the surface tension and makes a protective film that prevent bubbles to coalescence with each other. Stable foam is characterized by two processes; either the films between two or more bubbles get thinner or two or more bubbles fuse

together and form a single, larger bubble. These processes are termed film thinning and coalescence, respectively (Schramm and Wassmuth, 1994). Other factors influencing the foam stability is described below.

Disjoining pressure

When the thickness of liquid lamellae separating gas phases is reduced the surface of the foam film can interact with each other. When the forces acting between these two surfaces are in equilibrium, hence they balance, the disjoining pressure of a flat film equals the capillary pressure (defined by the Young-Laplace equation), which is given by equation (Farajzadeh et al., 2012):

$$\Pi = \Pi_{EL} - \Pi_{VW} = P_c = \frac{2\sigma}{r} \qquad [2.4]$$

Where the $\prod$ is the disjoining pressure, $\prod_{EL}$, is pressure dependent on the positive electrostatic forces $\prod_{VW}$ is the pressure dependent on negative van der Waals forces, P_c is the capillary pressure, σ is the interfacial tension between gas and liquid and *r* is the pore radius.

The disjoining pressure depends on the film thickness, electrolyte concentration and material densities of the neighboring phases. Strong repulsive forces between the film interfaces results in a high positive disjoining pressures and a stable film, whereas negative attractive forces result in negative disjoining pressure and unstable film where foam may collapse (Exerowa and Kruglyakov, 1998). Above a critical capillary pressure, the high capillary suction pressure becomes higher than maximum disjoining pressure, the lifetime of the lamellae and corresponding foam is short and macroscopic disturbances may rupture the foam. The disjoining pressure varies with surfactant type, surfactant concentration and salinity (Farajzadeh et al., 2012). As one can see from equation 2.3, smaller pore radius results in higher disjoining pressure, and the surface of the two liquid collapse.

Limiting Capillary Pressure

The dominant process that breaks down the foam is capillary suction coalescence (Kovscek and Radke, 1994). Khatib et. al. (1988) studied the understanding of coalescence and introduced a "limiting capillary pressure", P_c^*, for foam in porous media. Important variables affecting P_c^*, in addition to surfactant type and concentration, are gas velocity and the medium's permeability (Jiménez and Radke, 1989). The P_c^* corresponds to the water saturation, S_c^*, below which foam is unstable. The coalescence of all lamellae in a porous media do not occurs at once, but instead the foam coarsening, which means it translate from strong to weak foam (Khatib et al., 1988). Figure 2.12 shows an illustration of capillary curve where the limiting capillary pressure and respectively water saturation is shown.

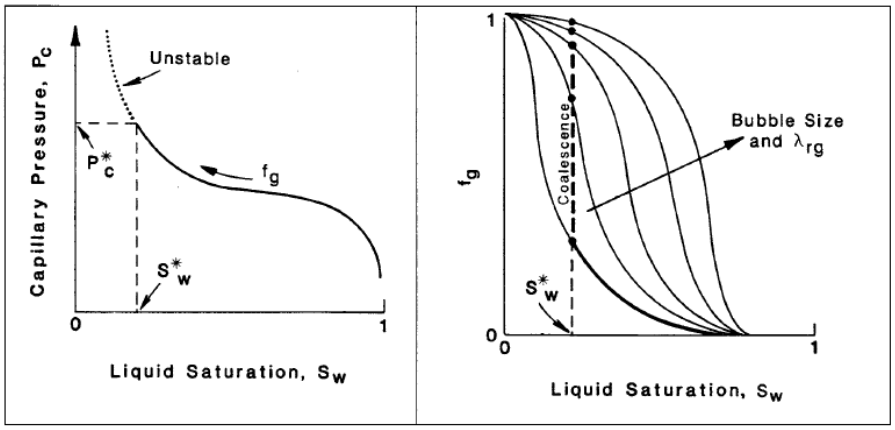

Figure 2.12 – Left: Capillary pressure curve vs. liquid saturation. The limiting capillary pressure is denoted P_c^* and the respectively water saturation is S_w^*. Capillary pressures above this critical value give unstable foam. Right: Gas fraction vs. liquid saturation. This figure shows that coalescence is affected by both bubble size and relative mobility of gas (Farajzadeh et al., 2012).

Two foam injection schemes were tested at the laboratory at Department of Physics and Technology. That was *in-situ* foam generation and pre-generated foam injection. The results from these experiments showed that pre-generated foam injection was the most stable one and gave an increase in oil recovery: (Haugen et al., 2010, Haugen et al., 2012).

Foam oil interactions

Oil can both stabilize and destabilize the foam and hence the influence of oil on foam stability is of important knowledge and one of the most important factors in EOR application of foam. What kind of foam to use in the petroleum industry for the best EOR project is depending on the foam-crude oil interaction in the porous media (Wasan et al., 1993). This means that the generation of foam may be reduced as the wettability of the rock changes from water wet towards oil wet. This was examined by Sanchez and Hazlet (1992) and from the experiments they concluded that new lamellae prefer water-wet conditions (Sanchez and Hazlett, 1992). In the present of an oil-wet medium the surfactant in the foam can alter the wettability towards less oil-wet and neutral wet medium (Farajzadeh et al., 2012). Laboratory experiments of core flooding are important to do because the oil influence the foam of some degree dependent on type of foam and oil presented. Influences of oil on foam stability were investigated by Vikingstad et. al. (2005), which concluded that the chain length of the hydrocarbon and salinity, in presence of oil, were the main factors that seemed to affect the stability of the foam. In addition the hydrocarbon molecular weight influenced the foam stability, where presence of longer alkanes than decane resulted in more stabilized foam (Vikingstad et al., 2005).

2.4 Foam injection for improving CO_2 flooding

Studies of foam and SAG injections at field scale have resulted in enhanced oil recovery and one important field scale project of foam injection is the East Vacuum Grayburg San Andres Unit, EVGSAU in New Mexico, USA.

Foam injection in EVGSAU, USA

Initially the full scale miscible CO_2 injection started in 1985 after almost 27 years of water flooding. The injection scheme used was WAG with a ratio of 2:1. As a result of this injection, 11.5% incremental oil was produced, but then it declined due to problem: 1) reservoir pressure below MMP, 2) observation of severe breakthroughs and 3) one area of the reservoir showed drastic permeability contrast between upper and lower zones. Detailed geological studies of the candidate pattern for CO_2 foam field trial could identify potential high permeability channels. (Harpole et al., 1994). Figure 2.13 illustrates a gas injection to the left injecting towards the right and a foam injection to the left injecting towards left (Sheng, 2013)

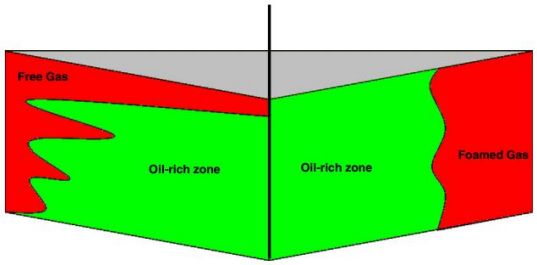

Figure 2.13 – Schematic of gas flooding (left) vs. foam flooding (right). Injections are from left and right towards the center. Foaming of the gas increase the viscosity and reduce the gas mobility (Farajzadeh et al., 2012).

Next a CO_2-foam field project began in 1989 (Stevens et al., 1992). The aim of this four-year project, which included reservoir studies, laboratory tests, simulation runs and field tests, was to evaluate the effectiveness of foam injection in the heterogeneous carbonate reservoir located in New Mexico, USA (Martin et al., 1992). The porosity ranged between 0.7 and 32.8% and the reservoir quality in different zones of the reservoir varied, and one zone even represented a non-reservoir rock. During evaluation of CO_2-foam injection in this field several core materials from different areas was examined where conventional core analysis measurements of porosity and permeability was available (Harpole et al., 1994). Before the CO_2-foam injection pilot started a history match of the previous CO_2 and WAG process was performed which showed encouraging results for most of the wells. During the field test of foam injection the reduction of CO_2 mobility was evaluated using a data collection program, which in addition evaluated the improvement in pattern sweep efficiency and production performance (Martin et al., 1992). Desirable foam was designed to flow in the high permeable layers and different

injection schemes were tested and continuously monitored. A rapid surfactant-alternating-gas (SAG) cycle with foam quality of 80% was chosen. This was tested to avoid operational problems and to achieve the benefit of simultaneously injection. The SAG cycle showed lower injectivity, *in situ* foam was generated and mobility of foam was one third of that during the WAG process(Martin et al., 1995) and incremental oil was produced and observed in three of eight producers. These positive responses, resulted in a second foam injection trial, with same conditions, but this time it stopped after two cycles of foam due to operation problems (Sheng, 2013). The two foam injection tests showed a positive economic result, and the total incremental oil produced was approximately 3045 l (19160 bbl).

Laboratory work is important to better understand the mechanisms at macro- and micro level during fluid displacement in a porous medium, such as a reservoir. And in the latter field case accurate measurements of the surfactant slug at the laboratory was important two achieve the favorable results. In the meantime there are some effects on the laboratory that might not happen at the field scale and vice versa, one of them are unfavorable capillary end-effect in drainage of oil by gas injection: due to a gradient in capillary pressure at the outlet the oil saturation may not decrease to the residual oil saturation when the injection rate is low (Hadley and Handy, 1956)

PART II – Experiments and results

3 Experimental setups and procedures

The following chapter describes the procedures of measuring important parameters such as porosity, permeability and how the core samples are prepared for each experiment. In addition there is also a description of the various setups used.

3.1 Rock material and Fluids

Analysis of rocks and fluids are important for reservoir characteristics and is time demanding and expensive to drill out cores from reservoirs. Pressure and temperature change when transporting the cores from the reservoir depth to the surface and thus the rock and fluid change. The experiments in this study are performed on both cores from real field and from outcrop rocks; the latter is used as an analogue to the reservoir rocks.

The chalk and limestone rocks are outcrop rocks. The chalk is from Portland cement factory in Ålborg, Denmark. This chalk is mainly consisting of cocolitt deposits with about 99% calcite and 1% quartz. Effective porosity and brine permeability of this chalk are in the range of 45-48% and 1-4 mD, respectively (Graue et al., 1999) and this outcrop chalk core are used as an analogue to the Ekofisk chalk field on the NCS. The limestone outcrop cores are from Edwards in Texas, USA, and it has a wide range of permeability values due to its heterogeneous rock material. The primary rock type is limestone, and minor rock types are dolostone and chert (Interior, 2014).

Carbonates are calcareous sedimentary rock and usually heterogeneous due to wide distribution of properties within the rock (Ahr, 2008). Oil Shale is an organic sedimentary rock, originally a source rock. The rock structure consists of complex systems which are comprised of hydraulically induced fractures, natural fractures and a complex matrix consisting of different minerals and kerogen (Hinkley et al., 2013).

Core samples are cut using water cooled circular saw, washed and dried in an oven at 80 °C for at least 24 hours. Length and diameter of the cores where measured using a slide caliper, and weighed before and after the water saturation. Chapter 4 presents the measured rock properties and it is listed in Table 4.1 and 4.2 and 4.3, respectively.

During the experiments several fluids were used and their characteristics, density and viscosity are listed in Table 3.1. The properties of CO_2 are listed separately in Table 3.2, due to different conditions of pressures and temperatures of each experiment. Brines were prepared by mixing the different components listed in table 3.1 and the salts were used as received.

Table 3.1 – Fluid characteristics

Fluid ID	Characteristics	Density, ρ 1 bar, 20°C [g/cm^3]	Viscosity, μ 1 bar, 20°C [cP]	Comments
Chalk Brine	Distilled water 50 g/m^3 NaCl 50 g/m^3 $CaCl_2 \cdot H_2O$ 0.05 cm^3 NaN_3	1.05	1.09	To avoid bacterial growth 0.05 ml/l NaN_3 is added. $CaCl_2$ was added to avoid dissolution of the carbonate rock (Graue et al., 1999)
Brine C	5.2362 g/m^3 Na_2SO_4 4.576 g/m^3 KCl 5.8247 g/m^3 $CaCl_2 \cdot 2H_2O$ 2.7599 g/m^3 $MgCl_2 \cdot 6H_2O$ 22.7968 g/m^3 NaCl	N/A	N/A	Closest approximation of amount of salt components from field water analysis to match the formation brine
n-Decane	$C_{10}H_{22}$	0.73	0.92	Isotopic purity > 95%
Paraffin oil	n-paraffines: C_9-C_{13}	0.74	1.43	Purity > 98%
Surfactant: Petrostep C-1 AOS $C_{14/16}$	Chalk brine 1wt% AOS $C_{14/16}$	N/A	N/A	To avoid bacterial growth NaN_3 is added to the brine.
Surfactant: Surfonic L24-22	Brine C 1 wt% Surfonic L24-22	N/A	N/A	To avoid bacterial growth 0.05 ml/l NaN_3 is added to the brine
Ekofisk-crude oil[1)]	53 wt% saturated HC 35 wt% aromatic HC 12 wt% resins 0.90 wt% asphaltenes	0.85	14.5[@ 20°C] 2.5 [@ 90°C]	Acid number: 0.094 Base number: 1.79

[1)] Composition of Ekofisk crude oil is from (Graue et al., 1999).

The purity of the salts used in the chalk brine is: NaCl 99.5%, $CaCl_2$ 99.5% and the sodium azide, NaN_3, has a purity of 99.5% (Graue et al., 1999).

Table 3.2 - Properties of different phases of CO_2

Fluid ID	Contents	Density [g/cm^3]	Viscosity [cP]	Conditions	Phase
CO_2	> 99.999% CO_2	0.856	0.081	T = 20 °C P = 100 bar	Liquid
		0.869	0.084	T = 28 °C P = 160 bar	Liquid
		0.662	0.051	T = 35 °C P = 90 bar	Supercritical
		0.599	0.046	T = 71 °C P = 178 bar	Supercritical
		0.468	0.035	T = 80 °C P = 160 bar	Supercritical
		0.291	0.026	T = 115 °C P = 150 bar	Supercritical
		0.418	0.033	T = 115 °C P = 200 bar	Supercritical

3.2 Porosity measurement

The cores were weighed both air filled and saturated with brine. The brine and core was vacuumed separately to remove air with a pressure less than 700 mTorr. After vacuuming the core was 100 % saturated with chalk brine for at least two hours. The salt contents and properties of chalk brine are listed in Table 3.1. A schematic drawing of the setup used for saturation is shown in Figure 3.1.

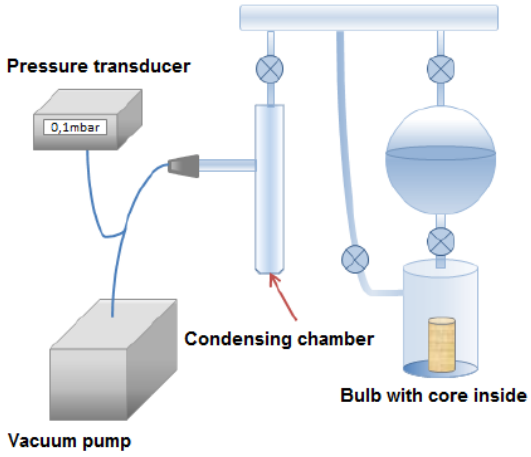

Figure 3.1 - Schematic drawing of the setup used for saturation of the cores.

The measured porosity, φ is the effective porosity and it is given by the fraction of pore volumes and the bulk volume. The rock samples may consist of a larger volume of voids, but if these are not connected to each other they are not filled with brine and hence not included in the porosity calculation. The percentage porosity is given by the equation:

$$\varphi = \frac{V_p}{V_b} \cdot 100\% = \frac{(w_{wet} - w_{dry})/\rho_{brine}}{\pi r^2 l} \cdot 100\% \qquad [3.1]$$

where V_p is the pore volume, V_b is the bulk volume, w_{wet} is the weight of dry core, w_{dry} is weight of saturated core, ρ_{brine} is the density of the brine, r is the radius of the core and l is the length of the core.

Each core was stored in a box and surrounded by the fluid they were saturated with to avoid evaporation of fluids and consequently change of saturation.

3.3 Absolute permeability measurements

Capability to transmit fluids through its network of pores is described by the permeability of a porous medium. Absolute permeability is measured if there is only one single fluid present in the medium. This measurement is performed by use of a Hassler core holder. Three different injection rates are used and the respective differential pressures are measured. The experimental set up is shown in Figure 3.2. Confinement pressure is 8 bar or 10 bar over the pressure in the system, for chalk and limestone, respectively.

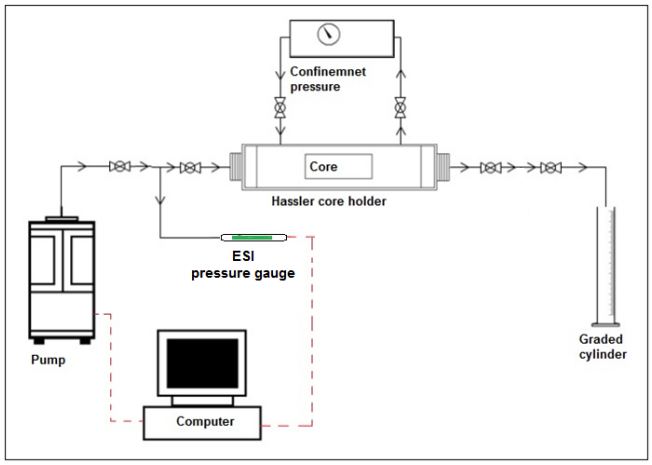

Figure 3.2 - Schematic drawing of the setup used for absolute permeability measurement and oil drainage. Pump injects brine/oil into the core from one side with different rates and the pressure gauge measure the respectively pressure. In the other end is the outlet and atmospheric pressure producing brine/oil.

Absolute permeability, *k* is calculated by use of Darcy's law, given in equation 3.2.

$$k = \frac{q}{\Delta P} \cdot \frac{\mu L}{A} \qquad [3.2]$$

where q is the flow rate [m^3/s], k is the permeability [$0.987 \cdot 10^{-12}$ m^2 = 0.987 Darcy], A is the area of the cross section [m^2], μ is the viscosity $\left[\frac{kg}{m \cdot s}\right]$ and $\frac{dP}{dx}$ is the pressure difference over the core length $\left[1\frac{atm}{cm} = 1.01 \cdot 10^7 \frac{kg}{m^2 s^2}\right]$.

By calculation of permeability the different flow rates are plotted versus respectively differential pressures and a straight line through the points gives a slope equal to $a = \frac{kA}{\mu L}$ (according to Darcy's law), where the slope a is used to calculate permeability, k. The viscosity of brine and length and cross sectional area of the core is constant.

3.4 Establishing S_{wi} by oil drainage

The same setup as the permeability measurement is used, Figure 3.2 for oil drainage. The irreducible water saturation, S_{wi} is obtained by injection of oil, either n-decane or paraffin oil at pressure of 2 bar/cm or 1.5 bar/cm into chalk and limestone, respectively. Care is taken to not exceed these pressures for the cores. 5 PV was injected in both directions of the core to achieve a uniform irreducible water distribution. The water and oil saturation were calculated from material balance.

3.5 Aging of cores and wettability measurements

Outcrop rock types are generally water-wet and by aging the core the wettability is changed. There are two kind of aging techniques, dynamic and static. The process used for aging the limestone core in this thesis was dynamic aging and was performed by Langlo and Ydstebø (2013). The dynamic aging was performed at 80°C, using Ekofisk crude oil. The high temperature is required to prevent precipitation of wax from the crude oil and for the aging to take place. The dynamic process was the same process as drainage process, where the oil was injected at a constant pressure of 1.5bar/cm in both directions to make sure the saturation distribution was uniform. After 2.5 PV of injection in both direction the cores were flooded for 90 hours with constant rate of 3 ml/h, this would result in neutral wettability (Graue et al., 1999). After the preferred wettability was reached the cores were flooded with 5 PV of both Decahydronaphtalene (Decaline) and n-Decane, this to prevent asphaltene precipitation. The wettability was measured with the Amott-Harvey method.

3.6 Preparation of cores: Fracture and Fracture permeability

The cores were cut longitudinally using a circular saw without water to maintain the stabilized residual oil saturation. The cores were weighed before and after the cutting and calculation of the new pore volume, denoted PV_{frac}, was done by a fraction of the weight before and after multiplied with the pore volume, equation given as

$$PV_{frac} = PV \cdot \frac{m_{frac}}{m_{whole}} \qquad [3.4]$$

where PV_{frac} [cm^3] is the new volume of the core after fracturing it, PV [cm^3] is the volume of the whole core before fracturing it, m_{frac} [g] is the weight of the fractured core and m_{whole} [g] is the weight of the whole core before fracturing it.

The porosity and fluid distributions were assumed constant before and after the core were cut. Figure 3.3 shows the longitudinal fracture and POM spacer used to ensure a constant fracture aperture. Figure 3.4 shows an example of a limestone core cut in two and a spacer placed between the two parts. The main purpose of keeping an open fracture is to easier compare the experiment. The spacer is made of polyoksymetylene, POM and was 1 mm wide. The extra volume of the spacer was excluded from the pore volume, hence included as dead volume. It was measured by adding up the volume of the window in the spacer.

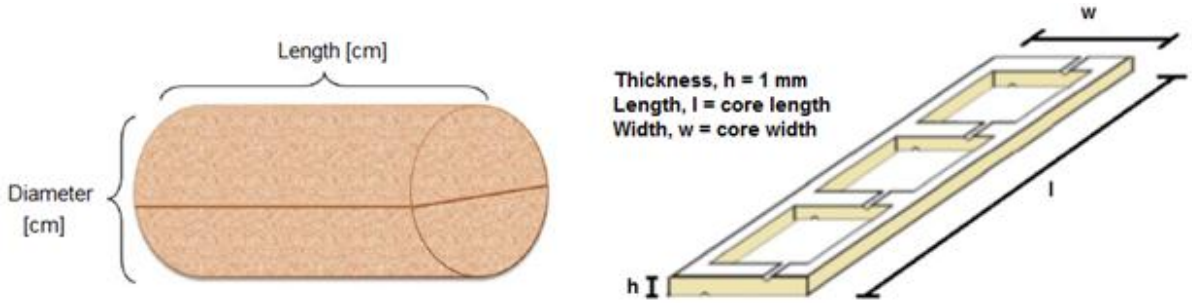

Figure 3.3 – Left: Schematic how the core was cut in two longitudinally. The new fractured PV was measured by weighting the core before and after the cutting. Right: POM spacer with three separate windows to create an open fracture. The one used in the experiments are cut in the right size to fit the core length. The width of the spacer is either 1.5" or 2" dependent on the core used for the experiments.

Figure 3.4 Fractured limestone core with spacer placed between the two parts. The chalk cores were cut in the same way and a similar spacer matching the length of the cores was used.

The cores were at irreducible water saturation and the effective permeability of the fractured core was measured after the system was pressurized with oil.

Figure 3.5 shows the procedure to wrap the core and end pieces with aluminum foil to reduce contact between the rubber and the sleeve and the injected CO_2. First the core is wrapped in aluminum foil and attached to the end pieces with aluminum tape. It is experienced during the experiments that after several time of injection of CO_2 the sleeve needed to be replaced. The sleeve used for these experiments was a Parker, Buna-N sleeve. Before attaching the core to the end pieces, the inlet end piece, consisting of a valve on top of it, was field with oil to avoid air coming into the core. The end pieces was mounted to the core by use of aluminum tape and afterwards the core and the end pieces was pushed through the core holder and attached to it. Because the two end pieces was attached to the core the core holder need to be taken out from the heating cabinet, and valves was attached to the core holder to keep the confinement oil inside the core holder.

Figure 3.5 – Top: Core before and after it is wrapped in aluminum foil and attached to end pieces.
Bottom: Core attached to the end pieces ready for montage to the core holder. Modified by (Haugen, 2012).

3.7 CO_2 and CO_2-foam injection

Five slightly different types of setups were used in this thesis dependent location the experiments were conducted and what pressures used during experiments. Figure 3.6 shows a general schematic of the setups. After the irreducible water saturation was established either water-, liqCO_2- , scCO_2- or scCO_2-foam injection was injected and oil production was recorded by volumetric measurement downstream of the BPR. The experimental setups were built in a heating cabinet, to accurately control temperature. The CO_2-injection was performed on limestone, chalk and shale cores either whole or fractured, where the fracture was aligned vertically and the injections were performed horizontally and thus gravity forces were neglected due to small dimensions of the core. Experiments performed on limestone and chalk cores when injecting supercritical CO_2 and foam was target at pressure of 90 bar and at temperature of 35°C. In this region the CO_2 is at supercritical conditions. The back pressure regulator was at the first placed outside the heating cabinet, but later moved inside due to large transition for the CO_2 when changing state from supercritical to gas. Each setup had to be tested for the desirable pressure before the experiment started.

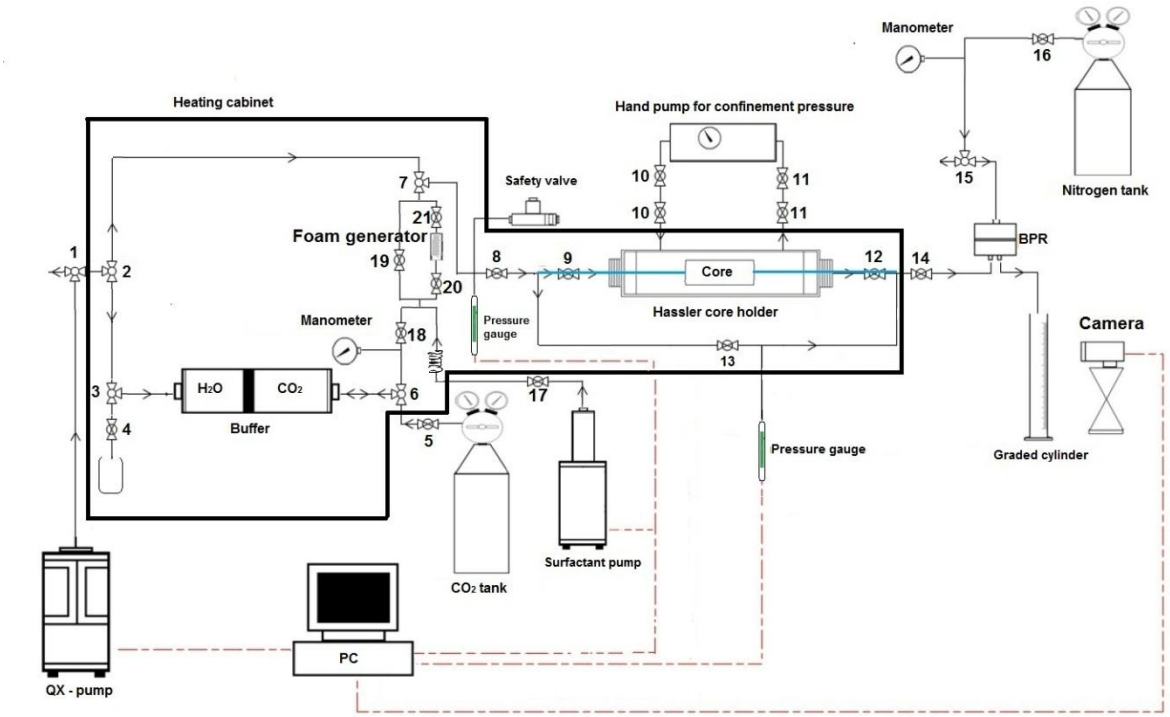

Figure 3.6 - Experimental setup for the CO_2 and CO_2-foam experiments. The dark line indicates what was mounted inside the heating cabinet. The arrows show possible flow directions. Valves are indicated by bows. Coiled dark line indicates coiled tubing to heat the CO_2 before injecting it into the core. The blue line denotes the dead volume. Included in the setup is a foam generator (between valve 20 and 21), which was used for the experiments when injecting CO_2-foam and bypassed when injecting pure CO_2.

Equipment used for the setup shown in Figure 3.6

- Accumulator containing CO_2 (volume 1.0 L)
- Backpressure regulator controlled by nitrogen, N_2
- CO_2 tank with a pressure of 60 bar
- Computer for operating pumps and logging
- 2x *ESI 200*, pressure transducer
- Foam generator (10 cm long and ¼" wide Swagelock tubing filled with glass beads)
- Hassler steel core holder
- Nitrogen tank with a pressure of 180 bar
- 2 Manometers
- *Quizix SP 5200* or hand pump, either one of the pumps for confinement pressure
- *Quizix QX 6000* or *QX 1500*, pump for pressurizing the line with oil and drive the accumulator
- Safety valve (set to 105 bar)
- Swagelock, tubings and valves
- Web camera

Detailed description of experimental procedure

The heating cabinet was set to test temperature before the accumulator was filled with CO_2 from the tank at 60 bar, through valve 5 and 6. Valve 3 was then opened, and the pump injected water at the bottom of the accumulator (through valve 1, 2 and 3) to pressurize the CO_2 to 90 bar. The pump was set to constant 90 bar for at least 3 hours (usually over the night) to establish equilibrium. The pump was switched from water to oil and the core was mounted and oil was flushed through the core (valve 9 and 12 opened, valve 13 closed) and tubes to pressurize the system, with low rate to avoid pressure build up so no more water was drained away from the core. Included in the setup is a foam generator (between valve 20 and 21), which was used for the experiments when injecting CO_2-foam and bypassed when injecting pure CO_2. Back pressure was regulated by a nitrogen tank, set to 90 bar (valve 15 and 16 opened). If the pressure exceeded 90 bar there was possible to close the nitrogen tank and remove some of the pressure carefully out trough valve 15. Next, the system, excluded the core (9 and 12 closed and 13 opened), was pressurized until 90 bar and how much volume used for pressurizing the oil from 0 bar to 90 bar was recorded. The back pressure was then removed and the system was depressurized to 0 bar. Then the core was include (bypass (valve 13) closed) in the pressurizing and the amount of oil injected to pressurize the system included the core was register. The confinement pressure was increased simultaneously and kept 10 bar or 8 bar above for limestone and chalk core, respectively. The fraction between the two different volume of oil used for pressurizing the system with and without the core was used as a pressurizing factor for the respectively oil, to correct for the extra volume injected when the system is pressurized. This was calculated for n-Decane and paraffin oil.

Oil was flushed through the core until the air from the system was observed at the outlet. Then the core was excluded from the system and CO_2 was flooded through bypass to remove oil and minimize dead volume. The foam generator was also excluded (valves 20 and 21 closed). When flooding the bypass it was used high flow rate to be sure that all possible oil was removed from the system. The CO_2 injection rate was set to experimental conditions before the valves to the core was opened. The injection rate was varied for each experiment to maintain the same frontal velocity. To achieve the same frontal velocity, desirable 2 cm/hour, for each core the rate was changed depending on rock type and size of cross sectional area. Limestone has half porosity of a chalk and thus different frontal velocity. After stabilized production through BPR the outlet valve (12) was opened, bypass valve (13) closed and inlet valve (9) opened, quickly. The production of oil was collected in a graded cylinder to read the produced amount of liquids.

In the case of scCO_2-foam injection the foam quality used in the experiments was 9:10 (90%), based on previous rate (Haugen et al., 2012) to generate a strong foam to give a favorable mobility ratio. Valve 17 was closed when the surfactant pump was pressurized before the injection. After 1-2 PV of CO_2 injected, the CO_2 injection was stopped and the CO_2 rate was adjusted to maintain the same total injection rate and simulta surfactant was set. Hence CO_2 and surfactant was co-injected (valve 17 now opened for surfactant injection). This time the foam generator was included (valves 20 and 21 opened, 19 closed) in the flooding (excluding the core) and foam was flushed through bypass.

Experience of foam injection resulted in no flooding of foam through bypass before injection to the core, which was performed in the latest experiments. The foam injection was then started after 1-2 PV of CO_2 injected. Predicting of when the foam exactly hits the core and thus one need to consider some uncertainty of this calculation. A web camera was on during the time of production, taking a photo every 10th minute.

Source of Errors

There were difficulties with maintaining a constant backpressure using the BPR because the production was either below or above the decided backpressure, and experiments were performed at pressures in a range of 85-99 bar. In addition, creating exactly the same setup in different heating cabinet may affect the results and may be an uncertainty when measuring the dead volume. To be sure that all dead volume is removed before starting the injection into the core may be difficult, and some of the produced oil which is counted as pore volume may be excessive for some experiements. There was also experienced fluctuation of differential pressure, which was also experienced previous by Langlo (2013) and Christoffersen (2010). These fluctuations may be due to the production through BPR, where it alternated between opening and closing as the CO_2 went from one state (supercritical/liquid) to another (gas)

3.7.1 Secondary oil recovery by liquid CO_2-foam injection

Secondary CO_2 injection in limestone core plugs were conducted at the Texas A&M University in College Station, Texas, USA. Two water wet and one oil-wet, at ambient temperature and at pressure of 90 bar. The schematic drawing of the setup is shown in figure 3.7.

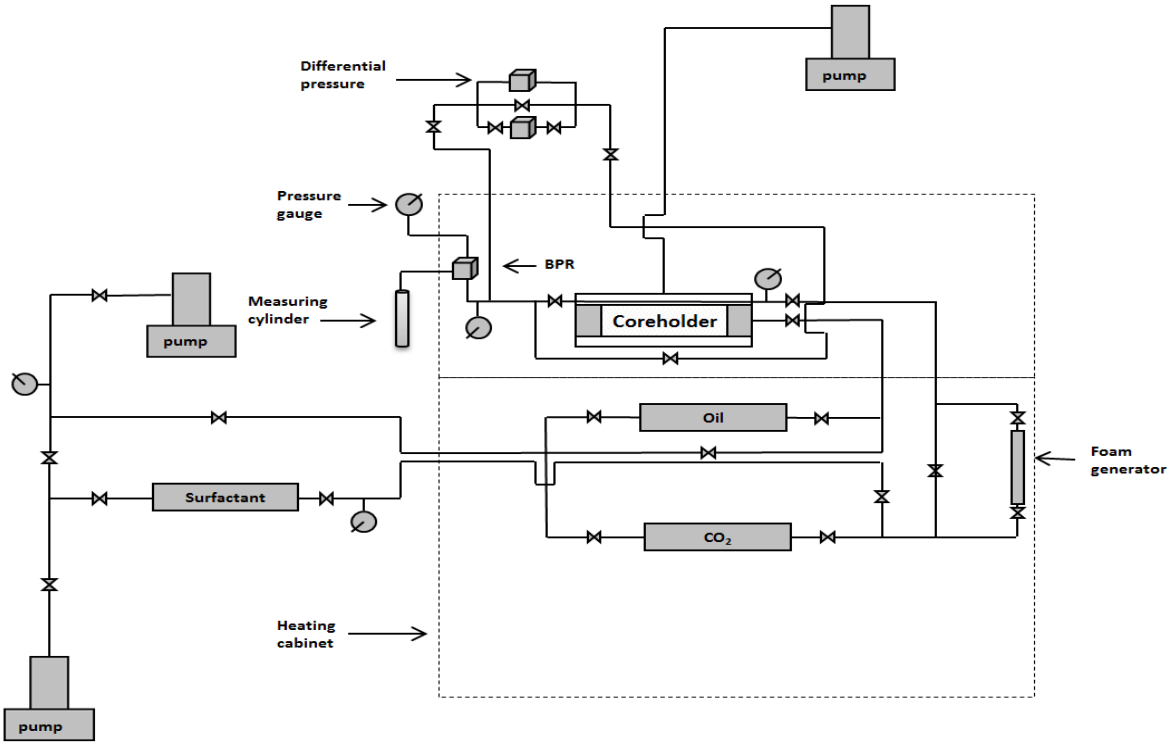

Figure 3.7 – Schematic of the experimental setup used for supercritical CO_2-foam injection at Texas A&M University (Langlo, 2013).

Equipment used for secondary recovery by CO_2-foam

- *3x Accumulators* containing oil, CO_2 and surfactant
- *Backpressure regulator* controlled by Nitrogen, N_2
- *Bi-axial (hydrostatic) core holder*
- *Foam generator* (10 cm long and ¼" wide Swagelock tubing filled with glass beads)
- *3x ISCO pumps* for injection of oil, CO_2 and surfactant
- *Pressure gauges*
- *Swagelock* tubings, fittings and valves
- *Validyne DP15*, differential pressure
- *Web camera*, monitoring the production and the differential pressure

These experiments were conducted by collaboration with Master students Stig A. Langlo and Tom Ydstebø (2013). The procedure was the same as the one described in chapter 3.7, but after flooding the lines with n-Decane, surfactant and CO_2 was co-injected and flooded through bypass instead of only

CO_2. The rate of co-injection of CO_2 and surfactant were 3.72 ml/h and 0.48 ml/h with a foam quality of 90%, respectively. The total injection rate of 4.2 ml/h was used to compare with pervious CO_2-injections (Langlo, 2013, Ydstebø, 2013). When foam was observed at the outlet, the inlet valve to the core was opened allowing foam injection through the core. A web camera taking photo of the graded cylinder and the differential pressure every half an hour made it possible to monitor the production also during the night. The fluctuation of differential pressure was also experienced here. Because most of the dead volume (90%) was at downstream of the core it was subtracted from the production. In these experiments the extra volume of oil injected to pressurize the system was subtracted from the production.

3.8 Tertiary CO_2 injection for EOR in Reservoir Carbonate Cores

CO_2 injection for EOR in reservoir carbonate cores from an onshore fractured carbonate field in Texas were conducted in collaboration with PhD-students Bergit Brattekås and Marianne Steinsbø. Schematic of the experimental setup is shown in Figure 3.8 and experimental equipment is listed below. The procedure was the same for all four cores.

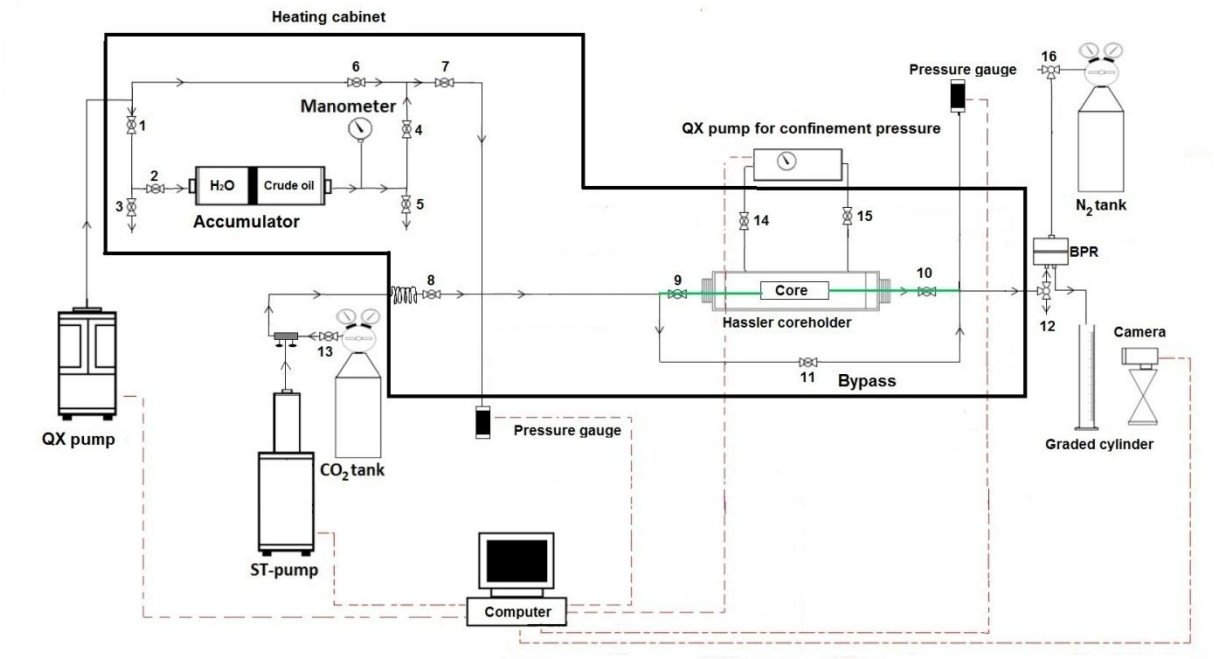

Figure 3.8 – Schematic drawing of the setup used for water and CO_2 injection in reservoir cores. The black box indicates the wall of the heating cabinet. The thicker line (green) before and after the core indicates the dead volume. Valves are indicated by a bow and numbered, 1 to 16. Red and dotted lines are communication cables connected to the computer.

Equipment used for the setup shown in Figure 3.8

- Accumulator containing CO_2
- *Autoclave* tubings and valves
- Backpressure regulator controlled by nitrogen, N_2
- CO_2 tank with a pressure of 60 bar
- Computer for operating pumps and logging
- *2x ESI 200*, pressure gauges
- *Foam generator* (10 cm long and ¼" wide Swagelock tubing filled with glass beads)
- *Hassler steel core holder*
- *Manometer*
- *Quizix SP 5200* for confinement pressure
- *Quizix QX 6000*, pump for pressurizing the line with oil and drive the accumulator
- Safety valve set to desirable pressure
- *Sanchez ST pump,* for injection of CO_2
- Web camera

Detailed description of experimental procedure

The cores were first saturated with chalk brine and permeability measured at ambient conditions performed as described in Chapters 3.2 and 3.3. The oil drainage and following water and CO_2 injection were performed at reservoir pressure and temperature of 180 bar and 71°C, in the system shown in Figure 3.8. Crude oil was stored in the accumulator inside the heating cabinet at experimental pressure. The core and tubes were pressurized by chalk brine (valve 6, 7, 9 and 10 was open) and the injected volume of brine to pressurize the system, excluding (valve 12 opened, 9 and 10 closed), and including the core, was measured to correct for extra volume injected to the system. Next water was injected at the bottom of the accumulator, through valve 1 and 2 (valve 6 was closed and 4 was opened) for injection of crude oil. S_{wi} was established by drainage with Ekofisk crude oil with the same procedure as described in chapter 3.4. The aim was to drain the cores with constant pressure buildup of 1 bar/cm injecting maximum 5 PV. It was not possible to reverse the flow direction. The water production at the outlet was measured and the S_{wi} for each core was calculated.

After the core was drained by crude oil, it remained shut-in for 20 hours before water flood initiation. Before injecting the water into the core the injection line had to be flushed with water. The inlet and outlet valve (9 and 10) to the core was closed, and water was injected through bypass (valve 11) to remove dead volume. During the water injection the bypass was closed and water was injected through the core (valve 9 and 10 opened). The flow rate of the water injection was set to the same frontal velocity as previous experiments (2 cm/hour) and was calculated by the cross sectional area and the porosity. Due to different porosity of the cores the rate was 5 and 3.5 ml/h. The water injection lasted for approximately 2 PV before it was switched to CO_2 injection.

CO_2 was injected from a pump placed outside the heating cabinet and injected to the system through valve 8. The CO_2 was pressurized to valve 8. The rate of the injection was set to the same as water injection, but due to increase in temperature (room at 26°C and heating cabinet at 71°C) the volume expansion of CO_2 resulted in a higher rate inside the heating cabinet. The flow rate was regulated on the pump and set to a lower rate calculated with use of volume ratio. The system was flushed with CO_2 (through bypass) to remove dead volume. The pressure transducers were placed outside the heating cabinet due to high temperature and after the first experiment the BPR was placed inside the heating cabinet due to hydrate plug.

Difficulties during the experiment:

- CO_2 pump at ambient temperature outside heating cabinet and system at 70 °C inside the heating cabinet

- Uncertainty in transformation of CO_2 from liquid to supercritical inside the heating cabinet.
- Hydrate plug, due to BPR first placed outside the heating cabinet
- Pressure transducers sensitive to temperature. The air conditioning was set to constant temperature to avoid pressure variation due to changes in room temperature.

3.9 Integrated EOR by Tertiary CO_2 and CO_2-foam Injection

Earlier experiment of tertiary oil recovery method by liquid CO_2-injection into chalk by Brautaset (2009) was reconstructed using limestone. The purpose of this experiment was to study the enhanced and improved oil recovery of a fractured system by tertiary CO_2 and the CO_2-foam injection, respectively. The foam used in the tertiary foam injection was generated *in situ* during co-injection of CO_2 and surfactant.

The following experiments were conducted using the same experimental setup as the supercritical CO_2-foam injection shown in Figure 3.6. The fractured network consisted of five parts, where the first part was a whole core and the following parts were one core cut in 4 where the middle core had a vertical fracture and the last core had a horizontal fracture, as shown in Figure 3.9. A spacer was not used between the fractures in this experiment. Figure 3.10 shows a photo of the cores before they were attached to the end pieces and put into the core holder. After the cores were cut there were some rough surfaces and thus difficulties when wrapping them in aluminum foil. In addition these rough surfaces could result in higher fracture permeability, and larger dead volume than expected, because no additional dead volume was added due to the absence of spacer. The fractured system permeability, K_{system}, was measured at reservoir conditions, but due to the whole core in the beginning the system's permeability might be strongly dependent on this one and there might be large uncertainty in these measurements. The whole fractured system was a bit uneven when it was attached to the end pieces and therefore some extra aluminum foil and tape was used to compensate.

The brine used for this experiment is listed as Brine C in Table 3.1. The following procedure for mixing the salts was used: The first salt mixed with 500 ml of deionized (DI) water was $CaCl_2$ $2H_2O$, $MgCl_2$ $6H_2O$, NaCl, and shaken to a clear solution. Na_2SO_4 was dissolved with additional 200 ml of DI water in a separate beaker until clear solution. Then the solution of Na_2SO_4 was added to the first solution and additional DI water was added until the total volume reached 1000 ml.

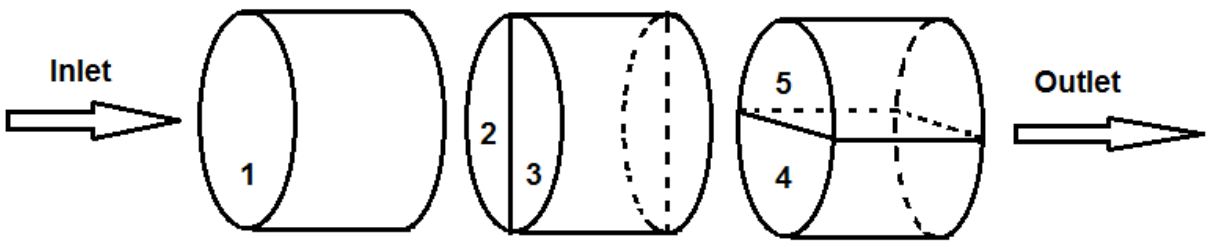

Figure 3.9 – Schematic drawing of the cores in the Integrated EOR experiment. Injection of fluids was from left towards right, initially injecting through the whole core. The middle core had a vertical fracture and the last core had a horizontal core. Part 1 was from a single core and part 2, 3, 4 and 5 was from the same core, cut in four.

Figure 3.10– Left: Five parts before and after assembling them into the core holder. Right: All five cores put together and wrapped in aluminum foil to avoid CO_2 wearing out the sleeve and to keep it inside the system. The core was attached to the end pieces as shown in Figure 3.6.

Experimental procedure

The procedure for this experiment was approximately the same procedure as described in chapter 3.8. The differences are after flushing the line with oil, the dead volume was removed by injection of brine because this was the first injection fluid introduced to the core. The experiment was performed at reservoir conditions, pressure at 90 bar and temperature at 35°C. First one injected 2 PV of brine, followed by 2 PV of $scCO_2$-injection and finishing with co-injection of $scCO_2$ and surfactant, with foam quality of 8:2. Instead of foam generator a whole core was placed at the inlet where the aim was to create foam in-situ in this whole core. The injection steps had a total injection rate of 10 ml/h and between the steps the injection was not stopped due to some problem of the BPR when stopping the experiment (the pressure inside the system was decreasing because the BPR was not holding the pressure if there was no injection). This problem was known and therefore taken into account.

4 Experimental Results and Discussion

This chapter presents the experimental results. A total of 55 cores were prepared, and 22 CO_2 and/or water injections were conducted. First section presents general comments and uncertainty during the experiments and subsequent section lists an overview of the core data and the results from the standard core analysis such as porosity, permeability, irreducible water saturations and residual oil saturation listed in tables.

4.1 Core properties

The reservoir cores and outcrop cores are divided into two different tables, Table 4.1 and Table 4.2, respectively. Cores that are not used is listed in a separately table, Table 4.3.

Table 4.1 – Core IDs and properties of reservoir samples

Core ID	Material	Length [cm]	Diameter [cm]	PV [ml]	Porosity [%]	S_{wi}	K_{matrix} [mD]	Fractured
RIK 1	Chalk	6.21	3.84	33.22	46.2	0.287	4.3	No
RIK 3	Chalk	6.04	3.80	31.06	45.3	0.292	3.8	Yes
RIK 4	Chalk	5.92	3.82	31.10	45.8	0.309	3.8	Yes
RIK 7	Chalk	6.04	3.83	31.96	45.9	0.307	4.7	Yes
RIK 9	Chalk	6.25	3.79	34.07	48.3	0.281	3.0	No
RIK 13	Chalk	5.97	5.10	54.58	44.8	0.224	4.3	No
KIR 1	Chalk	5.99	3.78	31.35	46.6	0.308	5.1	Yes
KIR 4	Chalk	5.85	3.80	31.38	47.3	0.286	4.1	Yes
RI2	Limestone	7.31	3.75	18.83	23.3	0.230	27.2	No
RI3	Limestone	7.76	3.76	20.22	23.4	0.258	21.9	Yes
RI4	Limestone	7.21	3.76	18.50	23.1	0.243	26.95	No
RI5	Limestone	7.33	3.76	18.15	22.3	0.245	20.19	Yes
RI6	Limestone	7.15	3.77	17.01	21.3	0.236	12.64	Yes
RI7	Limestone	7.45	3.77	18.83	22.7	0.256	19.11	Yes
RI8	Limestone	7.60	3.77	17.72	20.9	0.238	12.20	Yes
RI10	Limestone	7.38	3.78	19.56	23.6	0.233	21.41	Yes
L5	Limestone	7.59	4.95	33.76	23.1	0.227	23.31	No
L14	Limestone	7.27	4.96	32.84	23.4	0.285	28.20	No
L28	Limestone	7.67	4.96	35.67	24.0	0.243	19.88	No
L33	Limestone	7.05	4.97	34.01	24.9	0.294	33.55	No
E5[1)]	Limestone	5.91	3.81	17.21	25.5	0.227	N/A	Yes
L30[1)]	Limestone	7.41	3.78	18.82	22.6	0.245	21.00	Yes

[1)] Core E5 and L30 was prepared by Anders Christoffersen (2012) thus there is some lack of data.

Table 4.2 – Core IDs and properties of reservoir samples

Core ID	Length [cm] ± 0.01	Diameter [cm] ± 0.01	PV [ml] ± 0.04	Porosity [%]	S_{wi} [%][1)]	K_{matrix} [mD]
RC_A	6.17	4.70	16.05	15.0	46.4	15.3
RC_B	6.56	4.73	16.25	14.1	51.7	12.5
RC_C	6.75	4.79	11.32	9.30	47.0	2.6
RC_D	6.61	4.74	16.56	10.8	74.9	2.3

[1)] The cores was drained to high S_{wi} values explained in chapter 4.2.4

Table 4.3 – Core IDs and properties of reservoir shale cores

Core ID	Handled	Length, L [cm]	Diameter, d [cm]	Bulk volume, V_b [ml]	Weight, w [g]
SC_A	Unpreserved	3.80	3.80	43.10	114.40
SC_B	Unpreserved	3.92	3.80	44.46	111.27
SC_C	Preserved	2.45	3.82	28.08	70.28

Note that the size of the diameter is equal to a 1.5 inch diameter. Permeability and porosity measurements are presented in chapter 5 about reservoir shale cores

Table 4.3 – Core IDs and properties of outcrop chalk and limestone rocks not used

Core ID	Material	Length [cm]	Diameter [cm]	PV [ml]	Porosity [%]	S_{wi} [%]	K_{matrix} [mD]
RIK 2	Chalk	6.1	3.84	32.35	45.8	15.0	3.99
RIK 5	Chalk	5.83	3.83	30.41	45.3	-	3.92
RIK 6	Chalk	5.94	3.80	29.75	44.2	19.3	3.45
RIK 8	Chalk	5.65	3.82	29.25	45.2	12.8	3.55
RIK 10	Chalk	6.04	3.80	32.93	48.1	30.2	3.93
RIK 11	Chalk	6.40	5.08	63.41	48.9	28.2	4.35
RIK 12	Chalk	5.83	5.10	57.40	48.2	26.8	4.80
RIK 15	Chalk	6.08	4.95	55.96	47.8	12.4	4.56
RIK 16	Chalk	5.85	4.83	50.46	47.1	13.8	5.09
RIK 18	Chalk	6.02	5.09	57.81	47.2	27.3	5.97
RIK 20	Chalk	5.96	4.94	53.67	47.0	27.0	4.71
KIR 2	Chalk	5.93	3.80	31.91	47.5	-	4.02
KIR 5	Chalk	5.90	3.80	31.82	47.6	27.7	4.80
KIR 6	Chalk	5.89	3.79	32.44	48.8	30.9	4.82
RI9	Limestone	7.30	28.3	19.38	23.7	20.0	28.30
L3	Limestone	7.58	12.5	31.56	21.4	22.7	12.48
L8	Limestone	7.27	17.7	30.81	22.1	24.4	17.70
L11	Limestone	7.06	21.1	31.37	23.0	-	21.11
L12	Limestone	7.64	14.3	33.43	22.6	26.4	14.26
L13	Limestone	8.03	12.5	33.50	21.6	26.3	12.49

Permeability and porosity variation of the cores are illustrated in Figure 4.1 which shows a permeability-porosity plot. This plot shows a higher permeability of the limestone cores than the chalk cores, but the porosity value is inverted, where chalk has the highest value. The permeability of chalk cores are measured to be in a narrow range, between, 3 - 6 mD, whereas the permeability for limestone outcrop cores are in a wide range, between 12 - 33 mD. These significant permeability variations of limestone may indicate a heterogeneous material. The four reservoir carbonate samples are also plotted in Figure 4.1 and shows large distribution of permeability.

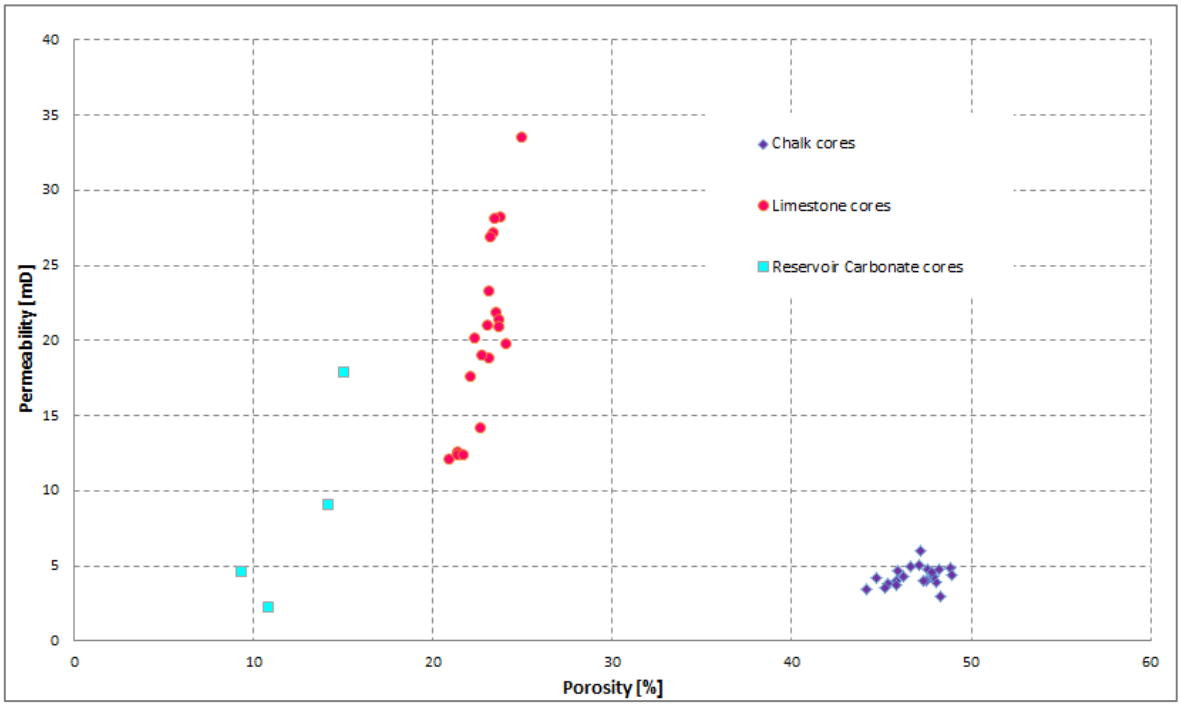

Figure 4.1 – Porosity vs. permeability plot for experimental cores. Diamond shape denotes chalk which has porosity in the range of 45-50% and permeability between 2.9-6.0 mD. Circle dots denote limestone which has a range in porosity between 21-26% and permeability range between 12.4-33.6 mD. The squares to the left denote the reservoir carbonate cores, with permeability ranging between 2.3-17.9 mD and porosity between 9.3-15.0%.

4.2 EOR and IEOR by CO_2 and CO_2-foam injection

4.2.1 Secondary Supercritical CO_2 injection

This chapter presents EOR by secondary supercritical CO_2 injection in outcrop chalk and limestone core plugs. Table 4.4 and 4.5 list the cores and their initial water saturation, S_{wi}, residual oil saturation after CO_2 injection ($S_{or,CO2}$) and oil recovery in % of OOIP (R_f).

Table 4.4 – Oil recovery in whole and fractured chalk cores during CO_2 injection

Core	Fractured	PV [ml]	S_{wi}	K_{matrix} [mD]	Pore pressure [bar]	Injection rate [ml/h]	$S_{or,CO2}$	$R_{f,CO2}$ [%OOIP]
RIK1	No	33.22	0.287	4.3	89 - 91	2	0.132	81.5
RIK3	Yes	31.06	0.292	3.8	90 - 93	10	0.224	68.4
RIK9[1)]	No	34.09	0.252	2.5	91 ± 2	2	-	-
RIK13	No	54.58	0.227	4.2	95 ± 2	20	0.124	84.0

[1)] CO_2 injection in core RIK9 was performed but uncertainty in the oil drainage resulted in wrong calculation of S_{wi} and as consequent oil recovery >100% OOIP was produced.

The results of CO_2 injection in chalk cores are listed in Table 4.4, and experimental results are shown in Figure 4.2 with oil saturation in fraction of PV versus PV injected, for core plugs RIK1, 3 and 13. In these three experiments the oil used was n-Decane. The whole core, RIK13 showed increased differential pressure shown in comparison plot Figure 4.4.

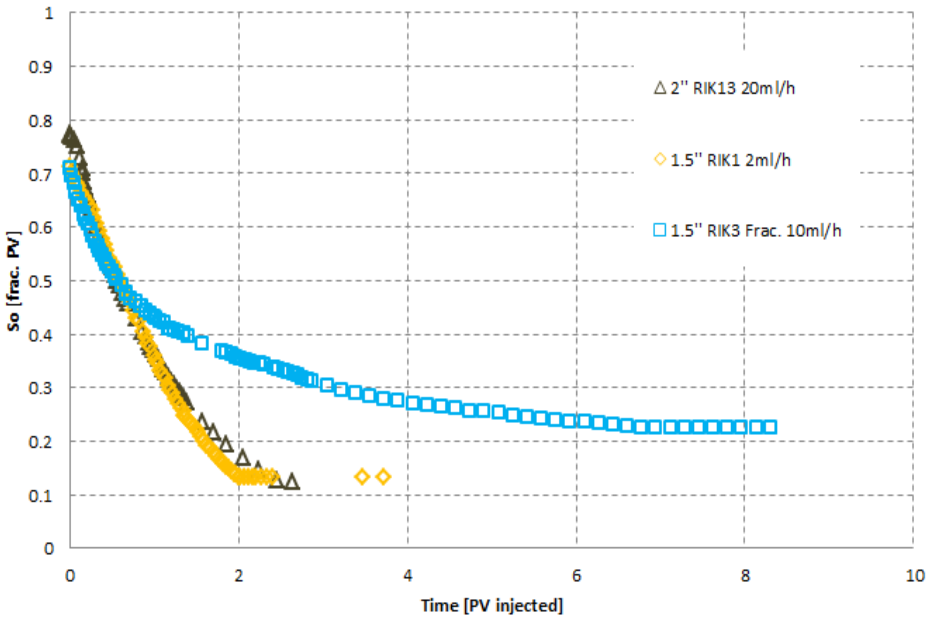

Figure 4.2 - Oil saturation vs. PV injected for $scCO_2$ injection in whole and fractured chalk cores. All cores are drained with n-Decane to S_{wi} and the injection rate for each core is given. The temperature for all experiment was at 35°C and the pressure ranged between 89-97 bar.

Whole chalk core RIK1 reached oil recovery of 81.5% Original Oil In Place (OOIP) produced after 2.0 PV (33 hours) of CO_2 injected and after this there was no more oil produced. The other whole core RIK13 reached an oil recovery of 78.3% OOIP produced after 2.0 PV injected, and additional 0.6 PV injected resulted in a total oil recovery of 84.0% OOIP produced. This experiment ended because no more CO_2 was available. From the oil saturation plot (Figure 4.2) one can see that the oil saturation was still declining and slightly more oil would probably have been produced if more CO_2 had been injected. The rapidly stop in oil production for RIK1 at 2 PV injected was unexpected because oil production rate suddenly reached zero.

CO_2 injection into fractured core plug RIK3 resulted in early CO_2 breakthrough, at approximately 1.0 PV of CO_2 injected, with maximum oil recovery at 68 % of OOIP after 6.6 PV injected. End point residual oil saturation was reached at 0.220 of total PV, and thus total oil recovery was lower than compared with whole cores. The two injection rates for RIK3 and RIK13 had comparable frontal velocity (cm/hour), and it is worth mentioning that Figure 4.2 indicates an identical oil production before CO_2 breakthrough for all three cores. There is a slightly variation in oil production rate, which may be because of pressure variation during the experiments.

The results of supercritical CO_2 injection in limestone cores are listed in Table 4.5 and a comparison of oil saturation from chalk and limestone cores are shown in Figure 4.4.

Table 4.5 – Oil recovery in whole and fractured limestone cores during CO_2 injection

Core	Fractured	Oil type	PV	S_{wi}	K_{matrix} [mD]	Pore pressure [bar]	Injection rate [ml/h]	$S_{or,CO2}$	R_f [%OOIP]
RI2	No	non-filtered paraffin oil	18.83	0.230	27.2	88 - 92	2	0.079	89.8
RI3	Yes	paraffin oil	20.22	0.258	21.9	93 - 95	5	0.310	58.2
RI4	No	paraffin oil	18.50	0.243	27.0	94 - 95	5	0.019	97.5
L5	No	n-Decane	33.76	0.227	23.3	93 - 94	4	0.091	88.2

Figure 4.3 shows oil saturation plotted versus PV injected for whole and fractured limestone core plugs during supercritical CO_2 injection. Total oil recovery ranged between 88.2-97.5 % of OOIP for whole cores compared to 58.2 % for fractured core plug RI4. No significant differential pressure was observed, with less than 0.05 bar.

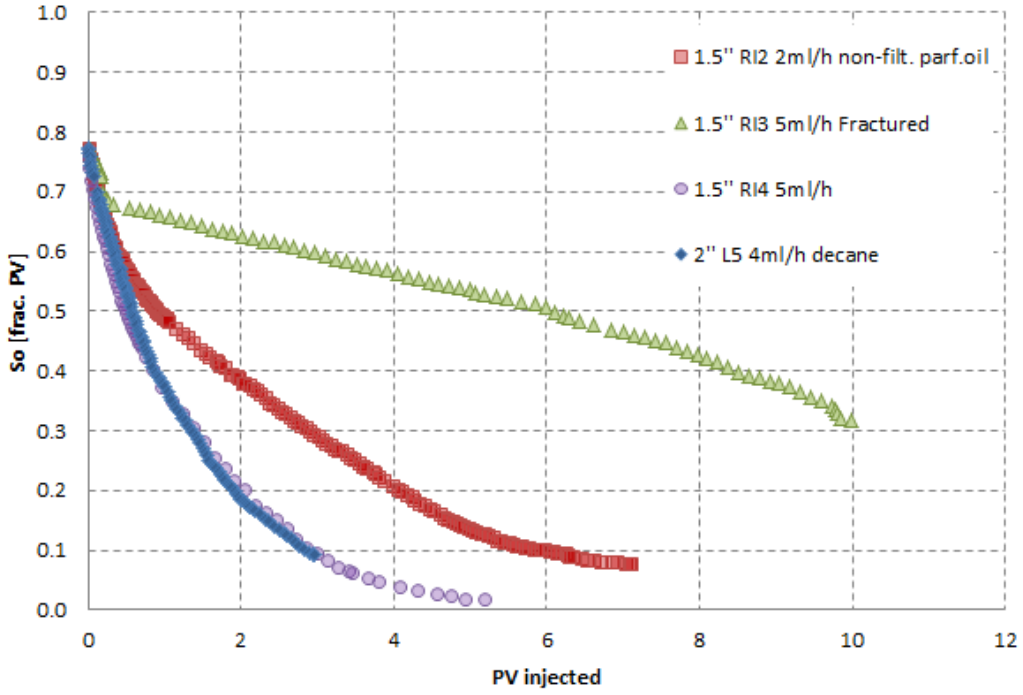

Figure 4.3 - Oil saturation vs. PV injected for $scCO_2$ injection in limestone cores. Initial oil saturation was in the range 0.742 – 0.773. The oil recovery for the whole cores ranged between 88.2 and 97.5% of OOIP, whereas the oil recovery for the fractured core was 58.2%. The experiments were performed at temperature of 35°C and a pressure range between 89-97 bar.

Compared to the whole cores, fractured core RI3 produced less oil with, approximately 58% of OOIP during a total of 10 PV (37 hours) injected. CO_2 displaced the oil in the high permeable fracture and less amount of matrix oil is produced before CO_2 breakthrough at approximately 0.25 PV injected. After this the continuous CO_2 flowing in the fracture resulted in oil recovery by diffusion due to concentration difference between the CO_2 filled fracture and oil-saturated matrix.

Residual oil saturation was not established in core L5 because CO_2 injection stopped after 3PV injected, but oil recovery versus PV injected for this core is identical to the oil recovery for Core RI4. Whole core RI4 reached maximum oil recovery 97.5% of OOIP after approximately 5.1 PV (19 hours) of injection. This was the highest oil recovery compared to the other two whole limestone cores (L5 and RI2). The oil saturation was low and ended at 0.019 of PV. The oil production is close to linear (same amount of CO_2 injected as oil produced) during the first 0.70 PV of injection for both RI4 and L5, where approximately 44% of OOIP is recovered, before the CO_2 breakthrough. Earlier CO_2 breakthrough is observed for the other whole core RI2 after 0.34 PV injected where the oil recovery is only 21.2 % of OOIP. Unfortunately, in this experiment, the paraffin oil used was not filtered. The polar compounds in the oil can alter the wettability by adsorption (Anderson, 1986), and this might influenced the oil production of Core RI2. Due to this uncertainty, this experiment is no longer discussed. The CO_2 injection for different oil compositions, like filtered paraffin oil and n-Decane, used in RI4 and L5 respectively, showed no significant discrepancy and hence one may assume the CO_2 develop first contact miscibility with both of these mineral oils.

Supercritical CO_2 injection in whole and fractured carbonate

Figure 4.4 shows a comparison of the oil saturation by supercritical CO_2 injection in both whole and fractured chalk and limestone cores. Differential pressure for whole and fractured chalk core is presented in the same figure for comparison and discussion.

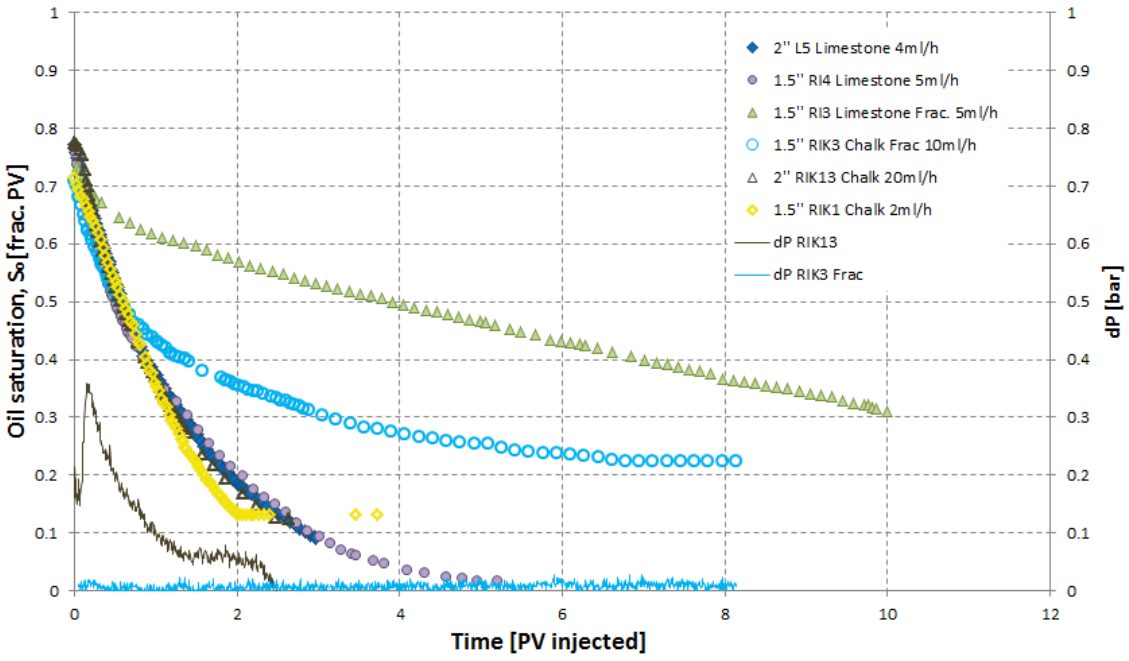

Figure 4.4 – Oil saturation (frac. of PV) versus PV injected for chalk and limestone cores. Differential pressure (plotted on secondary axis) versus PV injected is presented for whole and fractured chalk core. The limestone cores are denoted with filled marks and chalk cores denoted with unfilled marks.

The oil recovery by supercritical CO_2 injection resulted in oil recovery above 80% in whole cores for both limestone and chalk and a horizontal fracture present showed significantly lower oil recovery, between 58% of OOIP for limestone and 70% of OOIP for chalk. The differential pressure of the whole chalk core, RIK13 was increased to 0.35 bar during the first 0.2 PV injected due to higher injection rate and viscous forces dominating the displacement creating an oil bank in front. After this short period of increased differential pressure the pressure decreased assuming CO_2 developed first-contact miscibility with the oil and reduced the density difference. At CO_2 breakthrough it was approximately 0.05 bar and stabilized throughout the injection. After CO_2 breakthrough the oil displacement is dominated by molecular diffusion.

Lower total oil recovery and lower oil production rate is observed for fractured cores, both chalk core plug RIK3 and limestone core plug RI3 in addition no significant differential pressure was observed for these cores, where an example of L5 is shown in Figure 4.4. Production from whole cores is mainly by diffusion as the CO_2 diffuses from high concentration area into matrix with less concentration area. The main difference in oil production from whole and fractured cores is the amount of PV injected. The oil recovery from limestone showed after 4.0 PV injected above 90% OOIP produced, whereas for the same amount injected in fractured core was only 30% OOIP produced. The oil recovery for the whole chalk cores after 2.5 PV injected showed above 80% OOIP produced, whereas the fractured chalk core showed approximately 50% OOIP produced.

More efficient oil recovery is observed for fractured chalk core than limestone, where earlier CO_2 breakthrough for fractured limestone core (at 0.27 PV) and significant lower oil recovery (9.0% of OOIP) compared to chalk core (29.0% of OOIP) after 0.56 PV is observed. The earlier CO_2 breakthrough in limestone may be due to higher fracture permeability because of harder grain than the chalk core. When the chalk core was removed from the system it was observed marks from the spacer and inlet and outlet end pieces, which indicates that the chalk material has been squeezed. This effect is also shown in previous experiment (Haugen, 2012).

After CO_2 breakthrough the oil recovery is mainly by diffusion and the observation of higher total oil recovery in chalk emphasize more efficient diffusion in chalk than limestone because of higher porosity and narrower pore size distribution in the chalk core, which result in a higher contact area between pores and fracture aperture where diffusion occurs. The oil displacement by diffusion in chalk core has previously been observed from both PET/CT images (Lie, 2013) and MRI imaging (Haugen, 2012). Limestone may indicate a more heterogeneous material with respect to pore size and permeability streaks which will have an additional effect of oil production. This may, in addition to the fracture, explain the earlier CO_2 breakthrough. This is shown in Figure 4.1 where the permeability-porosity plot showed wide range for the limestone.

There is observed that supercritical CO_2 injection at these reservoir conditions develops first contact miscibility with both the mineral oils, n-Decane and paraffin oil. The cores where a fracture is presented (RIK3 and RI3) CO_2 first displaces the oil in the fracture (and a small amount of matrix) and the residual oil left in matrix is recovered by diffusion. CO_2 injection in whole cores displaces the oil by viscous forces, and due to low permeability of the chalk and more homogenous material it is low possibility for viscous fingers to appear for low injection rates hence the dispersion of CO_2 is larger. Whereas high injection rate in limestone cores and present of high permeable streaks can result in possible fingering of CO_2. In the presence of a fracture the CO_2 diffuses from fracture into matrix, displaces the oil from matrix into the fracture and hence the oil is produced

4.2.2 Secondary CO_2-foam injection

The secondary CO_2-foam injection was conducted to investigate the foam performance in the different core materials in the presence of high oil saturation. This chapter presents tables and figures of both secondary liquid CO_2-foam injection and supercritical CO_2-foam injection. The liquid CO_2-foam was injected in three whole limestone cores and was conducted at higher pore pressure than the supercritical CO_2-foam injection which was injected into a fractured chalk core. All experiments were conducted above the MMP for CO_2 and n-Decane, which means the experiments were first-contact miscible. Due to this various parameters during the foam-injection the results are presented in two different tables and plots. Table 4.6 shows the liquid CO_2-foam injection in limestone core plugs.

Liquid CO_2-foam injection in limestone cores with different wettability

Table 4.6 – Experimental conditions and results from experiments with foam injection in whole limestone cores.

Core	PV	S_{wi}	I_{A-H}	K_{matrix} [mD]	Injection rate [ml/h]	Avg. Pore pressure [bar]	$S_{or,foam}$	$R_{f,foam}$ [%OOIP]
L28	35.67	0.243	1	19.9	4.2	99	0.267	64.7
L33	34.01	0.294	1	33.6	4.2	98	0.064	90.9
L14[1)]	32.84	0.285	-0.06	28.2	4.2	99	0.012	98.3

[1)]Core L14 was moderately oil-wet and the wettability measurement using Amott-Harvey method were conducted by Langlo (2013) and Ydstebø (2013) which is described in chapter 3.5.

Figure 4.5 shows a comparison of the oil saturation vs. PV injected during liquid CO_2 injection in whole core with different wettability. Surfactant and CO_2 was co-injected, pre-generated in a foam generator, with foam quality of 9:1 for all experiments. The foam quality was applied to make strong foam to maximize foam viscosity, and reduce viscous fingering of the CO_2 (Haugen et al., 2012).

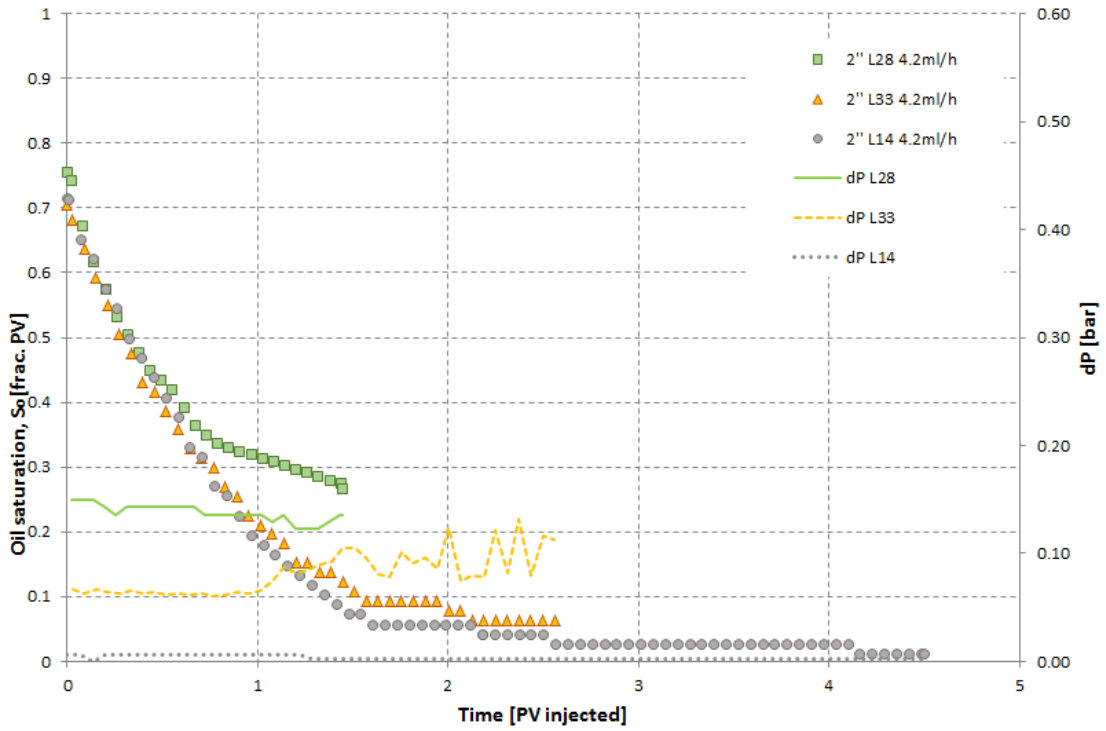

Figure 4.5 – Results of secondary CO_2-foam injection in whole limestone cores at S_{wi}. Oil saturation (primary axis) and differential pressure (secondary axis) vs. PV injected.

Foam injection in Core L28 ended at 1.5 PV (12.3 hours) injected and a total oil recovery of 65%. The oil production drastically decreased after only 0.5 PV injected compared to the other two limestone cores (L33 and L14). This might indicate that there was some more water and less oil than estimated. When the experiment stopped, one can see from Figure 4.5 that the oil production is still declining and the experiment was ended before end point residual oil saturation was reached. The permeability of this core was lower, 19.9 mD compared to the other cores. Differential pressure during the foam injection is fluctuating between 0.08-0.14 bar which may indicate foam generation, and this differential pressure during foam injection in fractured core has been observed (Christoffersen, 2010).

Figure 4.5 shows minor increased differential pressure during foam injection in core L33, which increases from 0.06 bar to 0.1 bar as the oil saturation decreases. After 2.56 PV (21 hours) of injection the oil recovery ended at 90.9% OOIP produced, and after only 1.5 PV injected a total of 84.7% OOIP was produced. The residual oil saturation ended at 6.4% of total PV. The permeability of this core was the highest 33.6 mD.

The moderately oil wet core L14, shows the same oil recovery trend as the strongly water-wet core L33. The injection lasted for 4.5 PV (35 hours), but reached the maximum oil recovery after approximately 4.2 PV (33 hours) injected. L14 has lower differential pressure than the other two strongly water-wet cores.

The oil recovery curves showed high oil recovery by foam injection in limestone cores and two of the limestone cores had repeatable oil recovery despite the different wettability. They started approximately the same initial oil saturation and ended at approximately the same residual oil saturation. Due to lack of differential pressure in the oil-wet core it is difficult to state any foam generation in this core, but as a result of miscible displacement of oil by CO_2 the recovery is high. It was observed a slightly differential pressure, fluctuating around 0.1 bar during the injection in core L33, which indicate resistance to flow and possibly foam generation. Because oil is destructive to foam and prefer water-wet medium (Sanchez and Hazlett, 1992), it was more foam created in the core plug when oil saturation decreased. There is not observed any differential pressure for the moderately oil-wet core during the injection, which may be due to that foam prefer water-wet medium, the pre-generated foam may be broken inside the core. The initially co-injection of surfactant and CO_2 might continue as separately injection, where CO_2 displaces oil by diffusion and oil swelling. More PV of foam is injected before CO_2-foam breakthrough compared to the pure CO_2 injection which is expected because the viscosity is increased.

Supercritical CO_2-foam injection in fractured chalk

Supercritical CO_2-foam was injected in a fractured chalk core which was drained with paraffin oil to S_{wi}. The result of the injection is listed in Table 4.7.

Table 4.7 – Experimental conditions and results from experiments with foam injection in fractured chalk core.

Core	PV	S_{wi}	Fractured	K_{matrix} [mD]	K_{frac} [mD]	Injection rate [ml/h]	Avg. Pore pressure [bar]	$S_{or,foam}$ ± 0.004	$R_{f,foam}$ [%OOIP]
KIR1	29.80	0.308	Yes	5.0		10	95	0.181	73.8

The foam injection was conducted at a higher pressure than previous supercritical CO_2 injection (chapter 4.2.1). Higher pore pressure decreases the permeability and a rigid chalk material may be more affected by increased pressure, where the rock material is squeezed towards the fracture. The oil saturation (fraction of PV) versus PV injected is shown in Figure 4.6. Oil recovery was 40.6% of OOIP at 0.84 PV of injection at foam breakthrough. The total oil recovery of 73.8% of OOIP was reached after 5.01 PV foam injected. Foam injection stopped in the transient period due to no more CO_2 available.

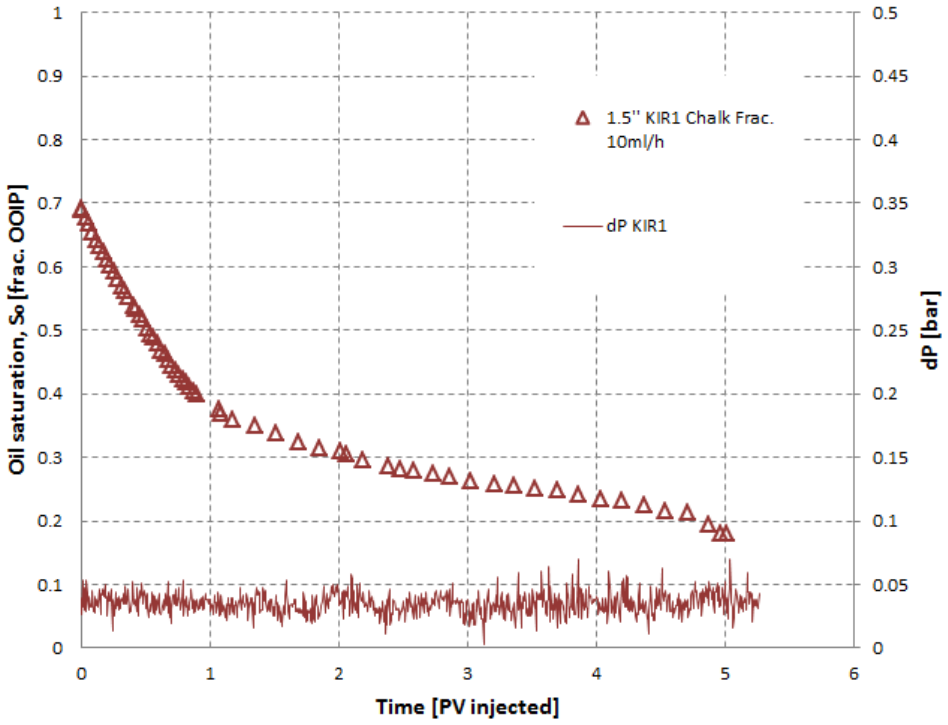

Figure 4.6 - Oil saturation vs. PV injected for fractured chalk core during supercritical CO_2-foam injection. The differential pressure (secondary axis) is plotted versus PV injected.

The differential pressure during the foam injection in fractured chalk was approximately 0.04 bar, which is low differential pressure and this might indicate no foam generation. The rupture of foam in chalk may be explained by small pore radii and high disjoining pressure, because the film is ruptured as it becomes thinner, as described in chapter 2.5.3. Observation of later foam breakthrough during injection of CO_2-foam compared to pure CO_2 injection was observed which was expected due to increased viscosity of injected fluid.

Earlier studies of foam injection in 100% oil saturated chalk core was visualized from PET/CT scans and showed low oil recovery (Lie, 2013). The low water saturation may have influenced the generation and foam was destroyed or weakened which is observed from previous experiment because the foam might dry out due to no water supply (Sanchez and Hazlett, 1992, Zanganeh et al., 2009). The stability of the lamellae in fracture depends on the capillary pressure in the surrounding medium, hence the matrix versus fracture, in the absence of water in a strong water-wet medium the high capillary pressure results in foam collapse (Khatib et al., 1988).

Viscosity and density of CO_2 decrease as the temperature and pressure increase, and the volume of CO_2 increases as temperature increases. Volume expansion is consequent of the latter one and results in higher velocity of the CO_2. Minor increase of temperature can result in major volume expansion of

the CO_2, influencing the gas fraction and as a consequent the mobility of the foam becomes more equal to the gas mobility. Previous experiment has shown that liquid CO_2- and supercritical CO_2-foam injection had no significant discrepancies in the displacement efficiency (Christoffersen, 2010). It is difficult to compare the foam injection in whole limestone core to the foam injection in fractured chalk core, due to different displacement when fracture is present.

4.2.3 Tertiary CO_2-foam injection for mobility control

This chapter presents results from secondary oil recovery method by $scCO_2$ injection and tertiary oil recovery method by CO_2-foam in fractured SWW limestone and chalk cores. The objective of tertiary CO_2-foam injection was to examine the oil recovery results by decreasing the mobility of the CO_2 and see if the foam injection could improve the oil recovery during injection in fractured cores. Table 4.8 lists the results such as initial water saturation, oil saturation and oil recovery after the two flooding processes.

Table 4.8 – Experimental results from experiment with $scCO_2$ injection followed by foam

Core	Material	Oil	PV	S_{wi}	K_{matrix} [mD]	Injection rate [ml/h]	$S_{or,CO2}$	$R_{f,CO2}$ [%OOIP]	$S_{or,foam}$	$R_{f,tot}$ [%OOIP]
RIK4	Chalk	n-Decane	31.10	0.309	3.8	10	0.334	52.4	0.158	77.2
RIK7	Chalk	n-Decane	31.96	0.307	4.7	10	0.323	53.3	0.165	76.2
RI5	Limestone	Paraffin oil	16.58	0.245	20.2	5	0.607	19.6	0.103	86.3
RI7	Limestone	Paraffin oil	17.24	0.256	19.1	5	0.548	26.4	0.156	79.0

The initial water saturation varied between 0.245 and 0.309 (water fraction of PV), and was calculated after fracturing the core, as described in chapter 3.6. The same frontal velocity of the injection was desirable, thus a different injection rate of 10 ml/h and 5 ml/h was used for chalk core and limestone core, respectively. Pre-generated foam was injected with quality of 9:1 while maintaining the total injection rate. The amount of 1-2 PV CO_2 injected prior to CO_2-foam was desired based on the pure CO_2 injection in fractured cores where the CO_2 breakthrough was at approximately 1 PV. Figure 4.7 shows oil saturation versus PV injected for the chalk cores.

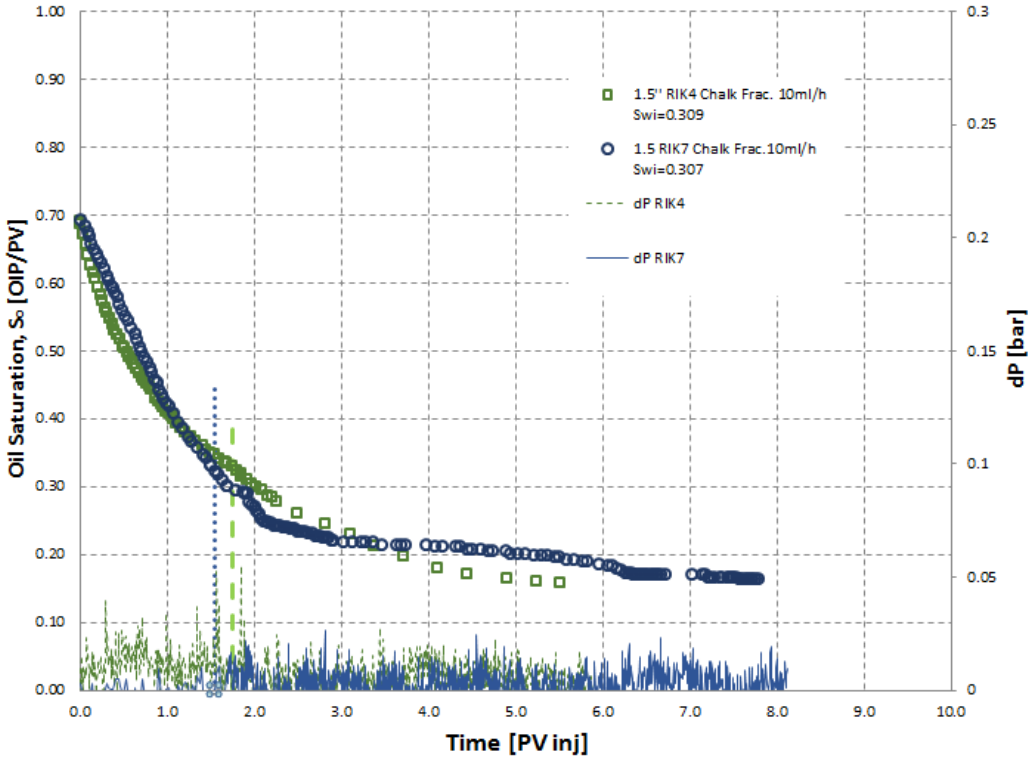

Figure 4.7 - Oil saturation vs. PV injected during a secondary injection of $scCO_2$ and tertiary injection of $scCO_2$- foam. For both graphs the dotted lines denote when foam is introduced to the core, where it is introduced to core RIK7 first. The differential pressure is plotted on secondary axis and shown with colors related to the oil saturation curve.

The secondary CO_2 injection for core RIK4 lasted for 1.7 PV (5 hours) and the oil recovered was 52.4% of OOIP (S_o was 0.476). Figure 4.7 shows a fast production of oil during the first 0.2PV injected and after CO_2 breakthrough (approximately 0.6PV of injection) the oil production declines. The injection was switched to pre-generated foam which lasted as long as CO_2 was available from the accumulator. The effect of foam shows no increased oil production rate, and the differential pressure was fluctuating around 0 bar, which might indicate no foam generated. The continued oil production looked like a pure CO_2 injection because of no significant increase in oil production rate. Compared to previous secondary CO_2 injection in fractured chalk (core RIK3), where 7 PV of CO_2 was injected to reach residual oil saturation at 22.4% PV, the total oil recovery after foam injection in RIK4 was 77.2% of OOIP (S_o equal to 0.158) after a total of 5.5 PV (16.4 hours) injected. The injection rate was 10 ml/h during both experiments.

CO_2 injection in RIK7 lasted for 1.5PV of injection and the oil recovery was 53.3% of OOIP. When surfactant and CO_2 was co-injected to the system, there was a stop during the flooding through bypass and extra oil coming out was added to the production based on the oil production rate from CO_2 injection. This might explain the different trend (the flat part) of the oil recovery curve compared to the other core RIK4. The total oil recovery was 79.0% after a total of 8.60PV of injection. In addition

discrepancies in the whole oil production curve for the two chalk cores are observed. The oil recovery for RIK7 was lower in the beginning compared to RIK4 (until 1.2PV injected and at oil saturation of approximately 0.40 PV and 45% of OOIP recovered). Figure 4.8 shows an increase in oil production after the foam is introduced to core RIK7, but no increase of the differential pressure, which may be due to that the pre-generated foam was destroyed. This observation was similar as for secondary foam injection in fractured chalk core, showed in Figure 4.7 in chapter 4.2.2.

After approximately 3.3PV of total injection the oil recovery was equal for core RIK7 and RIK4 (~68%), and the residual oil saturation ended at 0.165 and 0.158, respectively. The accelerated production in the end of the oil production for RIK7 may be due to generation of foam because less amount of oil was present in the core and assuming generation of weak foam (weak due to no differential pressure), but short time after destroyed. Oil recovery by tertiary foam injection is compared to secondary pure CO_2 and CO_2 –foam injection later.

Figure 4.8 shows the results of secondary $scCO_2$ injection and tertiary foam injection in fractured limestone core plugs RI5 and RI7, where oil saturation is plotted versus PV injected. This figure is related to the data about limestone cores listed in table 4.8.

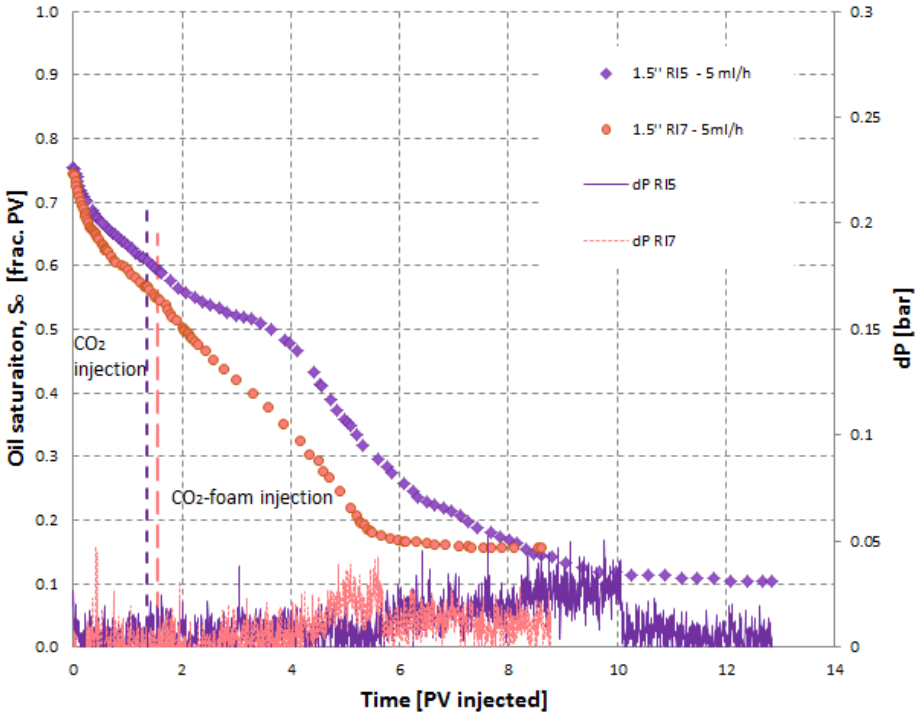

Figure 4.8- Oil saturation vs. PV injected during secondary injection by $scCO_2$ and tertiary injection of foam in fractured limestone core plugs RI5 and RI7. Diamond mark denotes RI5 and circle denotes RI7. Both cores drained with paraffin oil to S_{wi}. The differential pressure during each injection is separated by different colors and shapes of the line (pink dotted related to RI7 and purple non-dotted related to RI5). The heterogeneity of the limestone material might explain the different oil production profiles for RI5 and RI7.

The $scCO_2$ injection of core RI5 showed oil recovery of 19.6% of OOIP after 1.3 PV (4.2 hours). Injection was switched to foam and the oil recovery increased to 86.3% of OOIP after a total of 12.8 PV (42.5 hours), and the residual oil saturation ended at 0.103 PV. The oil production rate increased significantly after 2.8 PV (1.5 PV after foam was introduced to the core), and this is shown in Figure 4.10 (right) where oil production rate is plotted vs. time, compared with production rate of chalk core RIK4 (left). The differential pressure (plotted on the secondary axis in Figure 4.8) showed an increase short time after the foam was introduced to the core assuming generation of foam which propagated through the core. After the ended oil production the differential pressure decrease again

Injection of $scCO_2$ in Core RI7 resulted in oil recovery of 26.4% OOIP after 1.6PV (5.3 hours) injected. Fast oil production during the first 0.2PV CO_2 injected and rapidly decline after CO_2 breakthrough. The low amount of oil produced before CO_2 breakthrough may be due to high permeable streaks within the matrix displacing only a less amount of oil. The injection is switched to foam after the CO_2 injection and additional oil is recovered, approximately 55% of OOIP during 7.3 PV (25 hours) of foam injection. The total oil recovery ended at 79% of OOIP and the oil saturation of the core was then 0.156 fraction of PV. The foam injection was less visible for RI7, but from the plot of oil saturation (Figure 4.8) one can see the oil production is slightly decreased short time after the foam was introduced. The differential pressure for RI7 is increased 2.5PV after the foam is introduced, assuming generation and propagation of foam in the core. Next is a discussion of the CO_2-foam injection as mobility control.

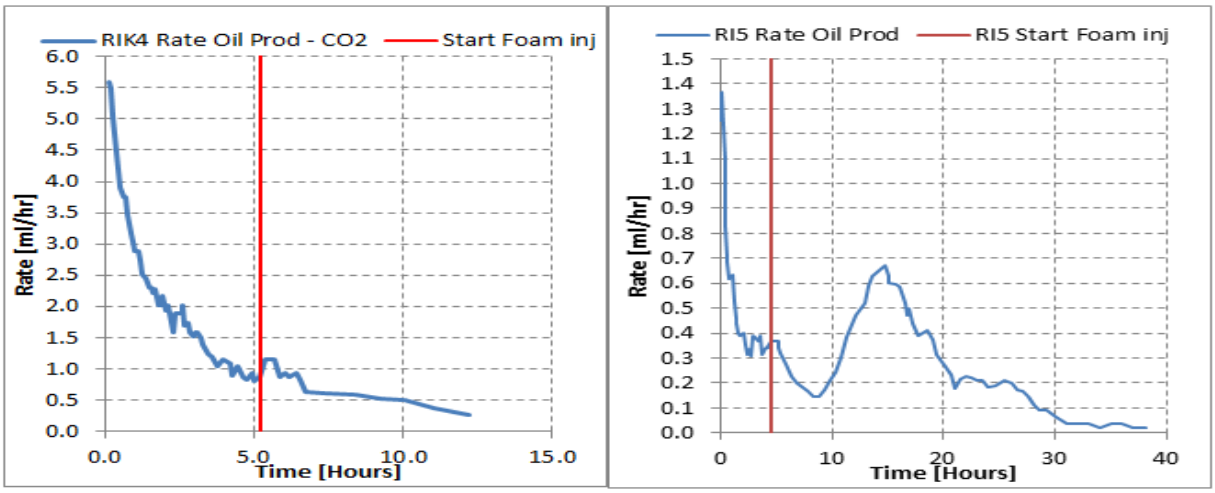

Figure 4.9 - Oil production rate (volume oil produced divided by hours) versus time (hours). Left: Fractured chalk core RIK4 with injection rate of 10ml/h. Right: Fractured limestone core RI5 with injection rate of 5ml/h. Red line indicates when foam hit the core and the oil production rate shows minor and major acceleration. Comparable frontal velocities results in different injection rates and the calculation of the rate is an average value of 5 points of production, which explain the fluctuations.

Mobility control by CO_2-foam injection into fractured chalk and limestone cores

Figure 4.10 shows highest oil recovery by pure CO_2 injection in whole core due to efficient oil displacement by viscous forces dominate by diffusion. Chalk is a homogeneous material with equal pore size distribution and low permeability of the chalk, where low viscous CO_2 cannot flow easily, resulting in later CO_2 breakthrough. The pure CO_2 injection in fractured cores, RIK4 and RIK3 shows similar CO_2 breakthrough, but as the foam is introduced in core RIK4 oil recovery increases. After 2 PV of injection the oil recovery for whole core RIK13 is significantly higher (~78%) than fractured RIK4 (~57%) and RIK3 (~33%). Diffusion is more efficient in the whole core than the fractured ones because the diffusion is dependent on the distance of molecule exchange. This distance is smaller between pores within matrix compared to the distance from fracture aperture to the pores outermost in the core.

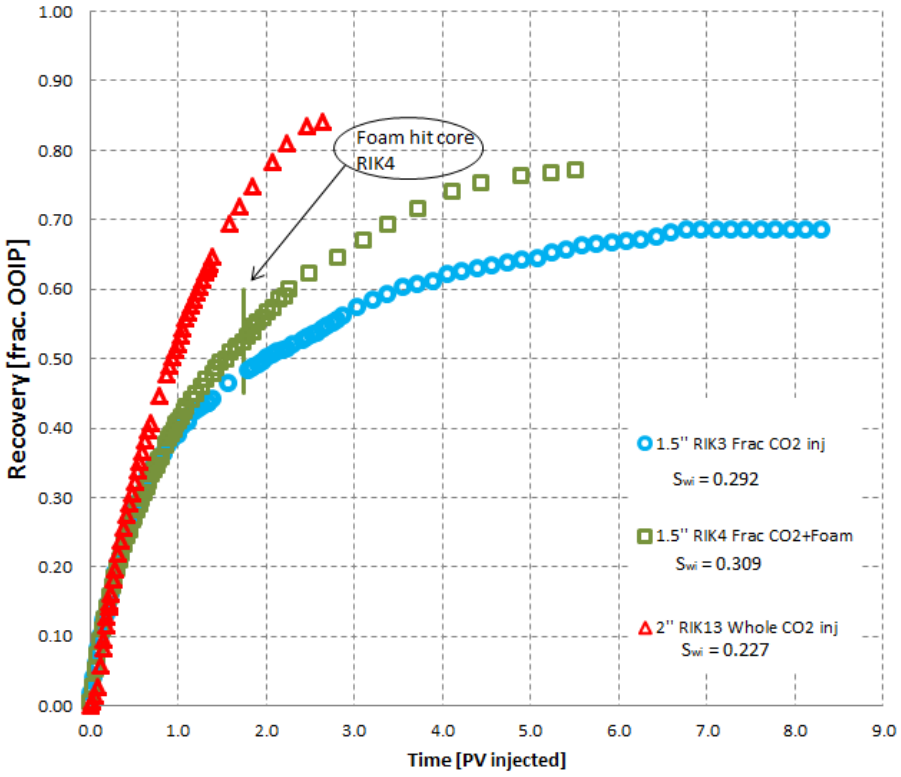

Figure 4.10 – Comparison of pure CO_2 injection (in whole and fractured chalk core) and CO_2-foam injection (in fractured core). Oil recovery vs. PV injected for the three different chalk cores, RIK3, RIK4 and RIK13.

Observation of no significant increased differential pressure during the foam injection in RIK4 may be due to no or weak foam present in the core. This can either be caused by 1) small pore throats and high disjoining pressure resulting in foam collapse 2) oil present in the core. The first one is explained by the chalk core consisting of small pore and pore throats (Hardman, 1982) where high disjoining

pressure can break down the foam, described in chapter 2.5.3. The latter one is explained by the foam sensitivity to oil, which has been tested by static foam test of alpha-olefin surfactant (AOS). The results from the experiments showed that the most important factor that affects the foam were the length of hydrocarbon and salinity in the presence of oil, where shorter alkane tended to destabilize the foam. In addition the hydrocarbon molecular weight also played an important role were decane and shorter alkanes act to destabilize the foam due to solubilizing in the micelles, which not happens for longer alkanes (Vikingstad et al., 2005).

The presence of n-Decane in the chalk cores might explain the reason why there is low or no effect of the foam injection because the n-Decane might solubilize in the micelles and destabilize the foam. The differential pressure shows minor pressure build up, but short time after it decreases again, which might indicate foam injection and later rupture of the foam, because when lamellae get in contact with more decane it might get destabilized (Vikingstad et al., 2005). During the foam injection in limestone this was not observed, thus it may be the chalk material and small capillaries that rupture the foam film.

The experiment conducted by tertiary foam injection in fractured chalk, showed approximately 5% additional oil recovered compared to the pure injection of CO_2 in fractured chalk. Additional oil recovery by tertiary foam injection was also reported by Haugen et. al. (2012) who injected pre-generated foam subsequent a water injection. The experiment was performed on strongly water-wet chalk, fractured, saturated with brine and drained to S_{wi} using decane. This might indicate that weak foam may propagate when less oil is present, despite the small pores in chalk rock which might break down the foam, the fracture may be a reason to generation of weak foam, due to the high permeable region (Tanzil et al., 2002).

In addition another factor that might affect the foam stability is the surfactant used and its sensitivity to rock material, because the positive charged surface (Ca^{2+}) of the rock material may influence the surfactant consisting of dipole molecules. When surfactant used for the experiments is an anionic surfactant (negative charged), adsorption might occur because the surface of carbonate rock is positively charged consisting of Ca^{2+} ions (Gogoi, 2011). The surfactant used in this experiment is a negative charged AOS, but the experiment of foam injection in limestone showed results of foam generation despite the positive charged surface of the rock, thus no conclusion drawn.

Figure 4.11 shows a comparison of the $scCO_2$ injection in whole and fractured limestone core plugs compared to $scCO_2$-foam injection in fractured limestone core plug.

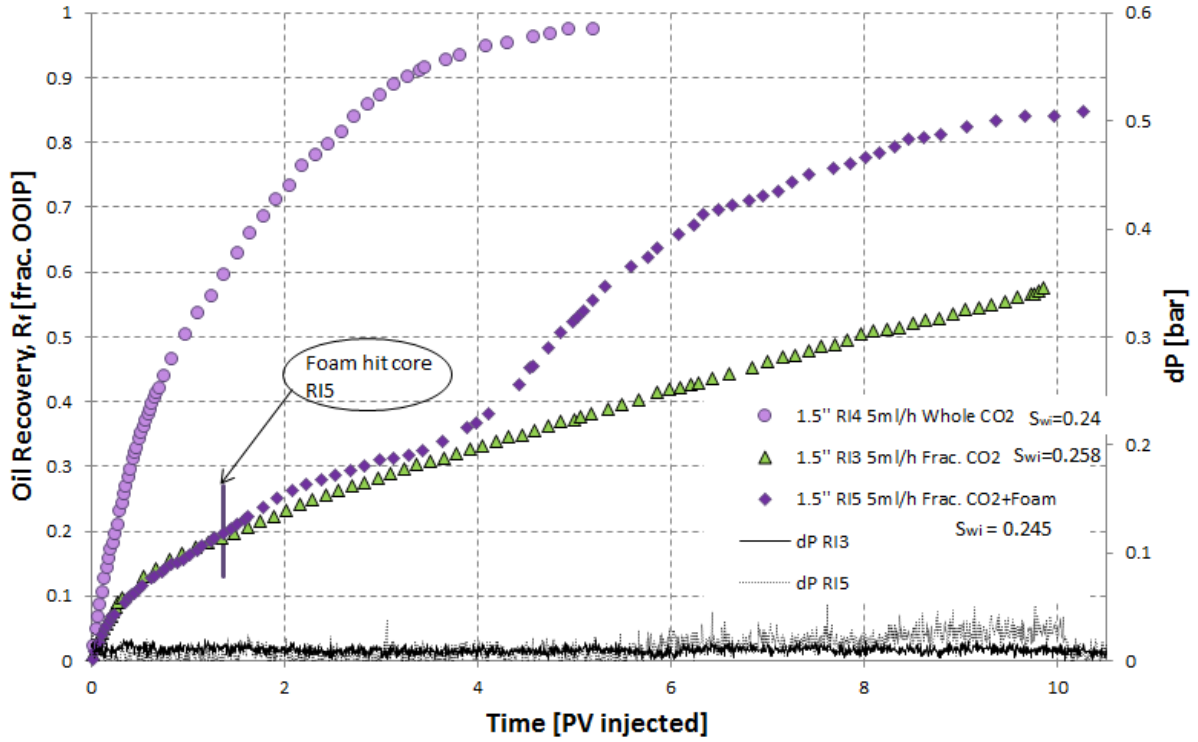

Figure 4.11 – Oil recovery vs. PV injected. Pure CO_2 injection in whole core RI4 and fractured core RI3 is compared to CO_2-foam injection in fractured core RI5. Time of PV injected when the foam is introduced to the inlet of core RI5 is marked.

Earlier experiment by pure CO_2 injection in fractured limestone core resulted in early CO_2 breakthrough and less efficient oil displacement, which may be due to the pore size distribution and high permeable streaks, as mentioned. The tertiary CO_2-foam injection shows increased oil production approximately 2.5 PV of foam injected, and increased differential pressure suggesting foam generation in the core. The late generation of foam may be due to the present of oil, and as the oil saturation decreased the foam was stronger and hence propagated in the core. The foam injection accelerated the oil production, and after approximately 4.5 PV foam injected the oil recovery was approximately 66% OOIP compared to 42% OOIP during pure CO_2 injection.

Stronger foam in limestone than chalk is shown by comparison of rate plots for chalk and limestone in Figure 4.9. This shows that the oil production decreased faster in the case of CO_2 injection into limestone than chalk and that the foam injection increased the production rate. Hence the foam may have blocked high permeable areas, such as the open fracture, diverted CO_2 into the matrix and more oil was produced.

Earlier studies of tertiary foam injection subsequent a water injection was conducted by Christoffersen (2012), but the secondary recovery method was water injection. The foam injection was then observed approximately after 0.5 PV of foam injected, which can be explained by the higher water saturation in the core which will supply the foam with water and strengthen it.

4.2.4 Tertiary CO_2 injection in Reservoir Carbonate Cores

This chapter presents four experiments of secondary water and tertiary CO_2 injection. The aim was to look at tertiary oil recovery by CO_2 injection after a water injection into reservoir carbonate cores. The following data and graphs present the results from four experiments. Table 4.9 lists oil saturation and oil recovery after both water and CO_2 injection. Because the cores were cleaned and not at native state the wettability of the material was assumed to be strongly water-wet (SWW). The cores were drained to high S_{wi} values by pressure build up, 1bar/cm. There were difficult to obtain maximum pressure during the drainage which might be due to high permeable streaks and this explains the high S_{wi} values, especially for RC_D. For one of the core, RC_C the drainage was successful. The permeability vs. porosity plot (Figure 4.1) showed wide distribution of permeability and porosity of the four cores. All the cores were whole.

Table 4.9 –Oil Recovery in Reservoir Carbonate cores during secondary water and tertiary CO_2 injection.

Core	S_{wi}	PV	K_{matrix} [mD]	Pore pressure [bar]	$S_{or,w}$	$R_{f,water}$ [%OOIP]	$S_{or,CO2}$	$R_{f,tot}$ [%OOIP]
RC_A	0.464	16.05	16.1	175 - 179	0.421	21.5	0.040	91.3
RC_B	0.517	16.25	11.4	177 - 180	0.397	17.8	0.040	91.7
RC_C	0.461	11.32	3.6	176 - 178	0.296	45.1	0.066	87.7
RC_D	0.749	12.56	2.3	175 - 179	0.191	23.8	0.008	96.8

Figure 4.12 shows oil recovery for the reservoir carbonate cores. Blue line indicates water injection and red line indicates supercritical CO_2 injection. Different injection rate for the cores are used because same frontal velocity for each core was desirable. Hence the velocity was dependent on the cross sectional area and porosity of the cores.

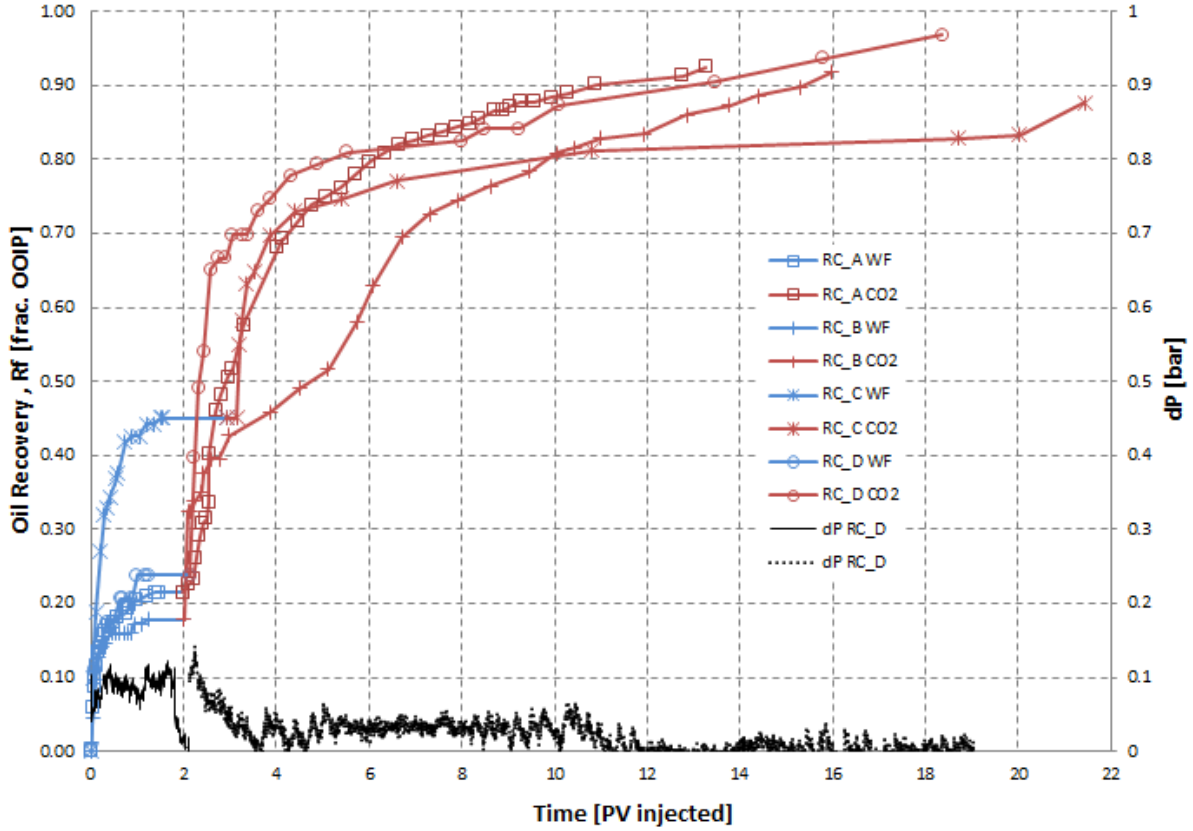

Figure 4.12 - Oil recovery as fraction of OOIP plotted versus PV injected. Blue dots denote the water injection (WF) and red dots indicates CO_2 injection (CO_2). The different cores have different marker to distinguish between them.

The oil recovery from water injection ranged between 17.8 and 45.1% of OOIP. The wide range in oil recoveries is due to the different initial oil saturations. RC_A and RC_C had approximately equal initial oil saturation, 0.464 and 0.461 respectively, but different oil recovery after ended water injection, 25.1 and 45.1% OOIP, respectively. Due to the successful oil drainage of RC_C there might be less permeable streaks in this core compared to the other ones and thus the oil is forced into the matrix. During water injection the strongly water-wet matrix imbibes water and the oil displacement is by spontaneously water imbibition. For the other three cores viscous forces dominated the displacement leading to earlier water breakthrough. The oil production during water injection for all cores was fast and more than 70% of the waterflood-recoverable oil was produced before 0.3PV injected. All four cores reached residual oil saturation after approximately 1.5PV water injected. After water breakthrough oil and water was produced simultaneously for a short period (termed transient period). And the residual oil by water injection was reached after 1.5PV injected for all cores. A total of 2PV water was injected for three of the cores, whereas RC_C had a total water injection of approximately 3PV.

The injection was switched to CO_2 with the same injection rate as water injection, but as the CO_2 goes from room temperature to reservoir temperature of 71°C the injection rate was calculated dependent on volume expansion of the CO_2 (volume at desire pressure and temperature according to (NIST, 2014). The additional oil recovery by CO_2 injection was in the range of 42.6-73.9% OOIP. The CO_2 injection was less efficient for core RC_C were the oil recovery by water injection was highest. Core RC_D had the highest total oil recovery (96.8% of OOIP) after the CO_2 injection. During the CO_2 injection the differential pressure is low and fluctuating around 0.05 bar during the transient period indicating oil recovery by viscous forces dominated by diffusion. The produced oil observed at the outlet was in the beginning of each water injection and CO_2 injection dark colored, similar to crude oil, and in the end of the CO_2 injection it was observed more light colored oil. Short time after the CO_2 injection had started in core RC_A the differential pressure increased, hence the pore pressure increased due to hydrate plug in the BPR, which in addition resulted in a delay of the oil production during the CO_2 injection.

Discussion of tertiary CO_2 injection subsequent secondary water injection

Table 4.9 shows variation in permeability for the cores and indicates the heterogeneity along with the range in irreducible water saturations. The shape of the oil recovery curve for the cores shows small discrepancies, where the oil recovery rate is high in the beginning of the water injection, short transient period after water breakthrough and increased again when CO_2 is injected. The CO_2 injection for RC_C resulted in the less efficient oil recovery, due to significant volume of water present in the core. Water presented in a strongly water wet medium covers the wall of the matrix, and some of the residual oil is trapped in the middle of the pores after water imbibition, which makes the diffusion process less efficient due to less contact area between the CO_2 and residual oil. These oil droplets trapped in matrix resist water flow and thus differential pressure increase again when only water is produced.

In cores with high S_{wi} there are less oil produced due to oil trapped in larger pores and as the water imbibes the small pores first where the capillary pressure is highest, the water bypasses the oil in the larger pores during the water injection.

In addition the core RC_D has low permeability which resulted in resistivity for water flow and the differential pressure decreased to 0bar when the injection is switched to CO_2 due to less density of the displacing fluid.

Because of combination of generally high oil recovery by CO_2 and observation of dark oil in the graded cylinder produced first and afterwards lighter oil, one may assume that the CO_2 developed multi-contact miscibility with the crude oil, meaning that the CO_2 extracted the lighter components

from the crude oil and developed a diffuse mixing zone (Sjævland and Kleppe, 1992). The oil recovery by CO_2 injection shows some different trend for core RC_B, which indicate less efficient diffusion in this core. The total PV injected in these experiments is not relevant on reservoir scale, because it requires a large amount of CO_2, but the experiments show potential of high oil recovery by CO_2 injection. In the cases RC_A, RC_B and RC_D all three cores reach high end-point oil recovery, which may be due to more oil present in the core, and hence diffusion is more efficient. In the case of water injection prior to CO2 injection it is possible that water shielding occurs, which is water films present in the core after water injection and inhibit CO_2 from contacting the oil phase, and leave residual oil in e.g. “dead-end” pores. This might be easier to observe on experiment conducted on larger cores of heterogeneous material, where a larger distribution of pore sizes may be present and where water covers the inlet of the pore throats.

4.2.5 IEOR by Tertiary CO_2 and CO_2-foam injection into fractured carbonate

This chapter presents results from $scCO_2$ and $scCO_2$-foam injection for IEOR in a fractured limestone network. The objective of these experiments was to look at the improved oil recovery by tertiary $scCO_2$ and $scCO_2$-foam injection subsequent a secondary water injection. In addition *in situ* foam generation was examined. These experiment was compared with previous study of EOR by $liqCO_2$ injection subsequent to water injection was previously reported in similar fractured chalk network using material balance and MRI technique (Brautaset, 2009). Different conditions for the experiment compared to the reference experiment are listed respectively: 1) "Brine C" and D_2O-brine 2) tertiary and liquid CO_2 injection 3) material used was limestone and chalk 4) mineral oil used was paraffin oil and n-Decane and 4) 10 ml/h and 2 ml/h . Table 4.10 lists core properties, such as length, PV, porosity and S_{wi} for the assembled fractured network, and Table 4.11 and 4.12 lists experimental conditions and results, respectively. Oil saturation and oil recovery vs. PV injected are plotted in Figure 4.13 and Figure 4.14, respectively.

Table 4.10 – Core properties of fractured system for IEOR experiment

Core ID	Core		Length [cm]	PV_{frac}	Porosity φ [%]	S_{wi}	Oil type	Injection scheme
AC_1	Limestone	RI10 RI8	9.7	21.4	21.9	0.237	Paraffin oil	I) Water II) $scCO_2$ III) $scCO_2$-foam
AC_3	Limestone	RI10 L30	9.7	23.1	23.6	0.242	Paraffin oil	I) Water II) $scCO_2$ III) $scCO_2$-foam
COJ2[1)]	Chalk		10.90	N/A	45.2	0.221	n-Decane	I) Water (D_2O) II) $liqCO_2$

[1)] Monitored in MRI, hence brine was exchanged with deuterium oxide (D_2O) brine at S_{or}

Table 4.11 – Experimental conditions during the IEOR experiments

Exp.	$K_{frac.system}$ (avg.) [mD]	Temp. [°C]	Pore pressure [bar]
AC_1	85 ± 57 [1)]	35	89
AC_3	146 ± 9	35	92
COJ2	2.95[2)] ± 0.94	23	83

[1)] High uncertainty due to problems with the BPR during the permeability measurements. The uncertainty in permeability measurements is measured by standard deviation. [2)] Absolute brine permeability

Table 4.12 – Experimental results from the IEOR

Exp.	S_{oi}	$S_{or,w}$	$R_{f,water}$ [%OOIP]	$S_{or,CO2}$	$R_{f,CO2}$ [%OOIP]	$S_{or,foam}$	$R_{f,foam}$ [%OOIP]	$S_{or,tot}$	$R_{f,total}$ [%OOIP]
AC_1	0.763	0.483	36.6	0.207	36.9	0.160	5.6	0.160	79.1
AC_3	0.758	0.566	25.3	0.384	24.0	0.309	9.9	0.309	59.2
COJ2[2)]	0.779	0.573	52.3	7.3	10.5	-	-	0.299	69.3

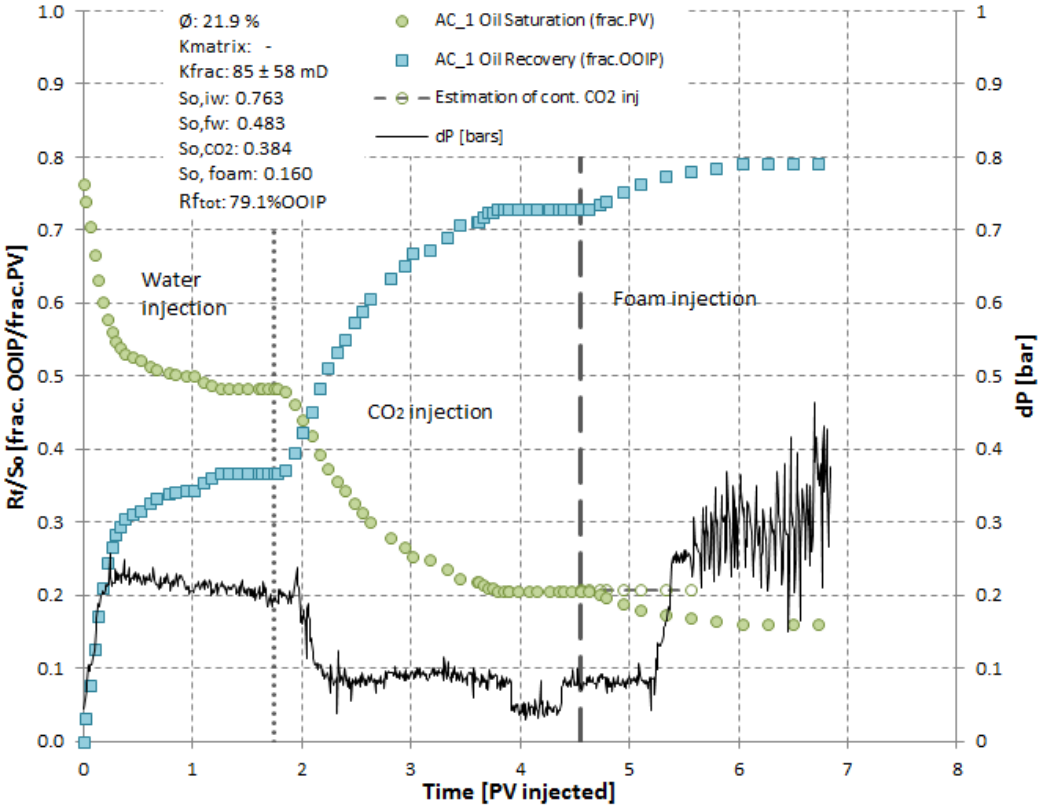

Figure 4.13 –Oil saturation and oil recovery vs. PV injected for core AC_1. Differential is plotted as dark line on secondary axis. The different injections schemes are separated by dotted lines and named specific.

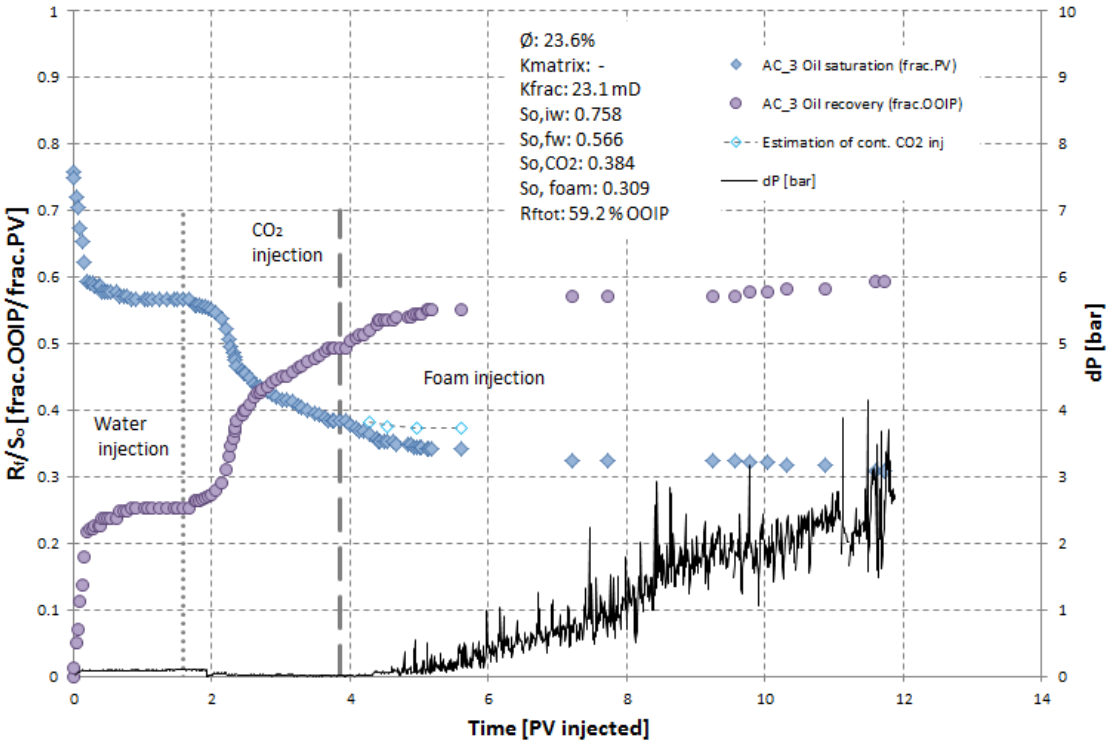

Figure 4.14 – Oil saturation and oil recovery vs. PV injected for core AC_3. Differential is plotted as dark line on secondary axis. The different injections schemes are separated by dotted lines and named specific.

Figure 4.13 and 4.14 shows a plot of oil saturation and oil recovery versus PV injected for the two cores, AC_1 and AC_3, respectively. The comparison of these figures shows a higher oil recovery in total for AC_1 and it is worth mentioning the low difference in S_{wi} (0.05) before injection started for the two fracture systems, which is later discussed and compared to the reference experiment COJ2.

During the water injection it is expected production from both cores, because of strongly water-wet media, where the rock imbibes water. Figure 4.13, 4.14 and Table 4.12 shows that after water breakthrough there is a short transient period and the total oil recovery by water injection for AC_1 and AC_3 are 36.6% and 26.3% OOIP, respectively. Water breakthrough occurs after injection of 0.3PV for AC_1 and 0.2PV for AC_2. Initially the differential pressure (notice the different scales in each figure) increased as a result of creation of an oil bank when water is injected into the first whole core. The oil displacement by water is capillary dominated in the strongly water-wet medium, due to spontaneous imbibition of water into the matrix. After water breakthrough the differential pressure decrease, due to high permeable zones in the present of fracture aperture and due to high injection rate, 10ml/h, the capillary forces is less dominant and viscous forces increase. The residual oil saturation after water injection was 0.483 and 0.566 for AC_1 and AC_3, respectively.

The following scCO_2 injection increased oil recovery due to diffusion of CO_2 in matrix, shown in Figure 4.13 and 4.14. In the end of the pure CO_2 injection there was no more oil produced and the residual oil saturation were approximately 0.20 and 0.40 for AC_1 and AC_3, respectively. An estimation of oil production if the CO_2 injection had continued is shown in the figures as transparent marks (estimation is based on oil production rate in the end of CO_2 injection). When CO_2 was injected the differential pressure was stabile for a short time which may be due to that CO_2 developed miscibility with the oil. Afterwards the differential pressure decreased as expected due to lower density difference between CO_2 and oil, as the CO_2 extract components from the oil. In the case of AC_3 (Figure 4.14) it is observed a sudden pressure drop towards the end of the CO_2 injection (approximately 4PV injected), this was caused by an unintentional temporary low CO_2 injection rate

The last part of the experiment was co-injection of surfactant and supercritical CO_2 with ratio 8:2. Foam was generated *in situ* the first whole core, where the dashed line to the right in Figure 4.13 and 4.14 indicates when the surfactant hit the core, approximately after a total injection of 4.6 PV for AC_1 and 3.85 PV for AC_3. The results from the foam injection showed further increased oil recovery, and additional oil produced was 5.6 and 9.9% of OOIP for AC_1 and AC_3 respectively. The residual oil saturation ended at 0.160 (AC_1) and 0.309 (AC_3) with a 20% difference in total oil recovery. The differential pressure increased during the foam injection and indicated generation of foam. The higher differential pressure in AC_3 may indicate stronger foam propagating through the core, and it may be due to blocking the fractures.

Discussion of tertiary scCO$_2$ and CO$_2$-foam injection

A comparison plot of oil recovery for the three different experiments is shown in Figure 4.15. The end-point oil recovery after water injection in AC_1 and AC_3 was lower than for COJ2, and in addition after water breakthrough it was observed a clean-cut for the latter one. The observation by MRI showed a capillary dominated, block-by-block displacement in this chalk core (Brautaset, 2009), and the oil recovery by water injection was higher than for AC_1 and AC_3. The different injection rates, 2ml/h for COJ2 and 10 ml/h for AC_1 and AC_3 may have influenced the oil recovery because the limestone cores may consist of high permeable streaks in addition to the fractures, where water can channel through.

The water imbibition in AC_1 was more efficient than AC_3, which showed approximately 10% less oil recovery than AC_1. This might be because AC_3 had a more open fracture in the outlet core than AC_1 (due to rough surface), and the water may has channeled through this high permeable fracture. The residual oil saturation after water injection was 0.483 and 0.566 for AC_1 and AC_3, respectively. The initial water saturation in the different cores was approximately identical and thus there was assumed minor differences in the oil recovery. The difference in oil production may be due to the heterogeneous material of limestone with respect to pore size and permeable streaks.

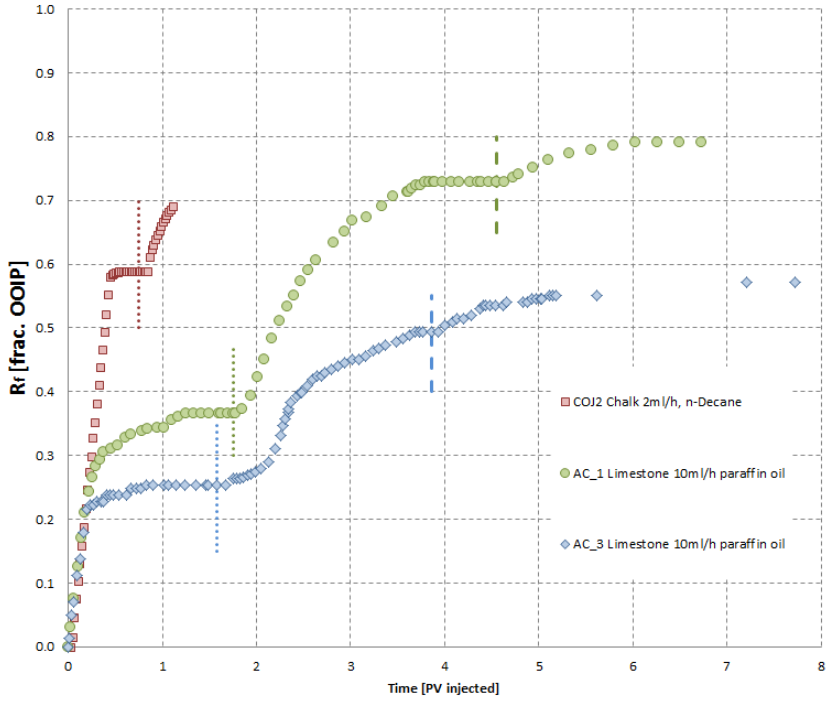

Figure 4.15 – Comparison of the experiments AC1 and AC3 with the reference experiment, COJ2 (Brautaset, 2009), where oil recovery is plotted versus PV injected. The fractured system was similar for all three experiments, but note that AC1 and AC3 was limestone and COJ2 was chalk. The injection rate for AC1 and AC3 was 5 times higher than COJ2, 10 and 2 ml/h, respectively. In all experiments there was performed a secondary water injection. The subsequent CO_2 and CO_2-foam injections are shown after the dotted lines, respectively.

The water injection was followed by a tertiary supercritical CO_2 injection which is indicated by the dotted lines to the left in Figure 4.15, showing rapid increased oil production. During the CO_2 injection the oil moved from the whole core and into the other cores and displaced the oil further, observed by MRI in Brautaset (2009). The increase in oil production rate is also observed in Figure 4.16 showing the production rate (ml/hr) of AC_1. The CO_2 injection ended at total oil recovery of 72.9% and 49.3% of OOIP for AC_1 and AC_3, respectively, whereas the CO_2 injection in COJ2 ended at 69.3, assuming the oil production was not finished if more CO_2 was injected. The result of tertiary CO_2 injection with respect to the oil saturation did not correspond with the result from Brautaset (2009) because the oil saturation in AC_3 was higher after water injection and thus higher oil recovery by CO_2 injection was expected. Which might be a result of the higher permeability of AC_3, hence region where CO_2 flows easily and the diffusion is less efficient due to minor contact with the oil in matrix.

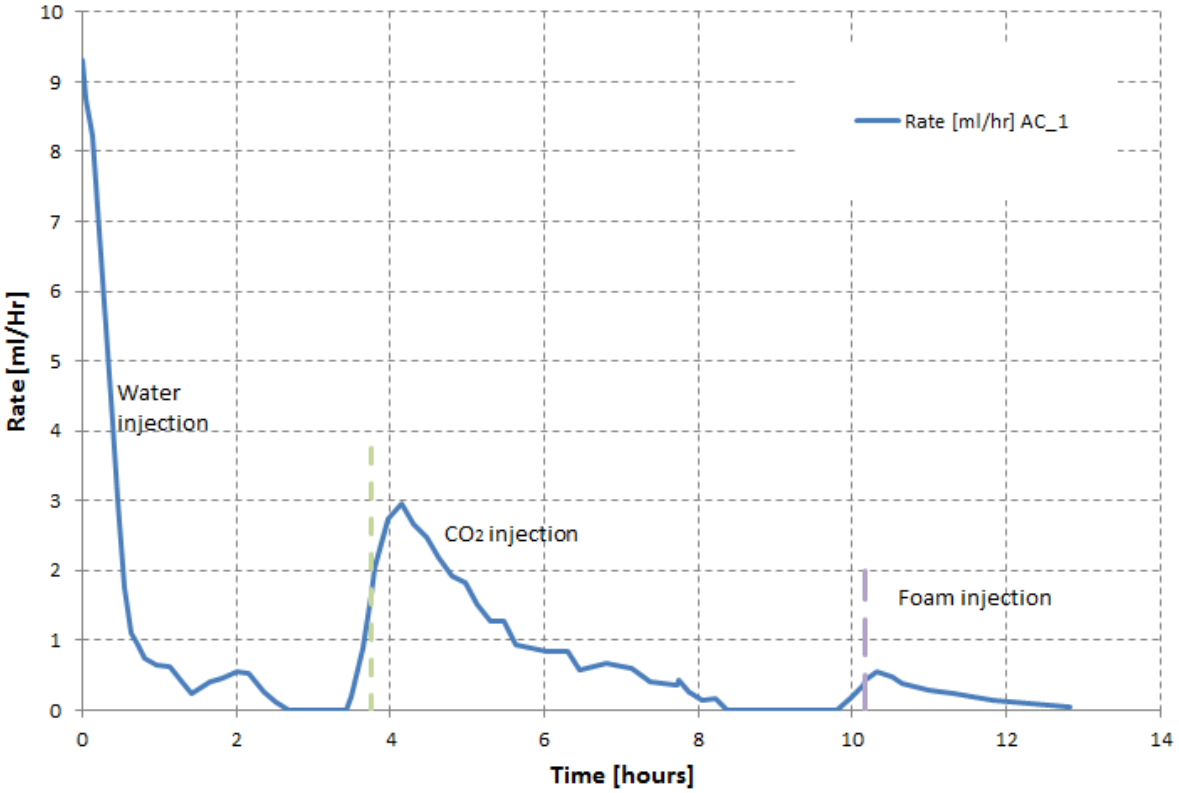

Figure 4.16 – Rate (ml/hr) versus time (hours) for AC_1. The green and purple dotted line indicates when CO_2 and co-injection of surfactant and CO_2 hit the core. The rate is calculated by an average of 5 rates, 3 values before and 2 values after the given hour.

In the beginning of the CO_2 injection it is assumed that the CO_2 develops first-contact miscibility with the paraffin oil. The low oil production rate of AC_3 during CO_2 injection may be influenced by water shielding, resulting in less efficient molecular diffusion as the amount of water saturation is higher than for a secondary CO_2 injection in cores at S_{wi}. Water films that are present after water injection can inhibit CO_2 from contacting the oil phase, and leave residual oil in e.g. “dead-end” pores (Gabitto,

1998). The more efficient molecular diffusion in chalk may be due to the smaller pore size which means the distance for molecular exchange between areas are smaller. In addition higher pore volume in chalk results in significant cross-sectional contact area between fracture aperture and matrix pores.

The increase in production by co-injection of surfactant and CO_2 for foam creation is due to increased viscosity of injected fluid (apparent viscosity), where the foam generated in the first whole part moving to the fractures blocking the apertures and deviate the CO_2 to the matrix and hence recover more oil (Kovscek and Radke, 1994). The production rate for AC_1 shown in Figure 4.16 showed increased oil production as a result of foam injection. The differential pressure did not increase initially, due to the time required for foam generation, but the differential pressure increased for both cores 0.5PV after the co-injection started in AC_1 and AC_3 which may be due to generation of foam and propagation further into the subsequent cores.

Higher differential pressure for AC_3 (one magnitude of order larger than AC_1) can be caused by generation of stronger foam, because large pressure drop across the core indicate stronger foam, hence flow resistance (Hirasaki and Lawson, 1985). Generation of stronger foam might be a result of less oil present in the cores (lamellae were not destroyed) and higher water saturation, stabilizing the lamellae. The fracture in outlet core of AC_3 was more open between the two parts (due to rough surface) than AC_1. This change in permeability when foam entering a larger fracture may have affected the foam because it is shown that foam is created by snap-off at permeability increase (Tanzil et al., 2002). And if the bubbles are of the same size, the apparent viscosity is higher in larger fractures compared to smaller (Hirasaki and Miller, 2006), which make a more favorable mobility ratio. Another explanation of the strong foam may be the surfactant used in these experiments, which was another type than previous experiments. This was not tested and should be investigated by injecting the surfactant solution into a brine saturated core. Earlier studies of foam injection as tertiary foam injection has been done by Christoffersen (2012), and the secondary recovery method was water injection. The result showed foam injection after 0.5 PV of foam injected, which can be explained by the higher water saturation presented in the core which will supply the foam with water and strengthen it.

All though the foam showed increased oil recovery, it is important to take into account the amount of pore volume required to achieve the maximum oil recovery. Less amount of CO_2 could be injected prior to the foam injection, but in these experiments it was injected that amount to clearly see if incremental oil was produced. If the foam injection had started earlier probably less amount of total injection was needed to achieve the residual oil saturation.

Previous tertiary CO_2 injection comparable with these CO_2 injection was oil recovery from CO_2 injection into strongly water-wet chalk cores were previously shown where supercritical CO_2 was

injected after water injection to enhance oil recovery, and the total oil recovery ended between 64.3 and 83.2% of OOIP (Svenningsen, 2011). The different oil recovery may be the water present in the core after a water injection, which can initially block the CO_2 for contacting trapped oil (water shielding). High water saturation when injecting CO_2 foam is favorable due to the water supply which strengthen the foam.

5 Shale - Unconventional Reservoirs

Unconventional reservoirs have been of large interest the last decades because there is estimated a large amount of petroleum reserves stored in these types of fields. There are several definitions of an unconventional reservoir and earlier distinctions between conventional and unconventional resources were primary based on economics (Law and Curtis, 2002), and later definition, by several organizations and authors, says that unconventional reservoirs require stimulation to be economically developed (Miskimins, 2009). There are challenges by producing from unconventional reservoirs, such as shale due to complex systems within the rock, where they are comprised of hydraulically induced fractures, natural fractures and a complex matrix consisting of different minerals and kerogen (Hinkley et al., 2013). Thus IEOR techniques and developing technologies are vital for oil recovery from these reservoirs. It is of large interest to obtain better understanding and more information about the shale rock, and thus the next chapter presents different trials of permeability and saturation experiments conducted on reservoir shale cores from a reservoir in the U.S.

Reservoir shale rock experiments

5.1 Experimental

Several experiments have been conducted on three shale core samples (SC_A, SC_B, SC_C), from a shale reservoir in the USA. The objective was to; 1) measure permeability by injection of CO_2 and 2) examine a "best practice" for saturating the shale cores with crude oil. Two of the core samples were unpreserved and one core sample was semi-preserved (covered in wax and aluminum foil). All cores were received at ambient temperature and pressure conditions. Table 5.1 summarizes properties obtained from the shale core samples, and includes length, diameter, bulk volume and initial weight.

Table 5.1 Properties of the shale cores

Core ID	State	Length [cm]	Diameter [cm]	Bulk volume [cm^3]	Weight [g]
SC_A	Unpreserved	3.80	3.80	43.10	111.27
SC_B	Unpreserved	3.92	3.80	44.46	114.40
SC_C	Semi-preserved	2.45	3.82	28.08	70.28

Permeability Measurements

Permeability measurements were performed on all core samples with both liquid and supercritical CO_2 injection, at various pressures, temperatures and flow rates. The experiments were performed on setup 3, see Figure 3.9. For the first experiment, a Back Pressure Regulator (BPR) was used at the outlet to control the pore pressure, as illustrated on the figure. For subsequent tests, constant outlet pressure was maintained by replacing the BPR with a retracting syringe pump for improved flow and pressure control. The supercritical CO_2 experiments were conducted at the Department of Physics and Technology (Setup 3), whereas the liquid experiments were conducted at Haukeland University Hospital (HUS) on a similar setup. A combined PET and medical CT scanner were used to get additional information about the flow behavior of the CO_2 phase. The injected CO_2 was explicitly labeled using ^{11}C to accurately visualize flow paths within the system.

During permeability tests, CO_2 was injected from the pump at experimental pressure conditions before CO_2 was injected through the core. The temperature was kept constant for each experiment, whereas net confining pressure and injection rate were varied. The rates were repeated in inverse direction. Due to temperature changes from the injection pump located at room temperature to the heating cabinet, the injection rate was re-calculated based on the volume expansion of CO_2. The experimental conditions for each experiment are listed in Table 5.2, and include temperatures, rates and net confining pressures. The injection rates and the measured differential pressures were then used to calculate the effective permeability by using Darcy's law (Equation 3.2.)

Table 5.2 Experimental conditions for different permeability tests

Core ID	**CO_2 state**	**Temperature *T* [°C]**	**Pore and net confinement pressure [bar]**
SC_B	Liquid	27	160 / 40
			160 / 80
SC_B	Supercritical	80	165 / 35
			165 / 85
SC_B	Supercritical	115	150 / 50
			150 / 100
			200 / 50
			200 / 100
SC_C	Supercritical	80	200/100

Rock structure

Rock structure for each core sample was also obtained with a medical CT scanner located at HUS, by dry scan of all core samples. The cores were first scanned to localize their position.

Positron Emission Tomography – Computed Tomography (PET-CT)

To obtain a three-dimensional visualization of rock material and to study in-situ displacements, a Siemens Biograph TruePoint PET/CT scanner, shown in Figure 5.1, with an extended axial field-of-view of 21.6 cm and a 16-slice CT has been used. This scanner is located at the PET center and nuclear medicine at the Haukeland University Hospital in Bergen (Jakoby et al., 2006).

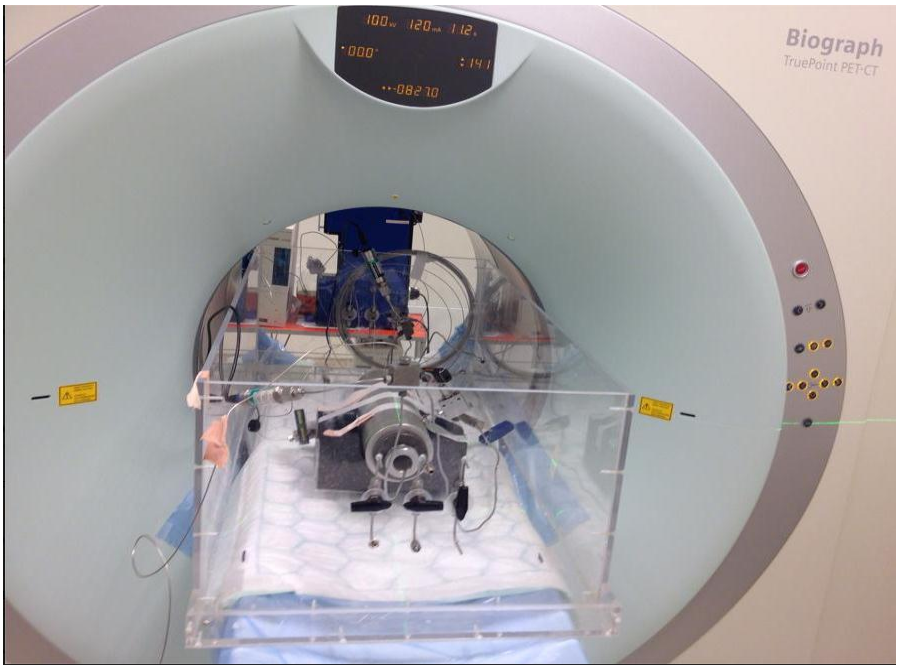

Figure 5.1 - Siemens Biograph TruePoint PET/CT scanner with core holder at Haukeland University Hospital in Bergen.

The PET/CT mainly consists of three parts: the PET scanner, the CT scanner, and the table where the patients or in this case the core holder is placed. Combining images from the PET scanner and the CT scanner, high-spatial-resolution 3D visualization of *in situ* fluid flow can be obtained. The CT-scan maps the initial variation of X-ray attenuation within the object, while the PET scan utilizes the annihilation radiation produced during decay of the radioactive isotope/tracer continuously to develop in-situ images (Jakoby et al., 2006).

CT scanning

Computed tomography (CT) scanning uses computer-processed X-rays to produce tomographic images of an object at different angles. The CT scanner consists of an X-ray source and detectors that measure how much the X-ray signals are attenuated as they pass through material with different densities. The CT value is the attenuation of the X-ray, and increases with increasing density, and is influenced by absorption and scattering which affect the intensity of the X-ray beam. The series of images produced in CT can be viewed individually as two-dimensional pictures or by combining the entire series as a three-dimensional visualization (Ketcham and Carlson, 2001).

PET

Positron emission tomography (PET) is a nuclear imaging technique to obtain a three-dimensional image volume of an object by using the unique decay characteristics of radionuclides that decay by positron emissions (Cherry and Dahlbom, 2006).

A PET scanner consists of a set of detectors that surround the object to be imaged and are designed to convert these high-energy photons into an electrical signal that can be fed to subsequent electronics. Labeled tracers (in this case ^{11}C was used to label CO_2) are introduced to the object, and when the radioactive atom on a particular molecule decays, a positron is ejected from the nucleus, ultimately leading to the emission of high-energy photons that have a good probability of escaping from the object. In a PET scan the decays will be detected and reconstructed into a tomographic image using mathematical algorithms to obtain a three-dimensional image. The signal intensity in a particular image is proportional to the amount of the radionuclide (Cherry and Dahlbom, 2006).

Best Practice for saturation shale cores

Different methods have been investigated in order to find a "best practice" for re-saturating dry reservoir shale cores with crude oil. Two saturation methods have been implemented for shale core SC_A and SC_B; 1) flowing crude oil through the cores for two weeks (dynamic) and 2) soaking the cores in crude oil under pressure in one week (static). Both experiments were conducted in a heating cabinet at 60 °C.

The first method dynamic method was to inject crude oil from an accumulator through the cores by a differential pressure of 100 bar, keeping the net confinement pressure at 50 bar. The samples were weighed during the test. The second method used for re-saturation was a static method, where the cores were placed inside an accumulator filled with crude oil under pressure (200 bar) for a longer

period of time (1-2 weeks) to force crude oil into the matrix. The added surface area could increase saturation.

5.2 Results and Discussion

Several experiments have been conducted on three shale core samples (SC_A, SC_B, SC_C), from a shale in the USA to measure permeability and find a "best practice" for saturating the shale cores. The experimental procedure is described in section 3.7.

Permeability Measurements

Permeability measurements by supercritical and liquid CO_2 injection was performed on core sample SC_B and SC_C, and additional information of fluid flow behavior was obtained in the PET/CT scanner at HUS on core sample SC_B by tracing the CO_2 marked with radioactive ^{11}C. Experiments conducted on core sample SC_A was aborted because of leaks from confinement pressure. The average effective permeability results from the tests are listed in Table 5.3, and include the net confinement pressure and the uncertainty by standard deviation.

Observations showed that temperature and net confinement pressure have a large impact on the effective permeability. An increase of net confinement pressure results in a decrease of the effective permeability, and is reasonable as it make it harder for the CO_2 to escape around the core sample. Increasing the temperature closer to reservoir conditions causes the effective permeability to decrease.

The summary table exhibits large variation for SC_B permeability results, and is suspected to be caused by a phase change of the CO_2 state, as viscosities of supercritical fluids are subjected to change when pressure or temperature varies. This is what may have happened during the experiment conducted in a heating cabinet (CO_2 at supercritical state), where constant outlet pressure was maintained using retracting pumps, located at room temperature outside the heating cabinet (CO_2 at liquid state). The higher discrepancy in the first experiment conducted at 80 °C is suspected to be caused by the fact that a Back Pressure Regulator (BPR) was used at the outlet, and might have caused instabilities in the outlet flow.

Table 5.3 - Experimental conditions and results

Core ID	CO_2 state	Temperature *T* [°C]	Pore and net confinement pressure [bar]	Average effective permeability, *k* [µD]	Comments
SC_B	Liquid	27	160 / 40	902 ± 74	With aluminum foil
			160 / 80	671 ± 32	
SC_B	Supercritical	80	165 / 35	498 ± 80	
			165 / 85	508	
SC_B	Supercritical	115	150 / 50	218 ± 55	
			150 / 100	142 ± 25	
			200 / 50	156 ± 39	
			200 / 100	133 ± 18	
SC_C	Supercritical	80	200 / 100	0.38	Without

Figure 5.2 illustrates the various pressures measured (outlet, inlet and differential pressure) and the injection rate as a function of time for core sample SC_B at 80 °C. When varying the injection rate, the outlet pressure remains stable, whereas the inlet pressure increases, and thus a higher differential pressure is observed, and indicates that the core sample is very tight and has a low permeability. One may also notice that by increasing the pressure more pressure fluctuations are observed, and is likely due to the back pressure regulator used in this experiment.

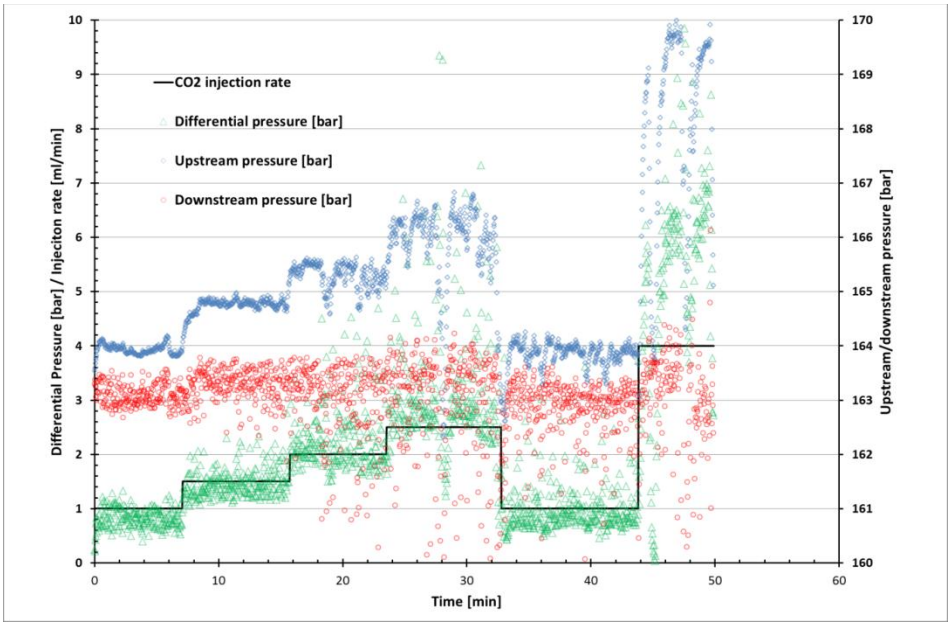

Figure 5.2 - Various pressures measured and injection rate as a function of time, for shale core sample SC_B at 80 °C

The images obtain from the PET/CT scan illustrated in Figure 5.3 showed that much of the CO_2 escaped around the core sample between the core and the aluminum foil protection, because of the consolidated nature of the shale matrix, and adds an uncertainty to all the effective permeabilities measured. Further experiment was conducted without aluminum foil to investigate if this could improve CO_2 flow through the core. This was conducted on core sample SC_C at 80 °C, and observations from Table 5.3 show a significant lower effective permeability of 0.38 µD and is more realistic compared to unconventional reservoirs that usually have permeability in the range of 0.1-10µD (Gorman et al., 1966).

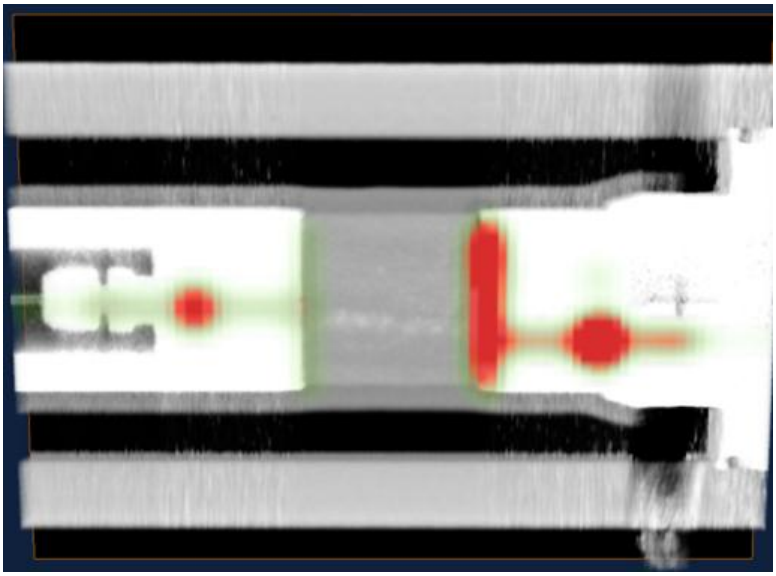

Figure 5.3 – Illustration of liquid CO_2 traced with radioactive ^{11}C injected into core SC_B. Warm colors (red) indicate high CO_2 saturation. Injection from right shows high concentration of CO_2. The middle grey part is the core SC_B and no CO_2, whereas to the left (outlet) it shows some CO_2 which was initially not there, indicating that the CO_2 was flowing around the core.

Rock structure

Dry scan of all the core samples, SC_A, SC_B and SC_C, was also conducted in the CT scanner and the images obtained are illustrated in Figure 5.4 respectively. A layered structure was observed in core sample SC_A and SC_B, whereas a more heterogeneous structure was observed from core sample SC_C. One reason for this could be that the core samples are taken from different parts of the reservoir.

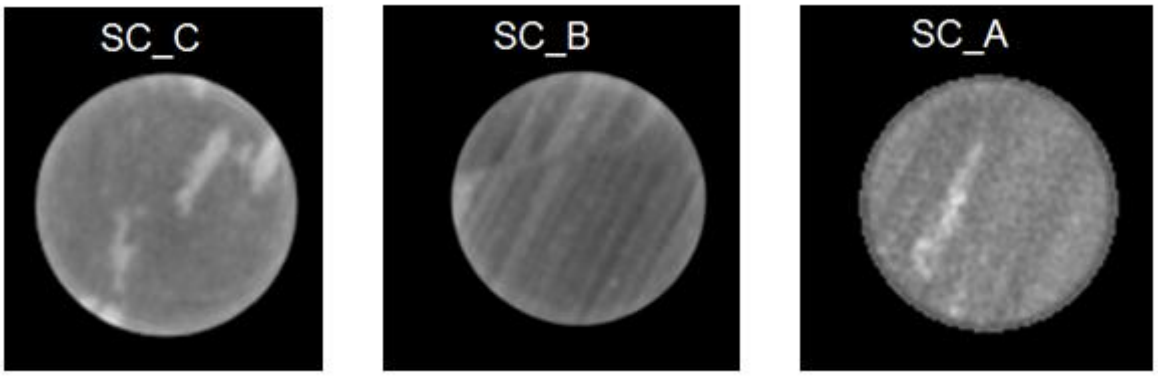

Figure 5.4 - Dry scan illustrating structured layers of core sample SC_A and SC_B and illustrating heterogeneities in core sample SC_C. The images are based on CT-values obtained from the scan and are vertical sliced. Darker areas indicate lower density, whereas lighter areas indicate higher density.

Best Practice for saturation shale cores

An investigation of a best practice for re-saturating reservoir shale cores was conducted on the two unpreserved core samples SC_A and SC_B. The different methods have been studied: 1) dynamic, by flowing crude oil through the core and 2) static, by soaking the cores in crude oil under pressure. The saturation results are listed in Table 5.4. The average porosity of unconventional shale reservoirs (~5%) was used to calculate the oil saturation, in addition to weight of dry and saturated core. Properties of the crude oil are listed in Table 5.1. The oil saturation was calculated by:

$$S_o = \frac{m_s - m_d}{V_{bulk} \cdot \varphi \cdot \rho_{oil}} \quad [5.1]$$

Where S_o is the oil saturation, m_d [g] and m_s [g] before and after saturation respectively, V_{bulk} [ml] is the bulk volume and φ [%] is the porosity.

Table 5.4 Results from the two re-saturations methods conducted on core samples SC_A and SC_B

Core ID	Saturation[%PV] (Dynamic method)	Saturation[%PV] (Static method)	Total saturation [PV%]
SC_A	65.2 ± 33	9.0 ± 33	74.2 ± 33
SC_B	71.1 ± 33	7.6 ± 33	78.7 ± 33

The results from dynamic re-saturation method provided an oil saturation of 65.2 % for shale core SC_A and 71.1% for shale core SC_B. The static method provided an additional increase in oil saturation of 9.0 and 7.6 % of core sample SC_A and SC_B, respectively.

It is worth noticing that approximately the same saturation percentage was obtained for both the dynamic and static method, and may indicate that the core structure is similar for the two cores, which was shown from the CT-scan illustrated in Figure 5.4.

The uncertainties are calculated to be 33% by equation A5 in Appendix A, and the high uncertainty in the porosity is the main contribution to this large number.

PART III – Conclusions and Future work

6 Conclusions

In this experimental study, miscible CO_2 and CO_2-foam was injected in fractured outcrop limestone and chalk cores to study the EOR and IEOR potential for these rocks. CO_2 injection in reservoir carbonate and shale cores from US reservoirs was also studied. Observation from the CO_2 and CO_2-foam injections are summarized below.

- Supercritical CO_2 injection performed on the same setup showed high oil recovery for both limestone and chalk cores. For whole cores, viscous forces and diffusion lead to high oil recoveries (88.2% OOIP on average for 5 cores). In fractured core plugs, oil recovery was lower (63.3% OOIP on average for 2 cores), and oil recovery was lower in limestone compared with chalk. This difference is due to large contact surface-area between matrix and fracture aperture in chalk, which result in more efficient diffusion in chalk.
- Pre-generated foam injection subsequent the CO_2 injection showed significant increased and accelerated oil recovery for limestone and minor increased oil recovery for chalk. The latter one showed no differential pressure, indicating no or weak foam generated, hence the foam was easily broken due to possibly high disjoining pressure because of small capillaries.
- Significant variation in S_{wi}, due to low pressure build up during oil drainage and along with different K_{abs} for the SWW reservoir carbonate cores indicated a heterogeneous material and possibly high permeable streaks. This resulted in oil recovery ranging between 17.8 - 45.1% OOIP produced during waterflood. Tertiary CO_2 injection in these cores resulted in a total recovery of 87.7 - 96.8% OOIP.
- Oil recovery by secondary water injection in SWW fractured limestone network resulted in oil recovery range between 26.3 and 36.6% OOIP produced by imbibition of water and viscous forces dominating the displacement process. Following tertiary CO_2 injection in fractured network resulted in additional 50% OOIP produced.
- By minimizing the undesired bypass of injected CO_2 a reasonable permeability measurement of 0.38 µD was achieved for the semi-preserved shale sample. A “best practice” for re-saturation the reservoir shale cores with crude oil was established using high pressure and temperature.

7 Further Work

- During the experiment use a transparent foam generator or tubing to visualize the foam
- Pre-heating the CO_2 when experiment is performed above ambient conditions
- Placing the BPR inside the heating cabinet to avoid drastic transformation of CO_2 when changing from supercritical to liquid/gas phase.
- Place a pressure gauge close to the core when this is shut-in to accurately measure the pressure inside and compensate with increasing/decreasing confinement pressure if the pore pressure changes.
- Use accurate pressure gauges to avoid uncertainty larger than the measured differential pressure.
- Further experiments by CO_2-foam injection in fractured chalk and limestone network should be conducted to investigate the foam behavior and obtain more knowledge.
- Co-injection of surfactant and air into brine saturated cores to study the foam creation in the cores (at ambient conditions).
- Tertiary CO_2-foam injection in reservoir cores for IEOR to examine if the oil production is accelerate and foam is stable with the crude oil.
- After several investigations of whole reservoir cores, investigate injection schemes in fractured reservoir cores and up-scaling by injection in blocks of the reservoir rocks. In addition PET/CT or MRI to visualize the fluid flow and structure of the reservoir rocks.
- Test of different surfactant solution to examine the best surfactant for carbonate rocks.
- HC or CO_2 injection in saturated shale cores to investigate the oil recovery
- Permeability measurements in unconventional shale without aluminum foil and by injection of noble gas instead of CO_2.

8 References

(NIST), T. N. I. O. S. A. T. 2011. *NIST Chemistry WebBook: Thermophysical Properties of Fluid Systems* [Online]. USA: U.S. Department of Commerce. Available: http://webbook.nist.gov/chemistry/ [Accessed 04.05.14 2014].

AARRA, M. G. & SKAUGE, A. 1994. A Foam Pilot in a North Sea Oil Reservoir: Preparation for a Production Well Treatment. *SPE Annual Technical Conference and Exhibition, 25-28 September, New Orleans, Louisiana.* Society of Petroleum Engineers.

AHR, W. M. 2008. *Geology of Carbonate Reservoirs: the identification, description, and characterization of hydrocarbon reservoirs in carbonate rock,* New Jersey, USA, Texas A&M University.

ALLAN, J. & SUN, S. Q. 2003. Controls on Recovery Factor in Fractured Reservoirs: Lessons Learned from 100 Fractured Fields. *SPE Annual Technical Conference and Exhibition, 5-8 October, denver, Colorado.* Society of Petroleum Engineers.

ANDERSON, W. G. 1986. Wettability Literature Survey - Part1: Rock/Oil/Brine Interactions and the Effects of Core Handling on Wettability. *Journal of Petroleum Technology,* 1125-1144.

ARDÈVOL, L. & GUTAMANIS, J. 2008. Pyrenees Hold Clues to Frac. *GEO ExPro*.

ARONOFSKY, J. S. & RAMEY, H. J., JR. 1956. Mobility Ratio - Its Influence on Injection or Production Histories in Five-Spot Water Flood. *Journal of Petroleum Technology*.

AWAN, A. R., TEIGLAND, R. & KLEPPE, J. 2008. A Survey of North Sea Enhanced-Oil-Recovery Projects Initiated During the Years 1975 to 2005. *SPE Reservoir Evaluation and Engineering*.

BABADAGLI, T. 2007. Development of mature oil fields — A review. *Journal of Petroleum Science and Engineering,* 57, 221-246.

BANGIA, V. K., YAU, F. F. & HENDRICKS, G. R. 1993. Reservoir Performance of a Gravity-Stable, Vertical CO2 Miscible Flood: Wolfcamp Reef Reservoir, Wellman Unit. *SPE Reservoir Engineering*.

BEAR, J. 1972. *Dynamics of Fluids in Porous Media,* New York, American Elsevier Publishing Company, Inc. .

BECK, J., LVOV, S., FEDKIN, M., ZIOMEK-MOROZ, M., HOLCOMB, G., TYLCZAK, J. & ALMAN, D. 2011. Electrochemical System to Study Corrosion of Metals In Supercritical CO2 Fluids. *CoRROSION 2011, 13-17 March, Houston, Texas, USA.* Houston, Texas, USA: NACE International.

BERTIN, H. J., APAYDIN, O. G., CASTANIER, L. M. & KOVSCEK, A. R. 1999. Foam Flow in Heterogeneous Porous Media: Effect of Cross Flow. *SPE Journal*.

BIJELJIC, B. & BLUNT, M. J. 2006. A Physically-Based Description of Dispersion in Porous Media. *SPE Annual Technical Conference and Exhibition, 24-27 September, San Antonio, Texas, USA.* San Antonio, Texas, USA: Society of Petroleum Engineers.

BLAKER, T., AARRA, M. G., SKAUGE, A., RASMUSSEN, L., CELIUS, H. K., MARTINSEN, H. A. & VASSENDEN, F. 2002. Foam for Gas Mobility Control in the Snorre Field: The FAWAG Project. *SPE Reservoir Evaluation & Engineering*, 5, 317-323.

BRAUTASET, A. 2009. *In situ fluid dynamics and CO_2 injection in porous rocks.* Dissertation for the degree philosophiae doctor (PhD), University of Bergen.

CAMPBELL, B. T. & ORR, F. M., JR. 1985. Flow Visualization for CO_2/Crude-Oil Displacements. *Society of Petroleum Engineers Journal*, 665-678.

CAPP. 2014. *Conventional and Unconventional* [Online]. Canada: Canadian Association of Petroleum Producers. Available: http://www.capp.ca/canadaIndustry/naturalGas/Conventional-Unconventional/Pages/default.aspx [Accessed 29/04/14 2014].

CHERRY, S. & DAHLBOM, M. 2006. PET: Physics, Instrumentation, and Scanners. *In:* PHELPS, M. (ed.) *PET*. Springer New York.

CHRISTOFFERSEN, A. 2010. *Økt oljeutvinning ved injeksjon av CO_2 -skum i en oppsprukket karbonatbergart ved forskjellige fuktforhold.* Master degree, University of Bergen.

CRAMEIK, T. D. & PLASSEY, J. A. 1972. Carbon Dioxide Injection Project Sacroc Unit, Scurry County, Texas. *Annual Meeting Papers, Division of Production, 6-8 March.* Houston, Texas: American Petroleum Institute.

CRAZE, R. C. 1950. Performance of Limestone Reservoirs. *Journal of Petroleum Technology*.

CRISCIONE, V. 2012. *Ekofisk – 40 years & still going strong* [Online]. nortrade.com: Norway Exports. Available: http://www.nortrade.com/sectors/articles/ekofisk-40-years-still-going-strong-/ [Accessed 21.05.2014 2014].

CUSSLER, E. L. 2009. *Diffusion: Mass transfer in fluid systems,* New York, U.S.A, Cambridge University Pres.

DA SILVA, F. V. & BELERY, P. 1989. Molecular Diffusion in Naturally Fractured Reservoirs: A Decisive Recovery Mechanism. *SPE Annual Technical Conference and Exhibition, 8-11 October, San Antonio, Texas.* Society of Petroleum Engineers.

DARVISH, G. R., LINDEBERG, E. G. B., HOLT, T., KLEPPE, J. & UTNE, S. A. 2006. Reservoir-Conditions Laboratory Experiments of CO_2 Injection into Fractured Cores. *SPE Europec/EAGE Annual Conference and Exhibition, 12-15 June, Vienna, Austria* Vienna, Austria Society of Petroleum Engineers.

ELY, J. F. & HANLEY, J. M. 1987. *TRAPP - Transport Properties Prediction [Computer] Program,* Boulder, CO, National Institute of Standards and Technology.

ESMAEILZADEH, P., BAHRAMIAN, A. & FAKHROUEIAN, Z. 2011. Adsorption of Anionic, Cationic and Nonionic Surfactants on Carbonate Rock in Presence of ZrO2 Nanoparticles. *Physics Procedia,* 22, 63-67.

EXEROWA, D. & KRUGLYAKOV, P. M. 1998. *Foam and Foam Films,* Netherlands, Elsevier Science B.V.

FALLS, A. H., MUSTERS, J. J. & RATULOWSKI, J. 1989. The Apparent Viscosity of Foams in Homogeneous Bead Packs. *SPE Reservoir Engineering*.

FARAJZADEH, R., ANDRIANOV, A., KRASTEV, R., HIRASAKI, G. & ROSSEN, W. R. 2012. Foam-Oil Interaction in Porous Media: Implications for Foam Assisted Enhanced Oil Recovery. *SPE EOR Conference at Oil and Gas West Asia, 16-18 April.* Muscat, Oman: Society of Petroleum Engineers.

FARAJZADEH, R., WASSING, L. B. M. & BOERRIGTER, P. M. 2010. Foam Assisted Gas Oil Gravity Drainage in Naturally-Fractured Reservoirs. *SPE Annual Technical Conference and Exhibition, 19-22 September.* Florence, Italy: Society of Petroleum Engineers.

GABITTO, J. F. 1998. Matrix-Fracture Mass Transfer. *SPE/DOE Improved Oil Recovery Symposium, 19-22 April, Tulsa, Oklahoma, USA.* Tulsa, Oklahoma, USA: Society of Petroleum Engineers.

GERNERT, J. M. & BRIGHAM, W. E. 1964. Meadow Creek Unit Lakota B Combination Water-Miscible Flood. *Journal of Petroleum Technology,* 16, 993-&.

GOGOI, S. 2011. Adsorption–Desorption of Surfactant for Enhanced Oil Recovery. *Transport in Porous Media,* 90, 589-604.

GORMAN, J. L., PASTO, J. K. & CROCKER, C. D. 1966. Soil Survey of Berkley County, West Virginia. *Soil Sruvey Series.* Berkley County, west Virginia, USA: United States Department of Agriculture in Cooperation with the Wet Virginia Agricultural Experiment Station.

GRAUE, A., VIKSUND, B. G. & BALDWIN, B. A. 1999. Reproducible Wettability Alteration of Low-Permeable Outcrop Chalk. *SPE Reservoir Evaluation & Engineering,* 2, 134-140.

GRUNDMANN, S. R. & LORD, D. L. 1983. Foam Stimulation. *Journal of Petroleum Technology,* 35, 597-602.

HADLEY, G. F. & HANDY, L. L. 1956. A Theoretical and Experimental Study of the Steady State Capillary End Effect. *Fall Meeting of the Petroleum Branch of AIME, 14-17 October, Los Angeles, California, USA.* Los Angeles, California, USA: Society of Petroleum Engineers.

HALLAND, E. K., MUJEZINOVIĆ, J. & RIIS, F. 2014a. CO_2 Starage Atlas - Norwegian Continental Shelf. *Petroleum activity on the Norwegian Continental Shelf* [Online]. [Accessed 25/05/2014].

HALLAND, E. K., MUJEZINOVIĆ, J. & RIIS, F. 2014b. CO_2 Starage Atlas - Norwegian Continental Shelf. *Storage options with EOR* [Online]. [Accessed 25/05/2014].

HAND, J. L. & PINCZEWSKI, W. V. 1990. Interpretation of Swelling/Extraction Tests. *SPE Reservoir Engineering*.

HARDMAN, R. F. P. 1982. Chalk Reservoirs of the North Sea. *Annual meeting of the Geological Society of Denmark.* Geological Society of Denmark.

HARPOLE, K. J., SIEMERS, W. T. & GERARD, M. G. 1994. CO_2 Foam Field Verification Pilot Test at EVGSAU: Phase IIIC--Reservoir Characterization and Response to Foam Injection. *SPE/DOE Improved Oil Recovery Symposium, 17-20 April.* Tulsa, Oklahoma: Society of Petroleum Engineers.

HAUGEN, A., FERNO, M. A., GRAUE, A. & BERTIN, H. J. 2010. Experimental Study of Foam Flow in Fractured Oil-Wet Limestone for Enhanced Oil Recovery. *SPE Improved Oil Recovery Symposium, 24-28 April.* Tulsa, Oklahoma, USA: Society of Petroleum Engineers.

HAUGEN, M. 2012. *CO_2 Injection in Fractured Chalk for Enhanced Oil Recovery*. Master degree, University of Bergen.

HAUGEN, Å., FERNØ, M. A., GRAUE, A. & BERTIN, H. J. 2012. Experimental Study of Foam Flow in Fractured Oil-Wet Limestone for Enhanced Oil Recovery. *SPE Reservoir Evaluation & Engineering*.

HEALY, R. N., HOLSTEIN, E. D. & BATYCKY, J. P. 1994. Status of miscible flooding technology. *14th World Petroleum Congress, 29 May-1 June.* Stavanger, Norway: World Petroleum Congress.

HELLER, J. P. 1984. Reservoir Application of Mobility Control Foams in CO_2 Floods. *SPE Enhanced Oil Recovery Symposium, 15-18 April.* Tulsa, Oklahoma, USA: Society of Petroleum Engineers.

HINKLEY, R., GU, Z., WONG, T. & CAMILLERI, D. 2013. Multi-Porosity Simulation of Unconventional Reservoirs. *SPE Unconventional Resources Conference Canada, 5-7 November*. Calgary, Alberta, Canada: Society of Petroleum Engineers.

HIRASAKI, G. J. 1989. Review of Steam-Foam Process Mechanisms, Supplement to SPE 19505, The Steam-Foam Process. *Society of Peroleum Engineers journal*.

HIRASAKI, G. J. & LAWSON, J. B. 1985. Mechanisms of Foam Flow in Porous Media: Apparent Viscosity in Smooth Capillaries. *Society of Petroleum Engineers Journal*, 25, 176-190.

HIRASAKI, G. J. & MILLER, C. A. 2006. Surfactant Based Enhanced Oil Recovery and Foam Mobility Control.

HOLM, L. W. 1986. Miscibility and Miscible Displacement. *Journal of Petroleum Technology*, 38, 817-818.

HOLM, L. W. & JOSENDAL, V. A. 1974. Mechanisms of Oil Displacement By Carbon Dioxide. *Journal of Petroleum Technology*, 1427-1438.

HUTCHINSON, C. A. & BRAUN, P. H. 1961. Phase relations of miscible displacement in oil recovery. *AIChE Journal*, 7, 64-72.

HØGNESEN, E. J., STRAND, S. & AUSTAD, T. 2005. Waterflooding of preferential oil-wet carbonates: Oil recovery related to reservoir temperature and brine composition. *SPE Europec/EAGE Annual Conference, 13-16 June.* Madrid, Spain: Society of Petroleum Engineers.

INTERIOR, U. S. D. O. T. 2014. *Mineral Resource On-Line Spatial Data - Edwards Limestone* [Online]. USA. Available: http://tin.er.usgs.gov/geology/state/sgmc-unit.php?unit=TXKed%3B0 [Accessed 2/5/14 2014].

JAKOBY, B. W., BERCIER, Y., WATSON, C. C., RAPPOPORT, V., YOUNG, J., BENDRIEM, B. & TOWNSEND, D. W. Physical Performance and Clinical Workflow of a new LSO HI-REZ PET/CT Scanner. Nuclear Science Symposium Conference Record, 2006. IEEE, Oct. 29 2006-Nov. 1 2006 2006. 3130-3134.

JENNINGS, J. W., JR. & LUCIA, F. J. 2003. Predicting Permeability From Well Logs in Carbonates With a Link to Geology for Interwell Permeability Mapping. *SPE Reservoir Evaluation and Engineering*.

JENNINGS, J. W., JR. & WARD, W. B. 2000. Geostatistical Analysis of Permeability Data and Modeling of Fluid-Flow Effects in Carbonate Outcrops. *SPE Reservoir Evaluation and Engineering*.

JENSEN, T. B., HARPOLE, K. J. & ØSTHUS, A. 2000. EOR Screening for Ekofisk. *SPE European Petroleum Conference, 24-25 October.* Paris, France: Society of Petroleum Engineers.

JIMÉNEZ , A. I. & RADKE, C. J. 1989. Dynamic Stability of Foam Lamellae Flowing Through a Periodically Constricted Pore. *In:* BORCHARDT, J. K. & YEN, T. F. (eds.) *Oil-Field Chemistry - Enhanced Recovery and Production Stimulation.* Department of Chemical Engineering, University of California, Berkeley: American Chemical Society.

KASRAIE, M. & ALI, S. M. F. 1984. Role of Immobile Phase Saturations in Tertiary Oil Recovery. *SPE Enhanced Oil Recovery Symposium, 15-18 April, Tulsa, Oklahoma, USA.* Tulsa, Oklahoma, USA: Society of Petroleum Engineers.

KETCHAM, R. A. & CARLSON, W. D. 2001. Acquisition, optimization and interpretation of X-ray computed tomographic imagery: applications to the geosciences. *Computers & Geosciences*, 27, 381-400.

KHATIB, Z. I., HIRASAKI, G. J. & FALLS, A. H. 1988. Effects of Capillary Pressure on Coalescence and Phase Mobilities in Foams Flowing Through Porous Media. *SPE Reservoir Engineering*, 3, 919-926.

KOVSCEK, A. R. & BERTIN, H. J. 2002. Estimation of Foam Mobility in Heterogeneous Porous Media. *SPE/DOE Improved Oil Recovery Symposium.* Tulsa, Oklahoma: Copyright 2002, Society of Petroleum Engineers Inc.

KOVSCEK, A. R. & RADKE, C. J. 1994. Fundamentals of Foam Transport in Porous Media. *Earth Science Division of Lawrence Berkley Laboratory and Department of Chemical Engineering, University of California*.

KULKARNI, M. M. & RAO, D. N. 2004. Experimental Investigation of Various Methods of Tertiary Gas Injection. *SPE Annual Technical Conference and Exhibition, 26-29 September, Houston, Texas, USA.* Houston, Texas, USA: Society of Petroleum Engineers.

KULKARNI, M. M. & RAO, D. N. 2005. Experimental Investigation of Miscible Secondary Gas Injection. *SPE Annual Technical Conference and Exhibition, 9-12 October, Dallas, Texas, USA.* Dallas, Texas, USA: Society of Petroleum Engineers.

LAKE, L. W. 1989. Enhanced Oil Reocvery. *Prentice Hall Incorporated.* Englewood Cliffs, New Jersey.

LAKE, L. W. 2007. *Petroleum Engineering Handbook,* USA, Society of Petroleum Engineers

LAKE, L. W., SCHMIDT, R. L. & VENUTO, P. B. 1992. A Niche for Enhanced Oil Recovery in the 1990s. *Oilfield Review by Schlumberger,* 4.

LANGLO, S. A. 2013. *Enhanced Oil Recovery by CO_2 and CO_2-foam Injection in Fractured Limestone Rocks* Master degree Master, University of Bergen.

LAW, B. E. & CURTIS, J. B. 2002. Introduction to unconventional petroleum systems. *APPG Bulletin,* 86, 1851-1852.

LIE, S. H. 2013. *Diffusion as an Oil Recovery Mechanism During CO_2 Injection in Fractured Reservoirs.* MSc, University of Bergen.

LUCIA, F. J., KERANS, C. & JENNINGS, J. W., JR. 2003. Carbonate Reservoir Characterization. *Journal of Petroleum Technology*.

MARTIN, F. D., HELLER, J. P., WEISS, W. W., TSAU, J.-S., ZORNES, D. R., SUGG, L. A., STEVENS, J. E. & KIM, J. E. 1992. CO_2-Foam Field Verification Pilot Test at EVGSAU Injection Project Phase I: Project Planning and Initial Results. *SPE/DOE Enhanced Oil Recovery Symposium in Tulsa (April 1992).* Tulsa, Oklahoma: Society of Petroleum Engineers.

MARTIN, F. D., STEVENS, J. E. & HARPOLE, K. J. 1995. CO_2-Foam Field Test at the East Vacuum Grayburg/San Andres Unit. *Society of Peroleum Engineers*.

MARZOUK, I., TAKEZAKI, H. & SUZUKI, M. 1998. New Classification of Carbonate Rocks for Reservoir Characterization. *Abu Dhabi International Petroleum Exhibition and Conference, 11-14 November, Abu dhabi, United Arab Emirates.* Society of Petroleum Engineers.

MATHIASSEN, O. M. 2003. *CO_2 as Injection Gas for Enhanced Oil Recovery and Estimation of the Potential on the Norwegian Continental Shelf.* NTNU – Norwegian University of Science and Technology.

MISKIMINS, J. 2009. The importance of geophysical and petrophysical data integration for the hydraulic fracturing of unconventional reservoirs. *The Leading Edge - Unconventional Resources and CO_2 Monitoring*.

MOORTGAT, J. & FIROOZABADI, A. 2012. Three-Phase Compositional Modeling with Capillarity in Heterogeneous and Fractured Media. *SPE Annual Technical Conference and Exhibition, 8-10 October, San Antonio, Texas, USA.* San Antonio, Texas, USA: Society of Petroleum Engineers.

NAGAI, R. B. & REDMOND, G. W. 1982. Numerical Simulation of a Gravity Stable, Miscible CO_2 Injection Project in a West Texas Carbonate Reef. *SPE Annual Technical Conference and Exhibition.* New Orleans, Louisiana, USA: Society of Petroleum Engineers.

NIST. 2014. *NIST Chemestry WebBook [Online]* [Online]. United States of America: Standard Reference Data Act. Available: http://webbook.nist.gov/chemistry/ [Accessed 04. March 2014].

NORWEGIANPETROLEUMDIRECTORATE. 2014. *Squeezing more out* [Online]. Stavanger, Norway: Norwegian Petroleum Directorate. Available:

http://www.npd.no/en/Publications/Norwegian-Continental-Shelf/No2-2013/Squeezing-more-out/ [Accessed 25/05/2014 2014].

ORGANICK, E. I. & BROWN, G. G. 1952. Prediction of hydrocarbon vapor-liquid ecuilibria. *Chem. Eng. Progr., Symposium Ser. No. 2,* 48, 97.

PATTON, J. T., HOLBROOK, S. T. & HSU, W. 1983. Rheology of Mobility-Control Foams. *Society of Petroleum Engineers Journal,* 23, 456 - 460.

PERKINS, T. K. & JOHNSTON, O. C. 1963. A Review of Diffusion and Dispersion in Porous Media. *Society of Petroleum Engineers Journal,* 3, 70-84.

PICHA, M. S. 2007. Enhanced Oil Recovery by Hot CO_2 Flooding. *SPE Middle East Oil and Gas Show and Conference.* Kingdom of Bahrain: Society of Petroleum Engineers.

RAGE, T. 1996. *Studies of Tracer Dispersion and Fluid Flow in Porous Media.* PhD, University of Oslo.

RANSOHOFF, T. C. & RADKE, C. J. 1988. Mechanisms of Foam Generation in Glass-Bead Packs. *SPE Reservoir Engineering,* 3, 573-585.

ROSSEN, W. R. 1988. Theories of Foam Mobilization Pressure Gradient. *SPE Enhanced Oil Recovery Symposium, 16-21 April, Tulsa, Oklahoma, USA.* Tulsa, Oklahoma, USA: Society of Petroleum Engineers.

SAHIMI, M. 2011a. *Flow and Transport in Porous Media and Fractured Rock,* Weinheim, Germany, Wiley-VCH.

SAHIMI, M. 2011b. *Flow and Transport in Porous Media and Fractured Rock,* Weinheim, Germany, WILEY-VCH Verøag GmbH & co. KGaA.

SANCHEZ, J. M. & HAZLETT, R. D. 1992. Foam Flow Through an Oil-Wet Porous Medium: A Laboratory Study. *SPE Reservoir Engineering,* 7, 91-97.

SCHECHTER, D. S., GRIGG, R., GUO, B. & SCHNEIDER, B. 1998. Wellman Unit CO_2 Flood: Reservoir Pressure Reduction and Flooding the Water/Oil. *SPE Annual Technical Conference and Exhibition, 27-30 September, New Orleans, Louisiana, USA.* Society of Petroleum Engineers.

SCHRAMM, L. L. & WASSMUTH, F. 1994. *Foams: Basic Principles,* Washington DC, American Chemical Society.

SERIGHT, R. S. 2010. *Mobility Ratio* [Online]. United States of America: New Mexico Petroleum Recovery Research Center - New Mexico Tech. Available: http://baervan.nmt.edu/research_groups/reservoir_sweep_improvement/pages/clean_up/mobility.html [Accessed 06.03.14 2014].

SHENG, J. J. 2013. *Enhanced Oil Recovery Field Case Studies,* USA, Gulf Professional Publishing.

SJÆVLAND, S. M. & KLEPPE, J. 1992. *SPOR - Recent Advances in Improved oil Reocvery Methods For North Sea Sandstone Reservoirs, Chapter 9,* Stavanger, Norwegian Petroleum Directorat.

STALKUP, F. I., JR. 1983. Status of Miscible Displacement. *Journal of Petroleum Technology,* 35.

STEVENS, J. E., HARPOLE, K. J., ZORNES, D. R. & MARTIN, F. D. 1992. CO_2 Foam Field Verification Pilot Test at EVGSAU: Phase II - Foam Injection Design and Operating Plan. *SPE Annual Technical Conference and Exhibition, 4-7 October.* Washington, D.C., USA: Society of Petroleum Engineers.

SVENNINGSEN, S. 2011. *An experimental study of CO_2 injection for enhanced oil recovery in chalk and limestone.* Master Degree, University of Bergen.

TANZIL, D., HIRASAKI, G. J. & MILLER, C. A. 2002. Mobility of Foam in Heterogeneous Media: Flow Parallel and Perpendicular to Stratification. *SPE Journal,* 7, 203 - 212.

TEIGLAND, R. & KLEPPE, J. 2006. EOR Survey in the North Sea. *SPE/DOE Symposium on Improved Oil Recovery, Tulsa (April 2006).* Tulsa, Oklahoma, USA: Society of Petroleum Engineers.

TORMODSGARD, Y. 2014. Norsk Petroleumsverksemd - Fakta 2014. *In:* DEPARTMENT, O. A. E. (ed.) *07 MEDIA.* Norway: Norwegian, Government, Oil and Energy Department.

TORSAETER, O. 1984. An Experimental Study of Water Imbibition in Chalk From the Ekofisk Field. *SPE Enhanced Oil Recovery Symposium, 15-18 April.* Tulsa, Oklahoma: Society of Petroleum Engineers.

VIKINGSTAD, A. K., SKAUGE, A., HØILAND, H. & AARRA, M. 2005. Foam–oil interactions analyzed by static foam tests. *Colloids and Surfaces A: Physicochemical and Engineering Aspects,* 260, 189-198.

WANG, F. P., LUCIA, F. J. & KERANS, C. 1998. Integrated Reservoir Characterization Study of a Carbonate Ramp Reservoir: Seminole San Andres Unit, Gaines County, Texas. *SPE Reservoir Evaluation and Engineering*.

WASAN, D. T., KOCZO, K. & NIKOLOV, A. D. 1993. Mechanisms of Aqueous Foam Stability and Antifoaming Action with and without Oil. *In:* SCHRAMM, L. L. (ed.) *Foams: Fundamentals and Applications in the Petroleum Industry.* Chicago: Illinois Institute of Technology, American Chemical Society.

WELLINGTON, S. L. & VINEGAR, H. J. 1985. CT Studies of Surfactant-induced CO2 Mobility Control. *SPE Annual Technical Conference and Exhibition, 22-26 September, Las Vegas, Nevada, USA.* Society of Petroleum Engineers.

YARBOROUGH, L. & SMITH, L. R. 1970. Solvent and Driving Gas Compositions for Miscible Slug Displacement. *Society of Petroleum Engineers Journal,* 10, 298 - 310.

YDSTEBØ, T. 2013. *Enhanced Oil Recovery by CO_2 and CO_2-Foam in Fractured Carbonates.* Master, University of Bergen.

YELLIG, W. F. & METCALFE, R. S. 1980. Determination and Prediction of CO2 Minimum Miscibility Pressures (includes associated paper 8876). *Journal of Petroleum Technology,* 32, 160 - 168.

YOKOYAMA, Y. & LAKE, L. W. 1981. The Effects of Capillary Pressure on Immiscible Displacements in Stratified Porous Media. *SPE Annual Technical Conference and Exhibition, 4-7 October, San Antonio, Texas, USA.* San Antonio, Texas, USA: Society of Petroleum Engineers.

ZANGANEH, M. N., KAM, S. I., LAFORCE, T. C. & ROSSEN, W. R. 2009. The Method of Characteristics Applied to Oil Displacement by Foam. *EUROPEC/EAGE Conference and Exhibition, 8-11 June, Amsterdam, The Netherlands.* Amsterdam, The Netherlands: Society of Petroleum Engineers.

ZOLOTUKHIN, A. B. & URSIN, J.-R. 2000. *Introduction to Petroleum Reservoir Engineering,* Kristiansand, Høyskoleforlaget AS - Norwegian Academic Press.

Appendix A – Uncertainty calculations

Value *R* dependent on several variables *x, y, z, ... i* with the uncertainty $S_{\bar{x}}$, $S_{\bar{y}}$, $S_{\bar{z}}, \dots, S_{\bar{\imath}}$ have the uncertainty calculated by the equation:

$$S_{\bar{R}} = \sqrt{\left(\frac{\partial R}{\partial x} S_{\bar{x}}\right)^2 + \left(\frac{\partial R}{\partial y} S_{\bar{y}}\right)^2 + \left(\frac{\partial R}{\partial z} S_{\bar{z}}\right)^2 + \cdots + \left(\frac{\partial R}{\partial i} S_{\bar{\imath}}\right)^2} \qquad [A1] \qquad \bar{x} = \frac{x_1 + x_2 + x_3 + x_N}{N} = \frac{1}{N}\sum_{i=1}^{N} x_i \qquad [A2]$$

where x, y, z, … , i, are uncorrelated variables and $\bar{x}$, $\bar{y}$, $\bar{z}, \dots$, $\bar{\imath}$, are the arithmetical middle value

If the value of R is given as a product of variable, a^2, b^2 and c^2, equation can be given by:

$$\frac{\partial_{\bar{R}}}{R} = \sqrt{a\left(\frac{\partial_{\bar{x}}}{\bar{x}}\right)^2 + b\left(\frac{\partial_y}{\bar{y}}\right)^2 + c\left(\frac{\partial_{\bar{z}}}{\bar{z}}\right)^2}$$

Uncertainty in porosity

The porosity is measured as pore volume divided by bulk volume of the core (equation 3.1). Pore volume is measured by weighting the cores dry and saturated by fluid and the uncertainty of the weight is ±0.02g and there is an uncertainty in the density of the fluids. Hence the uncertainty is given by equation:

$$\partial_{\bar{V}_p} = \sqrt{\left(\frac{\partial V_p}{\partial m}\partial_{\bar{m}}\right)^2 + \left(\frac{\partial V_p}{\partial \rho}\partial_{\bar{\rho}}\right)^2} = \sqrt{(2\pi L \partial_{\bar{r}})^2 + (\pi r^2 \partial_L)^2} \qquad [A3]$$

In addition the caliper used for measuring diameter and length for calculation of bulk volume is a contribution to uncertainty of porosity. The uncertainty in bulk volume is given by equation:

$$\partial_{\bar{V}_{bulk}} = \sqrt{\left(\frac{\partial V_b}{\partial r}\partial_{\bar{r}}\right)^2 + \left(\frac{\partial V_b}{\partial L}\partial_L\right)^2} = \sqrt{(2\pi L \partial_{\bar{r}})^2 + (\pi r^2 \partial_L)^2} \qquad [A4]$$

Combining these two equations, A3 and A4 the uncertainty in porosity is given by the equation

$$\partial_{\bar{\varphi}} = \sqrt{\left(\frac{1}{V_{bulk}}\partial_{\bar{V_p}}\right)^2 + \left(\frac{\partial V_p}{V_{bulk}}\partial_{\overline{V_{bulk}}}\right)^2} \qquad [A5]$$

Uncertainty in permeability

Permeability is measured by various variables in Darcy's law (equation 3.3). In addition to the uncertainty of the caliper there is uncertainty in the flow rate of the pump, viscosity of the fluid and the measured differential pressure. The total uncertainty of the permeability is given by equation:

$$\frac{\partial_{\bar{K}}}{K} = \sqrt{\left(\frac{\partial_{\bar{Q}}}{\bar{Q}}\right)^2 + \left(\frac{\partial_{\bar{\mu}}}{\bar{\mu}}\right)^2 + \left(\frac{\partial_{\bar{L}}}{\bar{L}}\right)^2 + \left(\frac{\partial_{\bar{A}}}{\bar{A}}\right)^2 + \left(\frac{\partial_{\overline{\Delta p}}}{\overline{\Delta p}}\right)^2} \qquad [A6]$$

Appendix B – Source of Errors

Instrumental Uncertainties

Pressure gauges: ± 0.25% of maximum value (250 bar)

Injection rate: ± 5% ml/h

Caliper: ± 0.01 mm

Weight: ± 0.02g

Experimental Uncertainties

PV injected: ± 0.5 ml

Oil Saturation, S_o: ± 0.008%

Reading the production from the graded cylinder due to the angle of the web camera sometimes made it hard to give an exact value and this was set to ± 0.05 ml.

Measurement of dead volume may be one of the major contributor to uncertainty in the oil produced, hence oil saturation and oil recovery.

Figure 4.2 shows a plot of oil saturation where uncertainty in both saturation and PV injected is included.

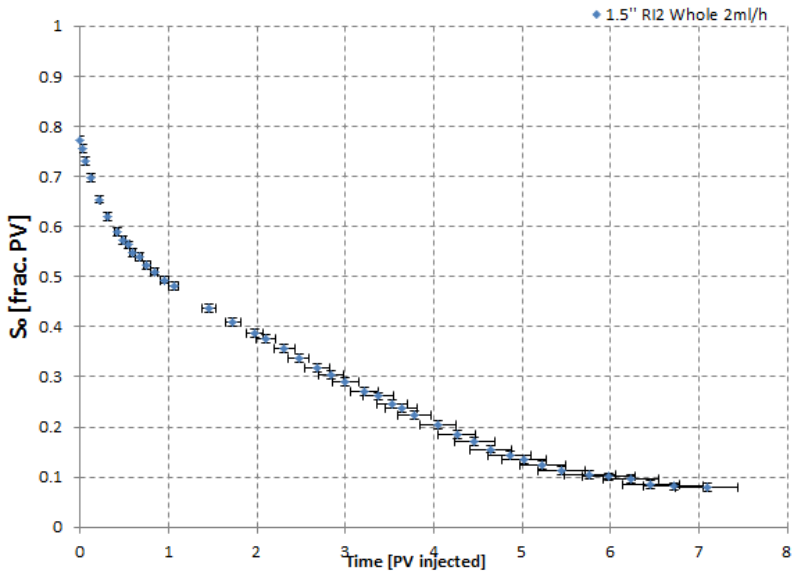

Figure 4.2 – Example of oil saturation curve vs. PV injected included error bars.

Appendix C - Nomenclature

K_{abs}	Absolute permeability
V_b, V_p	Bulk and pore volume, respectively
P_c, P_{nw}, P_w	Capillary pressure, pressure in non-wetting and wetting phase, respectively.
$\prod$	Disjoining pressure
$K_{e,i}$	Effective permeability of fluid *i* (water, oil or gas)
q	Fluid flow rate
IEOR	Integrated Enhanced Oil Recovery
IFT	Interfacial tension
$\sigma_{nw\text{-}w}$	Interfacial tension between non-wetting and wetting phase
S_{wi}	Irreducible water saturation
liqCO_2, scCO_2	Liquid CO_2 and Supercritical CO_2
λ_i	Mobility of fluid *i* (water, oil, gas)
M	Mobility ratio
OOIP	Oil Original in Place
PV, PV_{frac}	Pore volume and whole and fractured core, respectively
φ	Porosity
r_c	Radius of capillary
R_1, R_2	Radius of curvature
R_f	Recovery factor
$k_{r,i}$	Relative permeability of fluid *i* (water, oil or gas)
$S_{or,w}$, $S_{or,CO2}$	Residual oil saturation in the core after water flooding and CO_2 flooding, respectively
UoB	University of Bergen
υ	Velocity of displacing fluid
μ_i	Viscosity of fluid *i* (water, oil, gas)
θ	Wetting angle